

Electronic Thesis and Dissertation Repository

12-16-2019 1:30 PM

Biomechanical analysis of open-skull high-rate traumatic brain injury using finite element mouse brain model

Lihong Lu
The University of Western Ontario

Supervisor
Mao, Haojie
The University of Western Ontario

Graduate Program in Mechanical and Materials Engineering
A thesis submitted in partial fulfillment of the requirements for the degree in Master of Engineering Science
© Lihong Lu 2019

Follow this and additional works at: <https://ir.lib.uwo.ca/etd>



Part of the [Biomechanical Engineering Commons](#)

Recommended Citation

Lu, Lihong, "Biomechanical analysis of open-skull high-rate traumatic brain injury using finite element mouse brain model" (2019). *Electronic Thesis and Dissertation Repository*. 6723.
<https://ir.lib.uwo.ca/etd/6723>

This Dissertation/Thesis is brought to you for free and open access by Scholarship@Western. It has been accepted for inclusion in Electronic Thesis and Dissertation Repository by an authorized administrator of Scholarship@Western. For more information, please contact wlsadmin@uwo.ca.

Abstract

To better understand traumatic brain injury (TBI), it is necessary to correlate with injuries, which are observed from in vivo laboratory experiments, to brain mechanical responses, which can so far be best predicted by finite element (FE) models. Firstly, a previously validated FE model was improved to investigate the effect of repeated impacts and lateral movements on brain responses to ensure the accuracy and reproducibility of controlled cortical impact (CCI) across different labs. Then, a new FE mouse brain model with the detailed three-dimensional (3D), non-linear vasculature was developed to study how the vasculature affected brain response in CCI and predicted vasculature responses. Lastly, the correlation between brain mechanical strains and microvessel injury induced by CCI was investigated. In summary, the biomechanics of CCI was further characterized and a new mouse brain model with detailed vasculature was developed to understand brain mechanics and microvessel damage.

Keywords

Controlled cortical impact (CCI), finite element model, maximum principal strain (MPS), microvessel, traumatic brain injury (TBI), vasculature

Summary for Lay Audience

To better understand traumatic brain injury (TBI), it is necessary to correlate with injuries, which are observed from in vivo laboratory experiments, to brain mechanical responses, which can so far be best predicted by finite element (FE) models. The efforts of developing high-quality finite element (FE) head models have been conducted to increase the understanding of brain injury mechanism. In previous FE models, the brain was modeled without the whole three-dimensional (3D) vasculature and the result of the structural influence of the vasculature was contradictory, mainly because the brain vasculature network is of high complexity and is difficult to investigate. Also, very little was known on how the vasculature affects brain response under the open-skull controlled cortical impact (CCI), which is one of the most widely used in vivo laboratory neurotrauma models to observe focal brain injuries. In order to better understand CCI, a previously validated FE mouse brain model was improved to investigate the effect of repeated impacts and lateral movements on brain responses during CCI. The repeated impacts had minimal effect on peak strains. The lateral movements of the tip, however, greatly increased brain strains and affected large brain regions. Hence, it is necessary to monitor and control lateral movements to ensure the accuracy and reproducibility of CCI, for which no existing CCI devices can deliver, posing an opportunity for future developments. Then, a new FE mouse brain model with the detailed 3D, non-linear vasculature was developed to study how the vasculature affected brain response in CCI and predicted vasculature responses. Interestingly, the contribution of the vasculature on brain strains in CCI was limited, with less than 5% of changes by comparing brain models with and without vasculature. Lastly, CCI is a focal injury that induces microvessel damage in the cortical region. Hence, the correlation between brain mechanical strains and microvessel injury in CCI was investigated. In summary, the biomechanics of CCI was further characterized and a new mouse brain model with detailed vasculature was developed to understand brain mechanics and microvessel damage.

Co-Authorship Statement

Chapter 2 ('Quantifying the effect of repeated impacts and lateral tip movements on brain responses during controlled cortical impact') co-authored by Dr. Haojie Mao was published in Journal of Neurotrauma. Chapter 3 ('The effect of 3D vasculature on brain response under focal brain injury') co-authored by Dr. John G. Sled, Dr. Ken Monson and Dr. Haojie Mao and chapter 4 ('Investigate mechanisms and thresholds of the brain microvascular damage combining finite element modeling and experiments of CCI') co-authored by Joe Steinman, Dr. John G. Sled and Dr. Haojie Mao will be sent for review.

Acknowledgments

I would like to express my gratitude to Dr. Haojie Mao for his support of my research. I acknowledge Dr. Arthur Brown for his support as a committee member, as well as Dr. Kathy Xu for the support of the pneumatic CCI device. I acknowledge Mr. Steven Jevnikar and Dr. Kamran Siddiqui for the support of the high-speed camera. I acknowledge Dr. Joe Steinman and Dr. John G. Sled for the support of vasculature image and microvessel density image. I thank Mr. Kewei Bian for his help in taking high-speed videos and assisting with computer simulations. I acknowledge that the Canada Research Chairs program and NSERC for support. Lastly, I thank Mr. Jianyu Ma for his help with data analysis.

Table of Contents

Abstract.....	ii
Summary for Lay Audience.....	iii
Co-Authorship Statement.....	iv
Acknowledgments.....	v
Table of Contents.....	vi
List of Tables.....	x
List of Figures.....	xi
List of Appendices.....	xiv
Acronyms.....	xv
Chapter 1.....	1
1 Introduction.....	1
1.1 Traumatic brain injury (TBI).....	1
1.2 The mouse head anatomy and vasculature.....	1
1.2.1 Mouse head anatomy.....	1
1.2.2 The vasculature morphology.....	2
1.2.3 Material property of vasculature.....	3
1.3 Biomechanical methods to study TBI.....	5
1.3.1 Animal open-skull neurotrauma experimental models.....	5
1.3.1.1 Controlled cortical impact (CCI).....	5
1.3.1.2 Fluid percussion (FP) injury model.....	6
1.3.2 Finite element (FE) model.....	7
1.4 Brain biomechanics of vasculature.....	8
1.5 Objective.....	9
1.6 Thesis structure.....	10

Chapter 2.....	11
2 Quantifying the effect of repeated impacts and lateral tip movements on brain responses during controlled cortical impact.....	11
2.1 Introduction.....	11
2.2 Method.....	13
2.2.1 Investigation of the effect of repeated impacts and lateral movements....	13
2.2.2 FE simulation of electromagnetically driven CCI.....	15
2.2.3 High-speed imaging of pneumatically driven CCI.....	16
2.2.4 FE simulation of pneumatically driven CCI.....	17
2.2.5 FE mouse brain material property.....	17
2.3 Results.....	18
2.3.1 Electromagnetically driven CCI.....	18
2.3.2 Pneumatically driven CCI.....	24
2.4 Discussion.....	26
2.5 Conclusions.....	29
Chapter 3.....	31
3 The effect of 3D vasculature on brain response under the focal brain injury	31
3.1 Introduction.....	31
3.2 Method.....	34
3.2.1 Vasculature model development.....	34
3.2.2 Material property	38
3.2.2.1 FE mouse brain material property	38
3.2.2.2 Vasculature material property	38
3.2.3 FE simulation of focal injury	39
3.3 Results.....	40
3.3.1 Brain strain contour.....	40

3.3.2	Cumulative strain damage measure (CSDM)	41
3.3.3	Maximum principal strain (MPS)	43
3.4	Discussion	45
3.5	Conclusion	47
Chapter 4	48
4	Investigating the mechanisms and thresholds of brain microvascular damage combining finite element modeling and experiments of CCI	48
4.1	Introduction.....	48
4.2	Methods.....	50
4.2.1	CCI Experiments.....	50
4.2.2	Vessel density map and ASL MRI data	50
4.2.3	FE Simulation	51
4.3	Results.....	52
4.3.1	Brain strain contour.....	52
4.3.2	The correlation between the vessel length density and MPS.....	53
4.3.3	Thresholds of the brain microvascular damage	56
4.4	Discussion.....	57
4.5	Conclusion	58
Chapter 5	59
5	Conclusion and future work.....	59
5.1	Conclusion	59
5.1.1	Using CCI while understanding its tip movement.....	59
5.1.2	Vasculature and microvasculature in CCI	59
5.2	Contribution	60
5.3	Limitations	61
5.4	Future study	62

5.4.1	Develop an FE brain model with detailed 3D nonlinear, visco-elastic and anisotropic vasculature.....	62
5.4.2	Simulate the parcellated fiber axon clusters and blood flow	63
5.4.3	Diffuse injury	63
5.4.4	Validation.....	64
5.5	Significance and novelty.....	64
	Bibliography	67
	Appendices.....	78
	Curriculum Vitae	86

List of Tables

Table 2.1 FE model-predicted contusion volume for five CCI devices (a, b, c, d, and e). CCI: controlled cortical impact.	23
Table 2.2 The maximum lateral tip movements of five devices with and without considering the contact between impact tip and brain tissue and the corresponding MPS. MPS: maximum principal strain.	28
Table 3.1 Nomenclatures of the seven vasculature brain models. Whole-L: whole linear elastic vasculature model, Whole-NL: whole nonlinear elastic vasculature model, Major-L: major linear elastic vasculature model, Major-NL: major nonlinear elastic vasculature model, Small-L: small linear elastic vasculature model, Small-NL: small nonlinear elastic vasculature model, NV: non-vasculature model.	34

List of Figures

Figure 1.1 Mouse brain vasculature. Top left is the sagittal view. Top right is the dorsal view and the bottom is the ventral view [14].	3
Figure 1.2 The curve fitting of the constitutive model proposed by Fung (1981) for arteries (black line) and veins (gray line) compared with the stress-strain relations experimentally determined those by Monson (2001) [25].	5
Figure 1.3 Illustration of the controlled cortical impact model [34].	6
Figure 1.4 Illustration of fluid percussion injury model [34].	7
Figure 1.5 The developed finite element rat brain model [2].	8
Figure 2.1 Time-position profiles in electromagnetically and pneumatically driven CCI devices. (a) Example of the trajectory of an electromagnetically driven CCI tip (device a), digitized from Kim et al., 2018 [30]. (b) The videography of the x and y plane movements of the tip from the in-house pneumatically driven CCI device. CCI: controlled cortical impact.	17
Figure 2.2 Comparison of the maximum principal strain contours of the brain for three models for an electromagnetically driven CCI device. Distribution of strain predicted by (a) LC1, ideal impact along the impact axis; (b) LC2, with repeated impacts; and (c) LC3, with both repeated impacts and lateral movements. LC: loading condition.	19
Figure 2.3 (a) Three brain regions (the cerebral cortex, corpus callosum, and hippocampus) were investigated for the strain response. (b) Comparison of maximum principal strain for three regions in LC1, LC2 and LC3 over the entire brain for an electromagnetic driven CCI device. LC: loading condition. CCI: controlled cortical impact.	20
Figure 2.4 (a) Comparison of the histories of averaged maximum principal strain in LC1, LC2 and LC3 for an electromagnetic driven CCI device. (b) The time histories of average maximum principal strain predicted by the finite element model for five CCI devices (a, b, c,	

d, and e) for an electromagnetic driven CCI device. LC: loading condition. CCI: controlled cortical impact.....	21
Figure 2.5 Comparison of maximum principal strain for five cortical regions in the cortex for an electromagnetically driven CCI device. CCI: controlled cortical impact.	22
Figure 2.6 The effect of lateral tip movement on the contusion volume in CCI for an electromagnetically driven CCI device. CCI: controlled cortical impact.	23
Figure 2.7 Comparison of the maximum principal strain contours across LC1, LC2, and LC3. For LC2 and LC3, both the initial and later 5-ms time windows were simulated as high-speed videos demonstrated that there were larger lateral tip movements at the later stage. According, brain areas with high strains were largest for the later 5-ms time window at LC3. LC: loading condition. CCI: controlled cortical impact.	24
Figure 2.8 Comparison of maximum principal strain for three regions in LC1, LC2, and LC3. LC3 at the later 5-ms time window produced highest strains. LC: loading condition.	25
Figure 3.1 The top and side view of the geometry of the major arteries (dark red) and veins (blue).	36
Figure 3.2 The process of developing 3D mouse brain models with different vasculature under CCI. CCI: controlled cortical impact.....	37
Figure 3.3 Comparison of the maximum principal strain contours of the brain for linear vasculature models in CCI. L: linear; NL: nonlinear. CCI: controlled cortical impact.....	41
Figure 3.4 Four regions of brain selected for comparing strain of vasculature models in CCI. CCI: controlled cortical impact.....	42
Figure 3.5 CSDM (0.1) of four selected brain regions in linear and nonlinear vasculature models in CCI. L: linear; NL: nonlinear. CCI: controlled cortical impact.	43
Figure 3.6 Comparison of predicted maximum principal strain in these four regions and the global brain in CCI for linear and nonlinear vasculature. L: linear; NL: nonlinear. CCI: controlled cortical impact.	44

Figure 3.7 Vasculature strain in CCI. CCI: controlled cortical impact.	47
Figure 4.1 Microvasculature images with STPT from a healthy mouse. Maximum Intensity Projection (MIP) though 100 μm of tissue. Scale bar = 1mm. STPT: Serial Two-Photon Tomography [114].	49
Figure 4.2 Vessel density map of all cases. The green ASL MRI boxes represents a different vessel length density. The white dot shows the impact center. ASL: Arterial spin Labeling, MRI: magnetic resonance imaging.	51
Figure 4.3 Mouse brain CCI model with vasculature a. Brain CCI model b. CCI simulation with vasculature. CCI: controlled cortical impact.	52
Figure 4.4 Maximum principal strain contours of the brain for all cases.	53
Figure 4.5 The correlation between vessel length density and maximum principal strain for nine cases together.	54
Figure 4.6 The correlation between vessel length density and maximum principal strain for nine separated cases.	55
Figure 4.7 Logistic regression curves of nine cases together (800 mm/mm^3 threshold, 600 mm/mm^3 threshold, 400 mm/mm^3 threshold, and 200 mm/mm^3 threshold).	56
Figure 4.8 Logistic regression curves of case 4 (800 mm/mm^3 threshold, 600 mm/mm^3 threshold, 400 mm/mm^3 threshold, and 200 mm/mm^3 threshold).	57
Figure 5.1 Brain strain and motion. Strain contours predicted by: (a) Without-vasculature model; (b) With-vasculature model.	64

List of Appendices

Appendix A	Mouse ID and related slice labeled with the injury center.....	78
Appendix B	Vessel density map of seven sham mice.....	79
Appendix C	Logistic regression curves of nine separated cases (800 mm/mm ³ threshold, 600 mm/mm ³ threshold, 400 mm/mm ³ threshold, 300 mm/mm ³ and 200 mm/mm ³).....	80

Acronyms

ACA: Anterior cerebral arteries

ASL: Arterial spin labeling

BBB: Blood brain barrier

CBF: Cerebral blood flow

CCI: Controlled cortical impact

CHIMERA: Closed-head impact model of engineered rotational acceleration

CSDM: Cumulative strain damage measure

CSF: Cerebrospinal fluid

FP: Fluid percussion

ICA: Internal carotid arteries

ICP: Intracranial pressure

MCA: Middle cerebral arteries

MPS: Maximum principal strain

MRI: Magnetic resonance imaging

SCA: Superior cerebellar arteries

STPT: Serial Two-Photon Tomography

TBI: Traumatic brain injury

Chapter 1

1 Introduction

1.1 Traumatic brain injury (TBI)

Traumatic brain injury (TBI) is the main cause of death and severe disability worldwide with millions of people in different age groups, most of which suffered from TBI are young adults caused by vehicle accidents and the older people by falling. In the USA, the incidence of TBI has been reported at around 1.6 million, with the 52,000 deaths and 80,000 severe neurological disabilities annually [1]. For every mortality, more survivors suffered mild to moderate brain injury than severe injury, with short-term and long-term consequences of TBI, including the cognitive deficits and behavioral abnormalities. Although TBI is a big and severe medical problem with the enormous financial burden, the brain injury mechanism of TBI has not been fully understood.

1.2 The mouse head anatomy and vasculature

Human volunteers could provide some valuable data in the understanding of live brain but the responses of live human brain under injurious impact conditions are still rare, due to ethical and practical concerns. Thus, animal brain injury experimental data, especially mouse data, which were obtained under well-defined experiments, could greatly help to understand the mechanisms of TBI [2]. Also, animals like mice can be used to investigate various behaviors and assess the brain structure and pathways which are like those in human TBI [3-7]. Many mouse TBI models such as controlled cortical impact (CCI), and fluid percussion (FP) have successfully reproduced axonal injuries, vasculature damage and blood brain barrier (BBB) damage [8]. Furthermore, the advantage of using the mouse model under brain-injury experiment is small size, low cost, and availability of acquiring standard data [8].

1.2.1 Mouse head anatomy

The mouse head includes the hardest material (the skull) and the softest material (the brain). Unlike heart and muscles which can deform without damage under load condition, the

brain could not deform much under the same loading. The brain consists of many complicated anatomical components. The main components are cerebral cortex, hippocampus, thalamus, and brainstem. The cortex controls memory [9]. The cerebrum affects the speak, visual and spatial abilities [10]. The brainstem contains midbrain, pons, and medulla. The hippocampus, which is under the cortex, is important to the learning and memory abilities [10]. The thalamus is essential to cognitive processing [11]. The soft brain tissue includes gray and white matter. Gray matter includes neuron cells, glial cells, capillaries, neuropil, and neuron dendrites. White matter is composed of myelinated axons and named due to the color of myelin.

1.2.2 The vasculature morphology

The brain vasculature has a layered membrane structure to cover the entire brain. Brain tissue outside the arachnoid membrane is supplied with blood by the external carotid artery. The tissue from the inside arachnoid is perfused by the internal carotid and vertebral arteries, which flow through the bottom of the skull through a structure called the circle of Willis. There are four main arteries and branches to create a network of small arteries and capillaries over the brain lobes, some along the sulci, while others cross over them [12, 13]. The mouse brain vasculature is shown in Figure 1.1 [14]. Some of the major arteries and veins are identified in the image. Specifically, the arteries forming the circle of Willis can be seen at the bottom image. The arteries include internal carotid arteries (ICA), middle cerebral arteries (MCA), anterior cerebral arteries (ACA), olfactory artery, superior cerebellar arteries (SCA), basilar artery, and vertebral arteries. The veins depicted include transverse sinus and superior sagittal sinus. Large blood vessels in the subarachnoid space divided into small arteries downward into the cortex to join the cortical capillary plexus [15]. The gray matter contains more vascular than white matter [13, 16]. The cortical veins are formed by cortical capillaries draining into veins or venules in subarachnoid, returning though The Great Vein of Galen [17]. Veins form bridging veins from subarachnoid space to dural venous sinus. Bridging veins connect the cerebral veins to the superior sagittal sinus, including 11 pairs in the superior sagittal space.

For the blood vessel in deep circulation, the arteries supply blood to the brain and venules drain the venous blood into the sinus. The arteries supply nutrients and oxygen to brain tissue and the veins take the bio-waste from the brain [18].

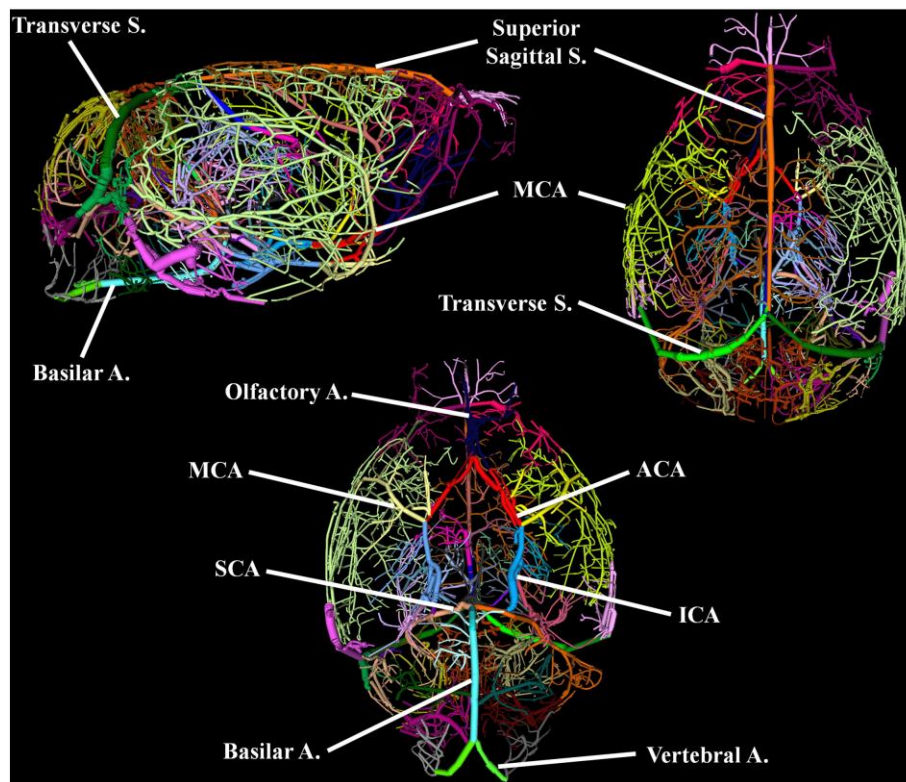


Figure 1.1 Mouse brain vasculature. Top left is the sagittal view. Top right is the dorsal view and the bottom is the ventral view [14].

1.2.3 Material property of vasculature

The investigation of the mechanical property of blood vessels has lasted more than one hundred years. Until now, blood vessels have been proved to be nonlinear, concave-upward, almost incompressible with stress-strain property based on the assumption of cylindrical orthotropy [19, 20]. However, there is a big limitation that many investigations were focused on the arteries because the relatively smaller size of veins provides much difficulty in experiments [21, 22]. To represent a nonlinear property of blood vessel, various material models and investigations have been proposed in the literature.

The Fung model (1981) was written with the Lagrangian stress T , uniaxial Green Lagrange strain E and uniaxial stretch ratio λ (Eqn. 1). The material constants of arteries and veins α and C are obtained from Levenberg-Marquardt (The MathWorks Inc., 1994). The experimental stress-strain curves are found [23].

$$T = \alpha EC \lambda \exp(\alpha E^2) \quad (1)$$

This Fung model had a limitation. For the small strain, the model gave a similar response in compression and tension. However, for large strain, the stress-strain relations gave a stronger response in tension than in compression, which could be explained by neglecting the compressive stiffness of collagen fibers. But no experiment investigation was found in the compressive and bulking response of vasculature.

According to Monson (2001), quasi-static and dynamic tensile tests to create experimental stress-strain curves and the cerebral blood vessel property were conducted [24]. A typical stress-strain curve is shown in Figure 1.2 [25]. In this study, the typical concave-upward stress-strain curves were found in both arteries and veins. The strain rate of arteries and veins have remarkable different between quasi-static and dynamic test. The ultimate stress and strain of arteries and vein in quasi-static were somewhat lower than those in the dynamic test. The results demonstrated that longitudinally strain rate was quite important in the material model of the vasculature, especially for veins. Also, post-mortem could affect the vessel stiffness because the arteries resected from the autopsy were stiffer than those from surgery. Similar results were concluded from the previous investigations on large arteries [26, 27]. They proved that cranial arteries were much stiffer than veins and extracranial vessels. The strain rate of human bridging veins was studied by Lee and Haut, concluding there was no rate dependence for the ultimate strain and stress. However, their results were obviously different with data of vein by Monson et al. (2000), proving that different structure of cranial veins didn't have a similar strain rate [24]. A continuous investigation by Monson (2005) stated that the sources and sizes of vessel affected vessel stiffness, which should be careful in defining the material property of vasculature.

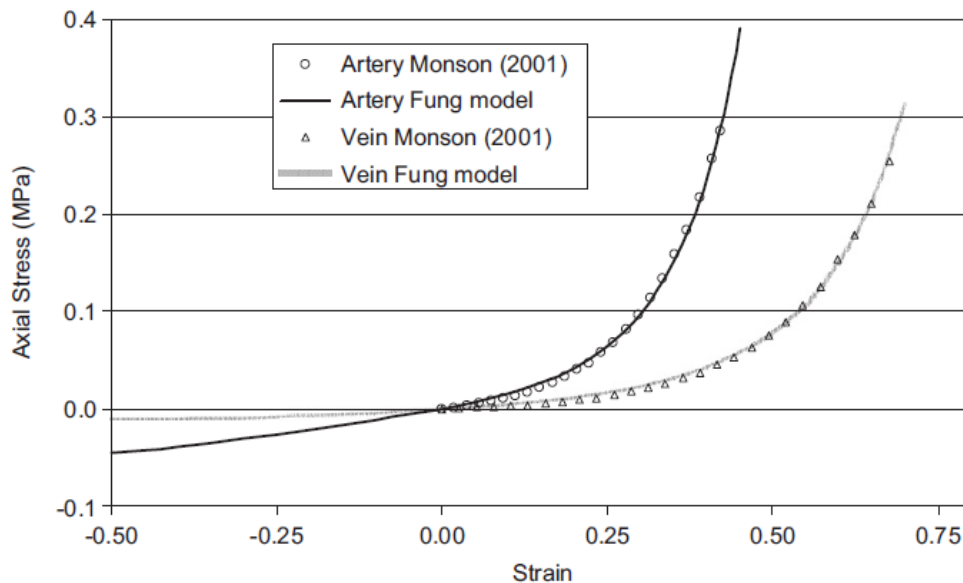


Figure 1.2 The curve fitting of the constitutive model proposed by Fung (1981) for arteries (black line) and veins (gray line) compared with the stress-strain relations experimentally determined those by Monson (2001) [25].

1.3 Biomechanical methods to study TBI

To better understand TBI, various animal neurotrauma experimental models such as CCI [28-31] and FP [32-34], and finite element (FE) models have been developed to explore the tissue-level responses of the brain due to impacts.

1.3.1 Animal open-skull neurotrauma experimental models

1.3.1.1 Controlled cortical impact (CCI)

CCI is an open-skull focal injury model that induces a cortical contusion. One of the main advantages of CCI model is that impact parameters, such as depth, velocity, duration, and craniotomy, can be well controlled. In general, CCI is considered as a single, well-controlled event driven by an electromagnetic or pneumatic actuator. The illustration of the controlled cortical impact model is shown in Figure 1.3.

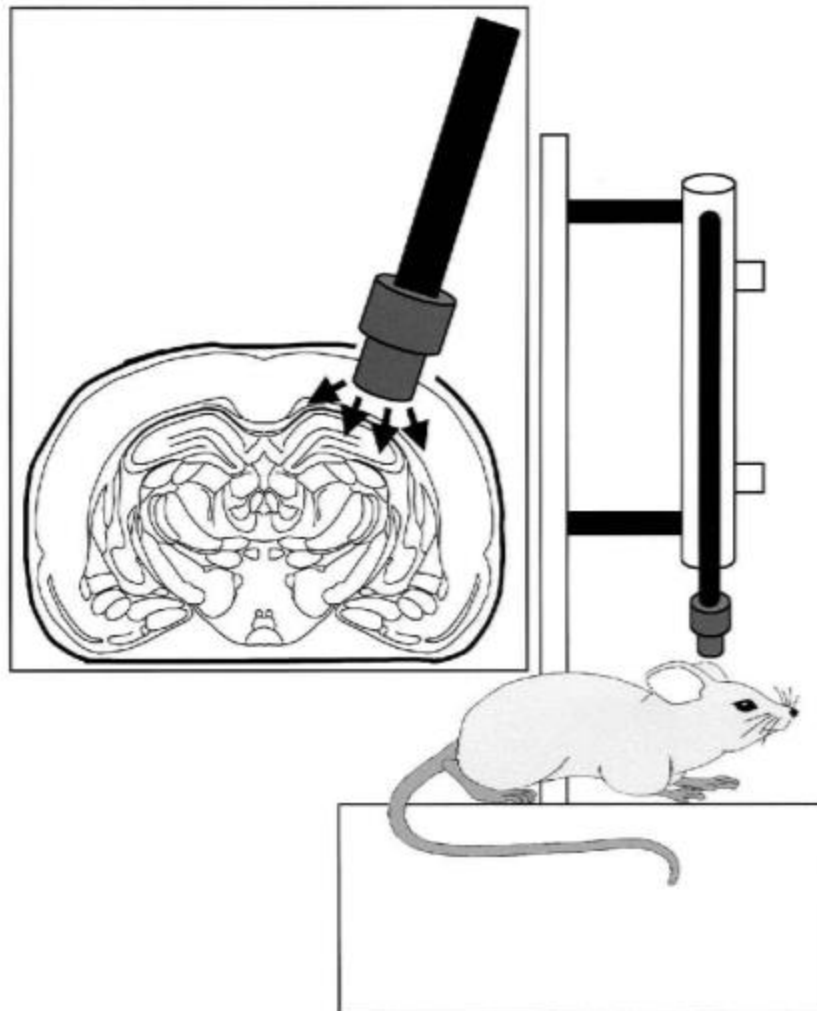


Figure 1.3 Illustration of the controlled cortical impact model [34].

1.3.1.2 Fluid percussion (FP) injury model

The FP injury model is the most commonly used mouse TBI brain model to induce a focal-diffuse brain injury like those in human closed-head TBI [32-34]. An anesthetized animal undergoes a craniotomy to show the intact dura matter of the brain. There was a hollow female luer lock sealed over the craniotomy, by which the animal was connected to fluid percussion. The adjustable hammer pendulum of the fluid percussion device released and stroked the piston located at the end of a fluid-filled horizontal cylinder.

Then a fluid pulse was produced and transmitted from the opposite end of the cylinder onto the brain [35]. The illustration of FP injury is shown in Figure 1.4.

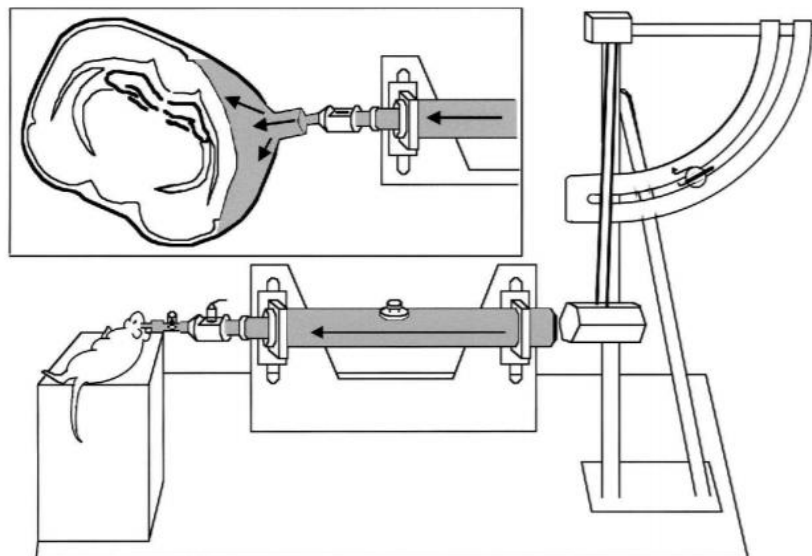


Figure 1.4 Illustration of fluid percussion injury model [34].

1.3.2 Finite element (FE) model

Brain injury data in the experimental models can be measured and used to investigate the mechanisms of TBI [36, 37]. Meanwhile, it is almost impossible to directly observe intracranial stress/strain responses *in vivo*. Therefore, FE models have been used to study brain mechanical responses and injury mechanisms. Also, FE model could predict mechanics-related head injury. These injuries include acute damages such as brain laceration and acute vessel breakage. Furthermore, FE model could help to understand the mechanical changes after the TBI, when brain neuronal damages such as axonal damage, dendrite activation, and cell damage, usually happen. However, these complicated biological process remains unknown. Thus, the high-quality FE head model provides the opportunity to see the mechanical world of the brain and predict brain damage.

In the study by Mao et al. [37], a detailed 3D FE rat brain model was used to investigate the intracranial brain mechanical response where the high occurrence of neuronal loss

was observed around the cortical regions (Figure 1.5). This developed rat brain model was further improved by incorporating some features such as a layer of cerebrospinal fluid (CSF), vasculature and others for the simulation of FP, CCI, and Closed-head Impact Mode of Engineered Rotational Acceleration (CHIMERA).

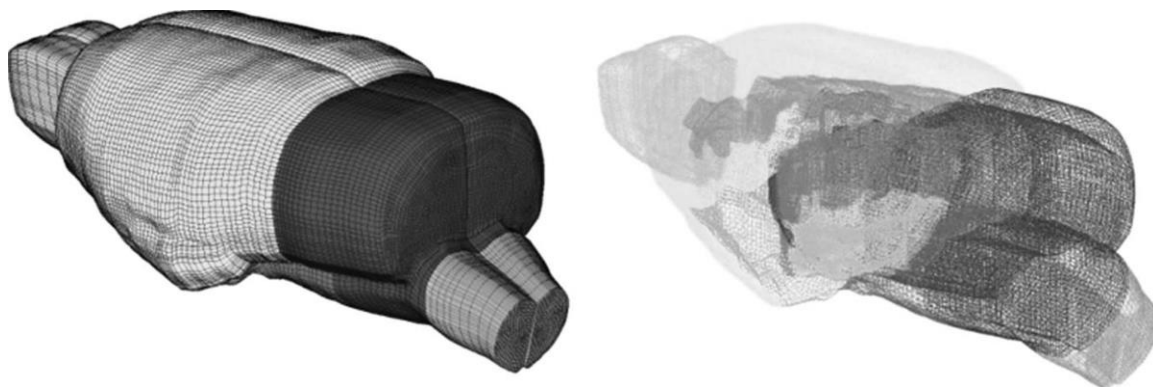


Figure 1.5 The developed finite element rat brain model [2].

1.4 Brain biomechanics of vasculature

The roles of the vasculature in the dynamic response of the brain were studied by several teams. However, confounding observations on the effect of the vessel have been reported and are summarized as follows. In a study by Ho et al. [25], three 3D FE models (without vessels, with linear-elastic vessels and with non-linear elastic vessels) were developed to study the dynamic responses of the brain under the rotational and translational acceleration impulses. Small reductions in the peak average strain were found in the models with vessels compared to the non-vessel model, with 2% reduction for non-linear elastic vasculature model and 5% for linear elastic vasculature model. This result illustrated that there was a small effect of the structural vasculature on brain response. However, other studies showed that the influences of the vasculature were remarkable. In the study by Zhang et al. [38], two 2D FE human head models were developed. Model 1 includes the skull, dura mater, cerebrospinal fluid (CSF), tentorium, brain tissue, and the parasagittal bridging veins. Based on Model 1, Model 2 further included main branches of cerebral arteries. Maximum principal strain (MPS) shear strain (SS) and intracranial pressure (ICP) were studied under two load conditions with linear and rotational accelerations. The overall reduction in MPS was around 37% compared Model 2 to

Model 1. SS in Model 2 was lower than those in Model 1 with the range from 7.4% to 36%. On the other hand, a similar study was done by Omori et al. [39] and their results were different from Zhang et al. Higher shear stress and SS were occurred in Model 2 including bridging vein and a major branch of an anterior cerebral artery because of tethering effect of the vasculature.

Under extremely high-rate blast loading conditions, in the study of the effect of blood vessel networks on dynamic responses of the brain by Hua et al. [40], using an FE human brain head model without vessel networks and an FE human brain model with statistically distributed 1D vessel elements. They found that the with-vessel model could predict higher strains in the brain, especially in the region with high vessel density (corpus callosum and brainstem). In the periphery region (cortex), there was a minimal difference in brain response between with and without vessel network models.

Unnikrishnan et al. [41], studied the effect of the 3D network of brain vasculature using rat brain FE model under blast overpressure. They found that including vasculature into rat FE model largely reduced the peak strain in cerebrum, cerebellum, and brainstem. Greatly strain reduction was found when using the human-brain properties in the FE simulation. They suggested that incorporating the vasculature into rat brain had a remarkable influence on brain strain under blast loading.

1.5 Objective

To better understand brain injury mechanism of open-skull, high-rate CCI, as well as the effect of brain vasculature, a previously validated FE mouse brain model was improved to incorporate vasculature modeling. The objectives of the research were to: 1) evaluate how the repeated impacts and lateral movements of CCI, which were observed in recent experimental measurements but have long been neglected and not reported, affect internal brain stresses/strains -- which are the direct cause of neuronal damage and affect the accuracy and reproducibility of CCI; 2) investigate how the detailed vasculature affect brain tissue responses on focal injuries; and 3) evaluate the intracranial mechanical responses within cortical brain regions where the remarkable 3D cerebral microvascular length density changes during CCI.

1.6 Thesis structure

Chapter 2 describes the effect of repeated impacts and lateral tip movements on brain responses in CCI by improving a previously validated FE mouse brain model.

Chapter 3 describes how the detailed vasculature affected brain tissue responses in open-skull focal injuries. A new FE mouse brain model with a detailed 3D, non-linear vasculature was developed. The contribution of the vasculature on brain strains in CCI was quantified by comparing brain models with and without vasculature.

Chapter 4 describes the intracranial mechanical responses within cortical brain regions where the remarkable 3D cerebral microvascular length density changes in CCI was found. The FE model-predicted intracranial strains were compared with the observed in vivo vessel length density. The correlation between the vessel length density and the predicted MPS of the microvascular in CCI was investigated.

Chapter 5 concludes the main findings of this study, lists the limitations and introduces the future study. The importance of the current study is also discussed.

Chapter 2

2 Quantifying the effect of repeated impacts and lateral tip movements on brain responses during controlled cortical impact

The effect of repeated impacts and lateral movements on brain responses during controlled cortical impact (CCI) was investigated using a previously validated, highly detailed three-dimensional (3D) finite element (FE) mouse brain model.

2.1 Introduction

Traumatic brain injury (TBI) is the main cause of death and severe disability worldwide affecting millions of people in different age groups. Generally, TBI happens when external forces such as those from sports-related head impacts, blast waves, vehicle accidents, and falls produce responses to the brain that exceeds its tolerance. Although TBI is identified as a severe medical problem, the injury mechanisms of TBI have not been fully understood. Partially due to this, effective treatments of TBI are still lacking. Continued investigations are needed using experimental TBI pre-clinical models.

Animal TBI models are widely used to study the pathogenetic, behavioral and histopathologic changes of TBI in a controlled and efficient manner. Many types of neurotrauma experiments have been developed in past decades, including CCI [28-31], weight-drop models [42-44], fluid percussion (FP) [32-34], blast injury models [45, 46] and closed-head impact model such as closed-head impact model of engineered rotational acceleration (CHIMERA) [36]. Each of these models simulates the certain histopathological and functional outcomes of clinical TBI. Among them CCI is a focal injury model that induces a cortical contusion. The proper model should be carefully chosen by researchers to represent human responses of TBI [47].

One of the main advantages of the CCI model is that impact parameters, such as depth, velocity, duration, and craniotomy, can be well controlled. In general, CCI is considered as a single, well-controlled event driven by an electromagnetic or pneumatic actuator. Since its adaption to rodents [48], CCI has been widely used among labs on various species including swine and primates [49]. Recently, due to greater portability (without a gas tank), the electromagnetic CCI devices have become commercially available [50-52]. However, a recent study using high-speed videography to evaluate five electromagnetic CCI devices brought about an awareness of repeated impacts and lateral tip movements during the supposedly single, axial CCI impact [30]. These repeated impacts and lateral tip movements might affect the accuracy and reproducibility of CCI as the complex tip movements would produce a greater degree CCI injury than a larger-diameter tip did [30]. Furthermore, repeated impacts of the tip were observed in both electromagnetic and pneumatic CCI devices [50].

Generally, the brain tissue response of CCI can be studied by physical, experimental and finite element (FE) models. Due to the difficulty of directly observe intracranial deformations, particularly in vivo, FE models work as efficient and reliable tools to investigate detailed brain tissue stretches/strains. These brain tissue responses are directly linked to neuronal/vascular/axonal damage and cell death [37, 53, 54]. In the study by Mao et al. [37], a detailed 3D FE rat brain model was used to investigate the intracranial mechanical brain response where the high occurrence of neuronal loss was observed around the cortical regions. In addition, delayed cell death was also studied and found to be related to initial mechanical stretches [55] using a brain tissue slice culture model.

Hence, using an FE model to understand brain tissue responses helps further reveal the mechanisms of TBI.

Here we used an established FE mouse brain model [55, 56] to investigate how the repeated impacts and lateral tip movements affected brain responses. Based on the previous studies on the electromagnetically driven CCI devices [30], our hypothesis is that the lateral movements of CCI impactor tip could affect brain stress/strain predictions while the effect of repeated impacts remains unknown. Also, we used a high-speed camera to record tip movements of a pneumatically driven CCI device. We simulated three loading conditions using the FE mouse brain model. Three brain regions including the cortex, corpus callosum and hippocampus were selected to compare model predicted maximum principal strain (MPS). Then the influence of concerned repeated impacts and the lateral tip movements were quantified.

2.2 Method

2.2.1 Investigation of the effect of repeated impacts and lateral movements

The effect of repeated impacts and lateral movements on brain strain responses was evaluated by comparing the results from three Loading conditions simulated using the FE mouse brain model: Loading condition 1 with an ideal CCI impact along the impact axis, Loading condition 2 with repeated impacts, and Loading condition 3 with both repeated impacts and lateral movements.

The FE mesh: The previously developed rat and mouse brain finite element models [55, 56] contained most of the anatomically essential features of the rodent brain, including the skull, dura matter, pia matter, hippocampus, corpus callosum, medulla oblongata, cerebral cortex, ventricle, internal capsule, cerebellum, spinal cord, optic tract, olfactory, pons, thalamus, and hypothalamus with a total of 255,700 hexahedral and 258 thousand solid elements. Element has a spatial resolution of 150 to 250 microns with an average of 200 microns approximately.

The FE boundary: The skull was assumed as rigid shell elements with the skull being held in still mimicking laboratory testing condition. The dura layer was directly connected to the nodes of the skull inner surface. For the interface between the brain and skull, there was a contact between PAC and dura using “CONTACT_AUTOMATIC_SURFACE_TO_SURFACE” in LS-DYNA (LSTC, Livermore, CA). A pia-arachnoid complex (PAC) including the pia and arachnoid membranes was modelled by a single layer of shell elements. The PAC was directly connected to the nodes of the brain outer surface.

The FE validation: The rat brain model was validated against the peak brain deformation data of CCI [56]. The mouse brain model was scaled based on the rat brain model. The correlations between experimentally observed injuries and input parameters, model responses and experimental injuries in CCI have been estimated [56]. Also, these FE models were well correlated through the linear relationship between the mechanical brain tissue strain and neural cell death [37]. The mouse brain model has been previously used to evaluate the effect of flat-shape and sphere-shaped impactor tips during CCI [55] and a CCI with reduced impact rate [57] demonstrating correlations between brain strain

predictions and histopathology observations. The same mouse brain model was used in this study.

2.2.2 FE simulation of electromagnetically driven CCI

For the electromagnetically driven CCI, we digitized the high-speed image data from the published trajectories of five devices (Impact One, Leica Biosystems, Concord, Ontario, Canada). Two kinds of stereotaxic devices were used: devices a, b, c with Stoelting stereotaxic device (Stoelting Co, Wood Dale, Illinois, USA) and devices d, e with a MyNeuroILab stereotaxic device (Leica Biosystems) [30].

The CCI simulations were conducted in LS-DYNA (Livermore Software Technology Corporation, Livermore, CA USA). By digitizing high-speed images of CCI device a and using reported experimental setups [30]. We simulated a 3 mm diameter flat tip impactor with 1 mm above the craniotomy. A 5 mm diameter craniotomy centered at 3.0 mm posterior to the bregma and 2.5 mm lateral to the midline was removed from the skull. We digitized the lateral movement curves from 5 devices (a, b, c, d, and e) along with the same vertical movement curve of the device a.

According to Saatman et al. [58], the impact depths of CCI in mouse were 0.5 mm and 1 mm. Also, the increased impact depths of 1 mm, 1.5mm and 2mm were used by Schwetye et al. [59]. In general, it was observed that 1 mm impact depth was frequently used [60, 61], and was referred in this study. For Loading condition 1, the impact speed was 5 m/s and the impact depth was controlled at 1 mm. For Loading conditions 2 and 3, the time-vertical position and time-horizontal position curves of CCI device tip movement were digitized from the experimentally measured CCI impactor tip trajectory

as shown in Figure 2.1a (device a). The vertical movement curve was adapted to the maximum impact depth of 1 mm [30].

The displacement-time curves of the CCI device tip were adopted in Loading condition 2 with repeated impacts using *BOUNDARY_PRESCRIBED_MOTION_RIGID_LOCAL available in LS-DYNA to control the CCI tip movements. CCI injuries of three loading conditions were simulated for 5 ms that includes the largest two repeated impacts and the largest lateral movements. Our test simulations demonstrated the highest MPS of the brain happened in 5 ms. Simulation results were plotted at every 0.1 ms. We investigated brain biomechanical responses for three models and quantified the effect of lateral movement and second impact at the tissue level using MPS.

2.2.3 High-speed imaging of pneumatically driven CCI

A pneumatically driven CCI device (TBI-0310 Impactor, Precision Systems, and Instrumentation, Fairfax Station, Virginia, United States) with a 2 Axis manual stereotaxic frame position controller was used, which was purchased in 2014. Tracker video analysis software (National Science Foundation, Alexandria, Virginia, United States) was used to analyze images recorded by a high-speed camera (Fastcam SA6, Photron Limited, Tokyo, Japan) at 10,000 frame/second. During video recording, we placed the camera on a stable table that is separated from the CCI device to avoid vibrations included by the impact. Poron cushioning material (2 cm thick, Rogers Corporation, Beijing, China) was used as the target. The marker was located in the center of the length of a 10-mm long, 3-mm diameter impactor tip. Data such as time and the impactor tip's position were calculated by the software. The impact velocity and depth were set as 5 m/s and 1mm, with a dwell duration of 500 ms.

2.2.4 FE simulation of pneumatically driven CCI

The same FE mouse brain model and three CCI loading conditions were used for investigating the pneumatic CCI device. For Loading condition 1, an ideal axial CCI impact was simulated. For Loading conditions 2 and 3, the time-vertical position and time-horizontal position curves of CCI device tip movements were harvested from the experimentally measured CCI impactor tip trajectory as shown in Figure 2.1b.

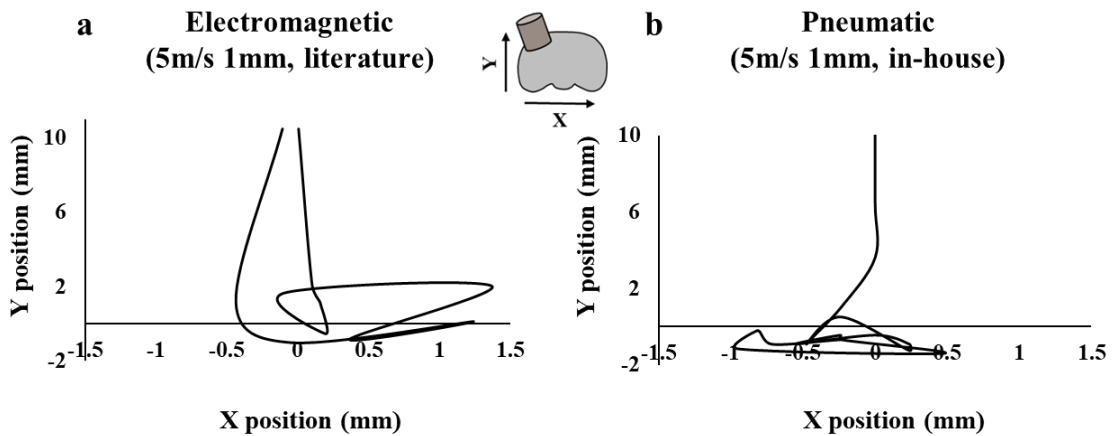


Figure 2.1 Time-position profiles in electromagnetically and pneumatically driven CCI devices. (a) Example of the trajectory of an electromagnetically driven CCI tip (device a), digitized from Kim et al., 2018 [30]. (b) The videography of the x and y plane movements of the tip from the in-house pneumatically driven CCI device. CCI: controlled cortical impact.

2.2.5 FE mouse brain material property

The linearly viscoelastic material law has been used in modeling the brain tissue simplifying the simulation. Eqn. 2 was used to calculate the shear modulus of a linearly viscoelastic material $G(t)$

$$G(t) = G_{\infty} + (G_0 - G_{\infty}) e^{-\beta t} \quad (2)$$

Where G_0 and G_∞ are the short-term and long-term shear moduli, respectively. The decay constant and the duration are given by β and t , respectively. A previously developed FE mouse model was used. More detailed material properties can be referred to in previous publications [55, 56].

2.3 Results

2.3.1 Electromagnetically driven CCI

The MPS contours at the time of maximum impact depth were illustrated in Figure 2.2. Similar strain contours were observed in both Loading condition 1 and Loading condition 2. The high MPS spread from the cortical layer into the deep brain in an ellipsoidal mode. Most of the high MPS regions of Loading condition 1 and Loading condition 2 were in the region directly under the impactor site (Figure 2.2a & b). Compared with Loading conditions 1 and 2, larger areas of MPSs were found in Loading condition 3. Also, some brain tissues were squeezed between the impactor and the edge of the craniotomy in Loading condition 3 (Figure 2.2c). These results show that the lateral tip movements not only affect the spatial distribution of the MPS responses, but also increase local brain tissue deformations while the repeated impact has minimal influence.

Brain strain
(Electromagnetic 5m/s 1mm, literature device a)

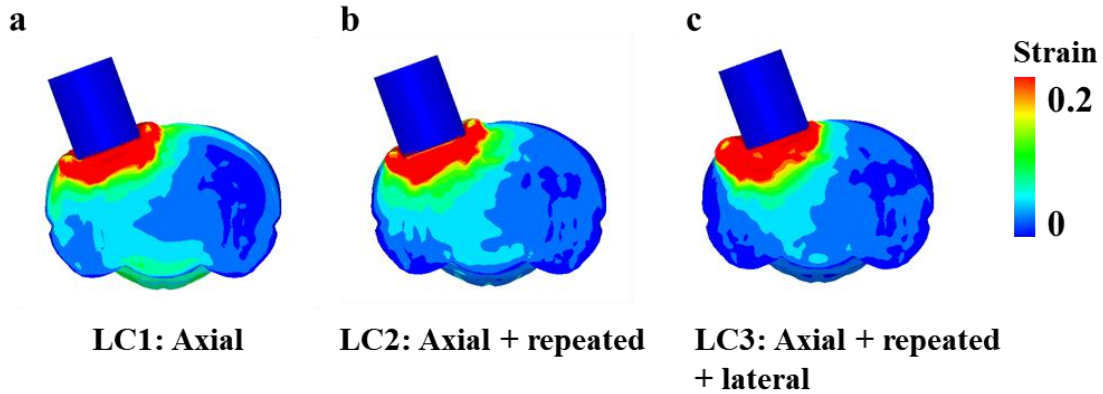


Figure 2.2 Comparison of the maximum principal strain contours of the brain for three models for an electromagnetically driven CCI device. Distribution of strain predicted by (a) LC1, ideal impact along the impact axis; (b) LC2, with repeated impacts; and (c) LC3, with both repeated impacts and lateral movements. LC: loading condition.

Three locations underneath the CCI impact site were selected to study the local effect of repeated impact and lateral tip movement (Figure 2.3a). These regions represent the cerebral cortex, corpus callosum, and hippocampus. The strain value, by default, was the averaged value of four elements in the same location. The predicted MPS in those three regions were compared in Figure 2.3b. The predicted MPS in Loading condition 1 (0.22 ± 0.09) was slightly higher than that in Loading condition 2 (0.19 ± 0.08), probably because the 1st impact depth (0.78 mm) in Loading condition 2 was less than the impact depth (1 mm) in Loading condition 1 even if the second impact depth in Loading condition 2 also reached 1 mm. These results indicated that repeated impacts had minimal effect on the brain and the MPS was mainly determined with the first impact depth. As indicated in Figure 2.3b, the predicted MPS ranged from 0.15 to 0.32 for Loading condition 1, 0.13 to 0.28 for Loading condition 2, and 0.24 to 0.52 for Loading condition 3. The cortex region in Loading condition 3 has the highest MPS (0.52), followed by the corpus callosum (0.27), and the hippocampus (0.24). Comparing Loading condition 2 to Loading condition 3, the largest MPS increase was in the cortex region (84.3%) followed

by corpus callosum (74.5%) and hippocampus (78.3%) (Figure 2.3b). It's concluded that the larger effect of lateral tip movements on predicted MPS was in the regions closer to the impact site than the deep brain regions.

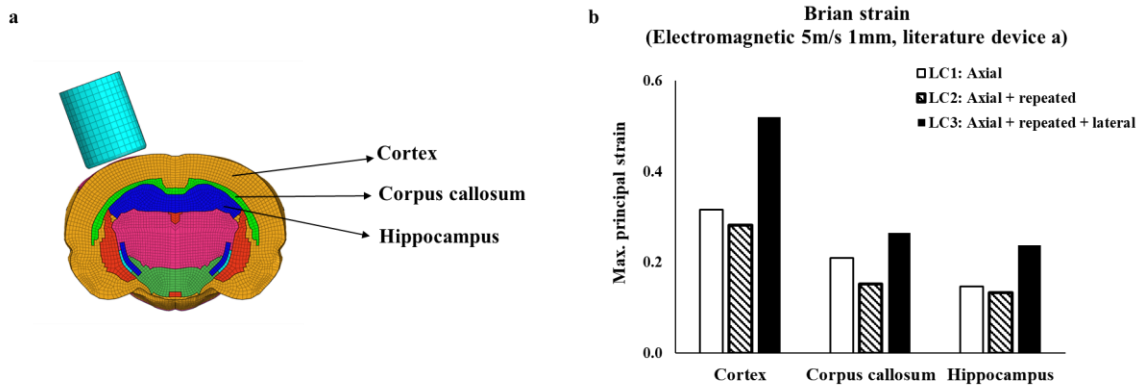


Figure 2.3 (a) Three brain regions (the cerebral cortex, corpus callosum, and hippocampus) were investigated for the strain response. (b) Comparison of maximum principal strain for three regions in LC1, LC2 and LC3 over the entire brain for an electromagnetic driven CCI device. LC: loading condition. CCI: controlled cortical impact.

Figure 2.4 depicts MPS histories in the brain. For Loading condition 2, the first impact induced slightly higher strains than the second impact did (Figure 2.4a) even though the first impact depth of 0.78 mm was smaller than the second impact depth of 1 mm. On the other hand, the highest MPS was observed in Loading condition 3 with three peaks (Figure 2.4a), illustrating that lateral movements had a large influence on model-predicted MPS. Figure 2.4b shows the time histories of average MPS for five CCI devices (a, b, c, d and e). Significantly higher MPS (0.36) was predicted in device a with the largest lateral movement. Similar time histories of MPS curves were found in device b, c, d, and e. Results suggested that the larger lateral tip movement in CCI would predict higher MPS responses.

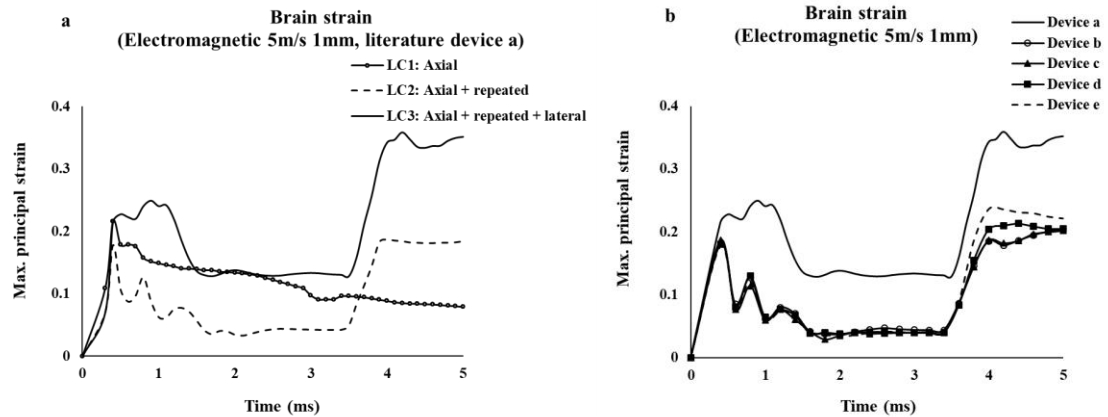


Figure 2.4 (a) Comparison of the histories of averaged maximum principal strain in LC1, LC2 and LC3 for an electromagnetic driven CCI device. (b) The time histories of average maximum principal strain predicted by the finite element model for five CCI devices (a, b, c, d, and e) for an electromagnetic driven CCI device. LC: loading condition. CCI: controlled cortical impact.

Five locations in the cortex were selected to further study the effect of the lateral movement on brain responses (Figure 2.5). According to Pleasant et al. [55], four elements were chosen for each location in the cortex: two in layer 4 and two in layer 5. Region C represented the center region under the impact tip. Region B and D were below the two sides of the impactor tip. Region A and E were outside of the impact site. The predicted MPS ranged from 0.14 to 0.45 in Loading condition 1, 0.11 to 0.44 in Loading condition 2, and 0.16 to 0.75 in Loading condition 3. Region D in Loading condition 3 had the highest MPS of 0.75 due to the large lateral movement. The predicted MPS of the cortex in Loading condition 1 (0.32 ± 0.14) was slightly higher than that in Loading condition 2 (0.27 ± 0.14), and the highest MPS was observed in Loading condition 3 (0.45 ± 0.25), indicating that repeated impacts had minimal effects on cortex strain, but lateral movements had large influence on cortex strain.

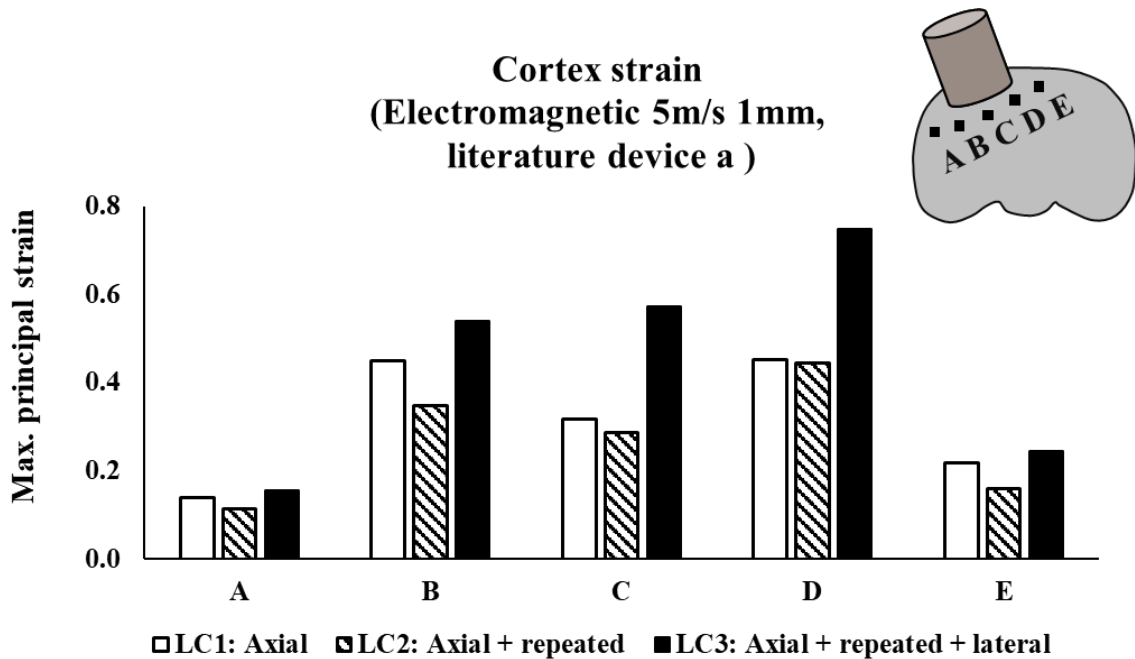


Figure 2.5 Comparison of maximum principal strain for five cortical regions in the cortex for an electromagnetically driven CCI device. CCI: controlled cortical impact.

The FE-predicted contusion volumes for five devices were listed in Table 2.1. For device a, the estimated contusion volumes using an MPS threshold of 0.3 were 17.86 mm³ in Loading condition 1, 17.25 mm³ in Loading condition 2, and 25.86 mm³ in Loading condition 3. These results indicated that the repeated impacts nearly didn't affect the contusion volumes because similar contusion volumes were found between Loading condition 1 and Loading condition 2. Comparing contusion volume between Loading condition 3 and Loading condition 2, lateral tip movement increased the contusion volume by about 50%. For all five electromagnetic CCI devices, the largest contusion volume was found in device a (25.86 mm³) with 1.38 mm lateral tip movement, followed by device e (20.28 mm³) with 0.4 mm movement, device b (18.58 mm³) with 0.34 mm movement, device c (18.28 mm³) with 0.19 mm movement, and device d (17.49 mm³) with 0.18 mm movement. There was a positive linear relationship between lateral tip movement and contusion volume in the CCI mouse FE model (Figure 2.6).

Table 2.1 FE model-predicted contusion volume for five CCI devices (a, b, c, d, and e). CCI: controlled cortical impact.

		Contusion Volume_0.3 (mm ³)
Device a	Loading condition 1	17.86
	Loading condition 2	17.25
	Loading condition 3	25.86
Device b	Loading condition 3	18.58
Device c	Loading condition 3	18.28
Device d	Loading condition 3	17.49
Device e	Loading condition 3	20.28

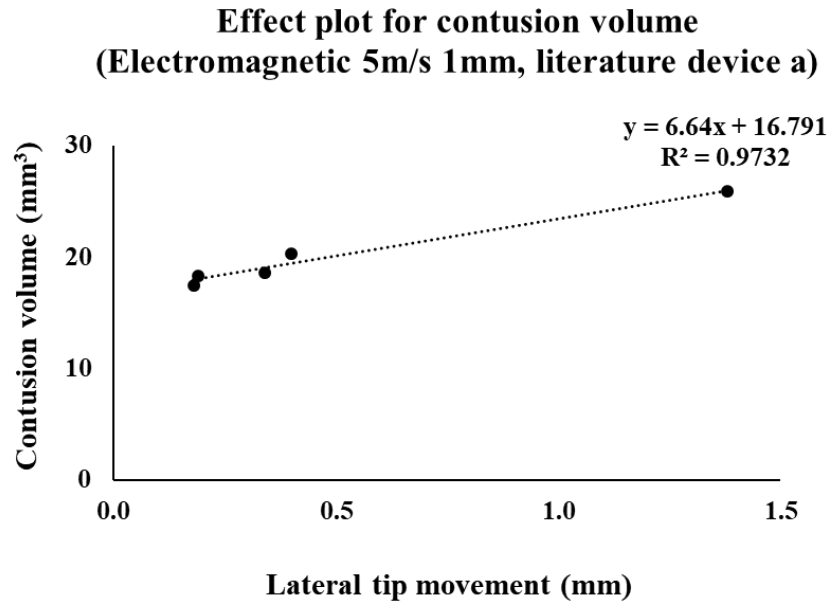


Figure 2.6 The effect of lateral tip movement on the contusion volume in CCI for an electromagnetically driven CCI device. CCI: controlled cortical impact.

The time histories curves of predicted average MPS in devices b, c, d and e were close at the initial 3.5 ms and demonstrated some variances (0.2 - 0.24) in the last 1.5 ms (Figure 2.4b). Similar to the MPS changes, the contusion volumes of these four devices demonstrated variances from 17.49 to 20.28 (Table 2.1).

2.3.2 Pneumatically driven CCI

The MPS contours of the brain were illustrated in Figure 2.7. Similar strain contours were observed in both Loading condition 1 and Loading condition 2. The high MPS spread from the cortical layer into the deep brain in an ellipsoidal mode. Compared with Loading condition 1 and Loading condition 2, larger areas of MPSs were found in Loading condition 3. Different from electronic CCI, pneumatic CCI demonstrated a tip movement of 0.95 mm at a later time and a tip movement of 0.48 mm initially, which were both smaller than 1.4 mm as measured from the electronic CCI device a. The results from the pneumatically driven CCI and electromagnetically driven CCI both demonstrated that the lateral tip movements not only affected the spatial distribution of the MPS responses, but also increased local brain tissue deformations while the repeated impacts had minimal influence.

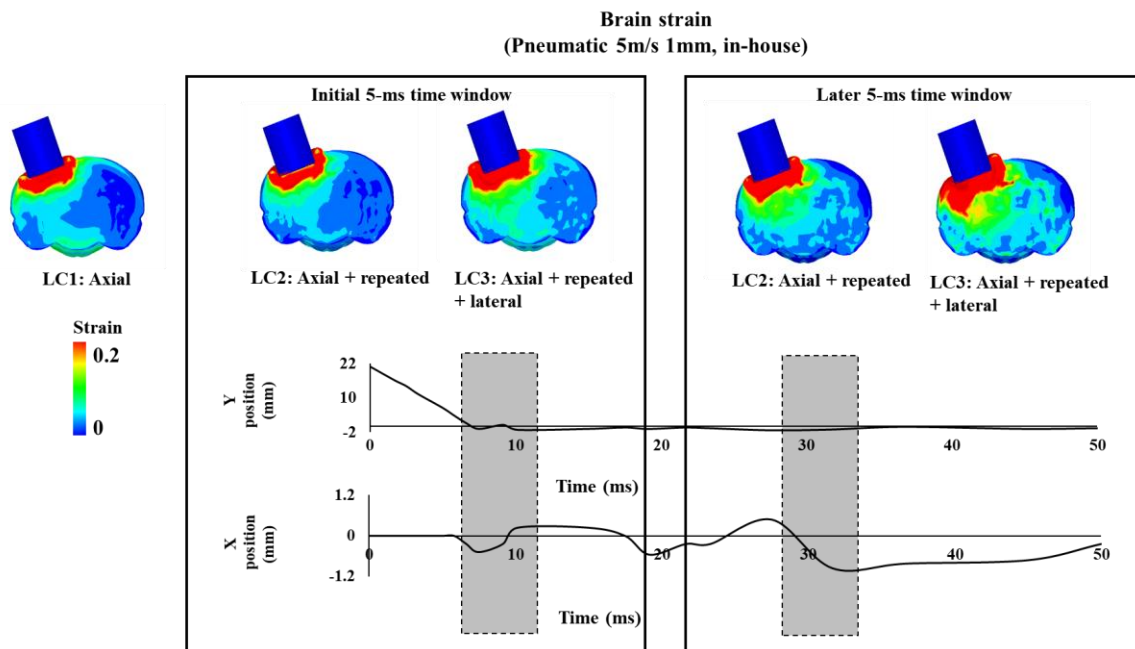


Figure 2.7 Comparison of the maximum principal strain contours across LC1, LC2, and LC3. For LC2 and LC3, both the initial and later 5-ms time windows were simulated as

high-speed videos demonstrated that there were larger lateral tip movements at the later stage. According, brain areas with high strains were largest for the later 5-ms time window at LC3. LC: loading condition. CCI: controlled cortical impact.

The cortex, corpus callosum, and hippocampus were selected to study the local effect of repeated impact and lateral tip movement (Figure 2.3a). The predicted MPS was compared in (Figure 2.8). For the initial 5-ms time window, the predicted MPS in Loading condition 1 (0.22 ± 0.09) was slightly lower than that in Loading condition 2 (0.24 ± 0.09). For the later 5-ms time window, the predicted MPS in Loading condition 1 was also slightly lower than that in Loading condition 2 (0.23 ± 0.07). Compared with the predicted MPS in Loading condition 3 for the initial 5 ms (0.31 ± 0.10), the predicted MPS in Loading condition 3 in later 5 ms (0.33 ± 0.14) was largest due to the maximum lateral movements (0.95 mm).

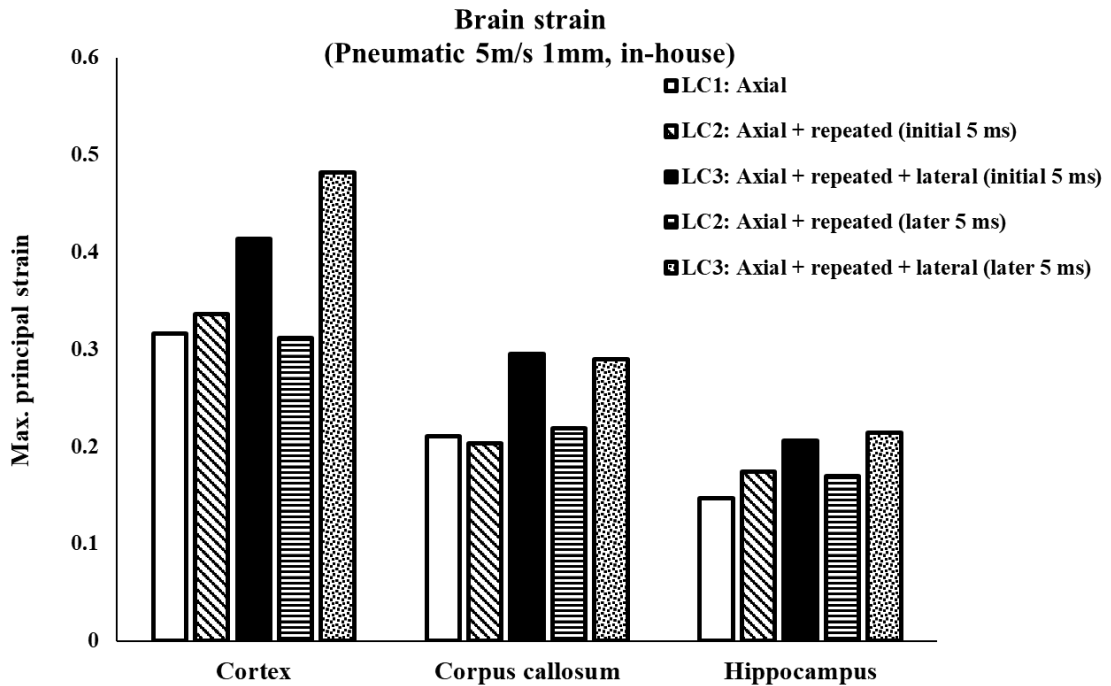


Figure 2.8 Comparison of maximum principal strain for three regions in LC1, LC2, and LC3. LC3 at the later 5-ms time window produced highest strains. LC: loading condition.

2.4 Discussion

Three loading conditions -- which included Loading condition 1 with ideal impact along the impact axis, Loading condition 2 with repeated impacts and Loading condition 3 with both repeated impacts and lateral tip movements -- were studied to investigate the effects of repeated impacts and lateral tip movements on brain strains. In general, predicted MPSs were similar between Loading condition 1 and Loading condition 2, indicating that the repeated impacts had minimal effect on brain strains. Higher MPSs were observed in Loading condition 3 with larger high-strain areas than those in Loading condition 1 and 2, indicating lateral tip movements increased brain strains. Overall, our results suggest that the strain predictions are largely affected by the lateral movement of the CCI impactor tip while the influence of the second impact on brain peak strain is limited.

The effect of repeated impacts during CCI is of particular interest to concussion research because repeated impacts have been reported to induce concussions [62-64]. Meanwhile, CCI has been adopted to induced closed head injury that mimics mild TBI [65].

However, it should be noted that the time intervals during the repeated impacts for concussion cases are as short as one day [66, 67] or longer [68]. Different time intervals affect the degree of brain damage caused by repeated impacts. Petraglia et al. reported that mice with six repeated impacts daily in seven days had increased anxiety, risk-taking behavior, and depression-like behaviors compared to a single impact [69]. Friess et al. found that the repeated head injury with one-day interval could worsen performance of the cognitive function in piglets compared to impacts with seven-day interval [70]. Meanwhile, Haar et al. demonstrated that repeated brain injury could reduce behavioral deficits given two weeks to recover [71]. Allen et al. proved that repeated mild brain

injury at the same site had no effect on motor function with three tests every two days [72]. Compared to these referred time intervals, the repeated impact during CCI happens in milliseconds and its effect remains to be investigated.

The MPSs were greatest in Loading condition 3 incorporating the lateral tip movements. The lateral movements from the pneumatically driven CCI were small at the initial stage (0.48 mm) but got larger at the later stage (0.95 mm). Accordingly, larger strains were produced at the later stage.

The significance of the current study for a better understanding and use of CCI can be described as follows. First, caution should be practiced when comparing CCI results among different labs without knowing brain tissue responses. As an example, a CCI with 1-mm impact depth may lead to remarkable intracranial tissue responses with MPS (0.15-0.52) if considering lateral tip movement (Figure 2.3b). Thus, a report of lateral movement is recommended besides reporting CCI parameters including impact depth, impact velocity, impactor tip shape and size, and craniotomy.

Second, the FE mouse brain model helps to understand the effect of repeated impacts on brain tissue responses. It was very difficult to explore the brain tissue response during CCI, not to mention exploring brain tissue response under repeated impacts with a time interval of several milliseconds. This study adopts an FE mouse model and helps to understand how the repeated impacts in milliseconds affect the tissue strain. Our data is unique in the literature, to the best of our knowledge. Even though the simulations of repeated impacts lacked validation, the technique we used to simulate CCI on the mouse

brain has been found to provide valid predictions when comparing brain strains to brain damage observed through histopathology [37, 55, 73].

Third, the FE mouse brain model helps to explain the importance of monitoring lateral tip movements. The maximum lateral tip movements of five CCI devices could happen when the tips were in contact with brain surface or were away from brain surface (due to the retractions during repeated impacts). It could be reasonably postulated that lateral movements with the tip away from brain surface do not induce any additional strains. Comparing device b and device e, device b had a larger maximum lateral tip movement (1.25 mm) but lower average MPS (0.20) (Table 2.2), while device e had a smaller maximum lateral tip movement (1 mm) but a higher average MPS (0.24). On the other hand, our studies proved that the lateral tip movement with contact was correlated well with the brain tissue strain (Table 2.2). Therefore, lateral tip movements should be monitored and those movements along with contact with the brain surface are expected to greatly affect brain responses.

Table 2.2 The maximum lateral tip movements of five devices with and without considering the contact between impact tip and brain tissue and the corresponding MPS. MPS: maximum principal strain.

	Lateral tip movement w/o. contact (mm)	Lateral tip movement w. contact (mm)	Average MPS
Device a	1.40	1.38	0.36
Device b	1.25	0.34	0.20
Device c	0.45	0.19	0.20
Device d	0.40	0.18	0.21
Device e	1.00	0.40	0.24

Fourth, the lateral tip movements in CCI devices are suggested to be added in the CCI FE modeling. In our previous work, CCI has been modeled as a single impact without considering the lateral tip movement. With this study demonstrating that lateral tip movements increased brain strains and contusion volumes, we could justify that previous CCI simulations might under-predict brain strain responses [37, 56]. To ensure the accurate prediction of brain response during CCI, lateral tip movements are suggested to be incorporated in simulations.

Fifth, our study highlights that intracranial brain tissue responses are better predictors of TBI than external mechanical parameters because these tissue responses are directly related to injury rather than impact parameters such as accelerations [74]. Impact depth and impactor shape were previously shown to be the main factors affecting CCI injury severity based on strain analysis [75]. In the current study, some lateral tip movements were shown to increase contusion volume as much as 50%. Such information could only be collected by describing brain strains. In the future, brain responses such as strain are recommended to be reported along with histopathological and behavioral damage, further helping establish a common language across labs [76].

2.5 Conclusions

We conclude that lateral tip movements increase brain strain predictions while the repeated impacts of the tip have minimal effect on peak strains during CCI. We justify that CCI could still be considered as a single event and the repeated impacts could be characterized as part of this single event without affecting peak strains. Also, our results suggest that lateral tip movements could play a major role in increasing contusion volume (by 50% for 1.4-mm lateral movement and < 20% for 0.4-mm and less lateral

movement). The lateral tip movements, which seem to take place in the CCI devices based on experimental studies, need to be explicitly monitored.

Chapter 3

3 The effect of 3D vasculature on brain response under the focal brain injury

The effect of the detailed three-dimensional (3D) vasculature on brain tissue responses in open-skull focal injuries was investigated. A new FE mouse brain model with a detailed 3D, non-linear vasculature was developed.

3.1 Introduction

Traumatic brain injury (TBI) has been considered as a serious problem in the world. In the USA, the incidence of TBI was around 1.6 million, with 52,000 deaths and 80,000 severe neurological disabilities annually [1]. TBI Survivors usually suffered neurologic deficits, cognitive deficits, and behavioral abnormalities, bringing enormous societal and financial burden. Among all TBI injuries, vessel damage is critical as brain tissue injury often accompanies brain vessel injury in TBI, damaging neural tissues [77-79]. The most direct symptoms of vessel injury are laceration and bleeding. Also, vessels may experience subtle deformation which is not severe enough to cause bleeding but can damage the microstructure of brain vessels, and even change their structure and function [80]. In addition, vessel injury in the central nervous system can damage the exchange of nutrients, molecules, and cells between blood and brain parenchyma, making neural tissues suffering from toxins and pathogens [81]. Post-trauma biochemical cascade has been proven as a reason for vessel dysfunction [77, 82, 83]. Vessel dysfunction also includes the injury of vascular cells and extracellular matrix in the absence of hemorrhage. Although the vessel injury plays an important role in understanding the mechanism of TBI, how the mechanical forces cause vessel injury during TBI and what are the vessel response to these forces lack in the current literature.

Despite the lack of study of brain vessels, many investigations have been conducted to explore the brain injury mechanisms using both experimental models [84-87] and finite element (FE) models [36, 38, 88-94]. Impact animal experiments, especially rodents, have been widely used, including rotational load, closed-head impact model of engineered rotational acceleration (CHIMERA), controlled cortical impact (CCI) and

fluid percussion (FP). Rotational load is a common impact that delivers the defined energy from controlled impacts to a closed unconstrained head. These rapid acceleration and rotation during TBI impact lead to the stretch and deformation of the brain tissues in the skull, representing as a diffuse injury. However, CCI is a focal injury model that induces a cortical contusion. Brain injury data in these experimental models can be measured and used to investigate the mechanisms of TBI [36, 37]. Meanwhile, it is almost impossible to directly observe intracranial stress/strain responses in vivo. Therefore, FE animal models have been used to study brain response and injury mechanisms. However, in many FE brain models, the entire 3D vasculature has not been fully modeled. From a mechanics standpoint, the blood vessels are hundreds of orders stiffer than brain parenchyma [25, 95-97]. which could probably affect the dynamic response of the brain, especially the load-bearing property of the brain.

The roles of the vasculature in the dynamic response of the brain were studied by several teams. However, confounding observations on the effect of the vessel have been reported and are summarized as follows. In a study by Ho et al. [25], three 3D FE models (without vessels, with linear-elastic vessels and with non-linear elastic vessels) were developed to study the dynamic responses of the brain under the rotational and translational acceleration impulses. Small reductions in the peak average strain were found in the models with vessels compared to the non-vessel model, with 2% reduction for non-linear elastic vasculature model and 5% for linear elastic vasculature model. This result illustrated that there was a small effect of the structural vasculature on brain response. However, other studies show that the influences of the vasculature are remarkable. In the study by Zhang et al [38], two 2D FE human head models were developed. Model 1 includes the skull, dura mater, cerebrospinal fluid (CSF), tentorium, brain tissue, and the parasagittal bridging veins. Based on Model 1, Model 2 further includes main branches of cerebral arteries. Maximum principal strain (MPS) shear strain (SS) and intracranial pressure (ICP) were studied under two load conditions with linear and rotational accelerations. The overall reduction in MPS was around 37% compared Model 2 to Model 1. SS in Model 2 was lower than those in Model 1 with the range from 7.4% to 36%. On the other hand, a similar study was done by Omori et al. [39] and their results were different from Zhang et al. Higher shear stress and SS were occurred in Model 2

including bridging vein and a major branch of an anterior cerebral artery because of tethering effect of the vasculature.

Under extremely high-rate blast loading conditions, in the study of the effect of blood vessel networks on dynamic responses of the brain by Hua et al. [40], using an FE human brain head model without vessel networks and an FE human brain model with statistically distributed 1D vessel elements. They found that the with-vessel model could predict higher strains in the brain, especially in the region with high vessel density (corpus callosum and brainstem). In the periphery region (cortex), there was a minimal difference in brain response between with and without vessel network models.

Unnikrishnan et al. [41], studied the effect of the 3D network of brain vasculature using rat brain FE model under blast overpressure. They found that including vasculature into rat FE model largely reduced the peak strain in cerebrum, cerebellum, and brainstem. Greatly strain reduction was found when using the human-brain properties in the FE simulation. They suggested that incorporating the vasculature into rat brain had a remarkable influence in brain strain under blast loading.

These published brain models included a two-dimensional (2D) vasculature model, a simple-geometry model, a 3D vasculature model with major branches and a 3D vasculature model with a detailed vasculature network. Many publications were under rotational impact loading, plus two papers under blast loading. Overall, how the detailed and major branches of vasculature affect brain tissue responses in focal injuries has not been investigated in the literature. In this study, we developed seven vasculature models including a 3D, anatomically detailed vasculature model with the arteries and veins, major branches vasculature model, small branches of vasculature model with nonlinear/linear vasculature. We investigated the effects of the detailed vasculature with nonlinear/linear elastic vasculature on mouse brain tissue responses for focal injury. The hypothesis of this study was that vasculature should have a small effect on focal injury and the similar influences for the major and small branches of the vasculature. Model-predicted biomechanical parameters, such as the MPS and cumulative strain damage measure (CSDM) were identified at selected brain regions and were compared to quantify the effect of the vasculature.

3.2 Method

The effect of the detailed 3D cerebral vasculature on brain responses under focal injury was evaluated by comparing the results from the seven vasculature brain models. The nomenclature of these models is summarized in Table 3.1.

Table 3.1 Nomenclatures of the seven vasculature brain models. Whole-L: whole linear elastic vasculature model, Whole-NL: whole nonlinear elastic vasculature model, Major-L: major linear elastic vasculature model, Major-NL: major nonlinear elastic vasculature model, Small-L: small linear elastic vasculature model, Small-NL: small nonlinear elastic vasculature model, NV: non-vasculature model.

Models/Material	Linear elastic vasculature	Non-linear elastic vasculature
Whole vasculature	Whole-L	Whole-NL
Major vasculature	Major-L	Major-NL
Small vasculature	Small-L	Small-NL
Non- vasculature		NV

3.2.1 Vasculature model development

Vasculature geometry - We obtained the cerebral vasculature geometry based on the previous work [98]. Four CBA male mice (ages 6 and 16 months) were anesthetized with ketamine (50 mg/kg) and xylazine (10 mg/kg). A radio-opaque silicone rubber (Microfil® MV-122, Flow-Tech Inc.) was used as a contrast agent at the pressure of 160 mm Hg for 90 min. Heparinized PBS (1unit heparin/ml) was the contrast agent which was injected into the left ventricle of the heart and drained from the right ventricle. Removing the skin, lower jaw, ears and nose tip from a mouse head, the remaining mouse head was soaked in 4% paraformaldehyde at 4 °C for 12 h. After a series of specimen preparation, brain was extracted from skull, kept brain in 1% agar, and obtained the X-ray Micro CT imaging of cerebral vasculature with 20 μm isotropic resolution.

The meshes of the 3D brain vasculature of a mouse brain were generated based on data with a spatial resolution of 20 microns. The original number of triangles meshes was 10,484,908. The meshes were further improved using MeshLab 2016 (National Research

Council, Rome, Italy) because too many small meshes affected the efficiency of computational simulation. After mesh simplification, element size ranged from tens to hundreds of microns with an average of approximate 20 microns. The vasculature model contained 317,294 shell elements. The arteries and veins were separated based on the mouse anatomy of brain vasculature [99, 100]. Major arteries such as the anterior cerebellar arteries (ACA), inferior cerebellar arteries (ICA), middle cerebellar arteries (MCA), superior cerebellar arteries (SCA), olfactory arteries, basilar arteries, and vertebral arteries, and veins such as superior sagittal sinus and transverse sinus, were identified as shown in Figure 3.1. Therefore, the Whole vasculature model contained all the detailed 3D vasculature with the highest vasculature area (283cm^2). The Major vasculature model only included several major arteries and veins of the vasculature. The small vasculature model included the rest of the vasculature (shown in Figure 3.2a). The thickness of the blood vessel wall was assumed as 0.0039 mm for artery and vein, which were calculated from 3D brain vasculature of a mouse brain [24].

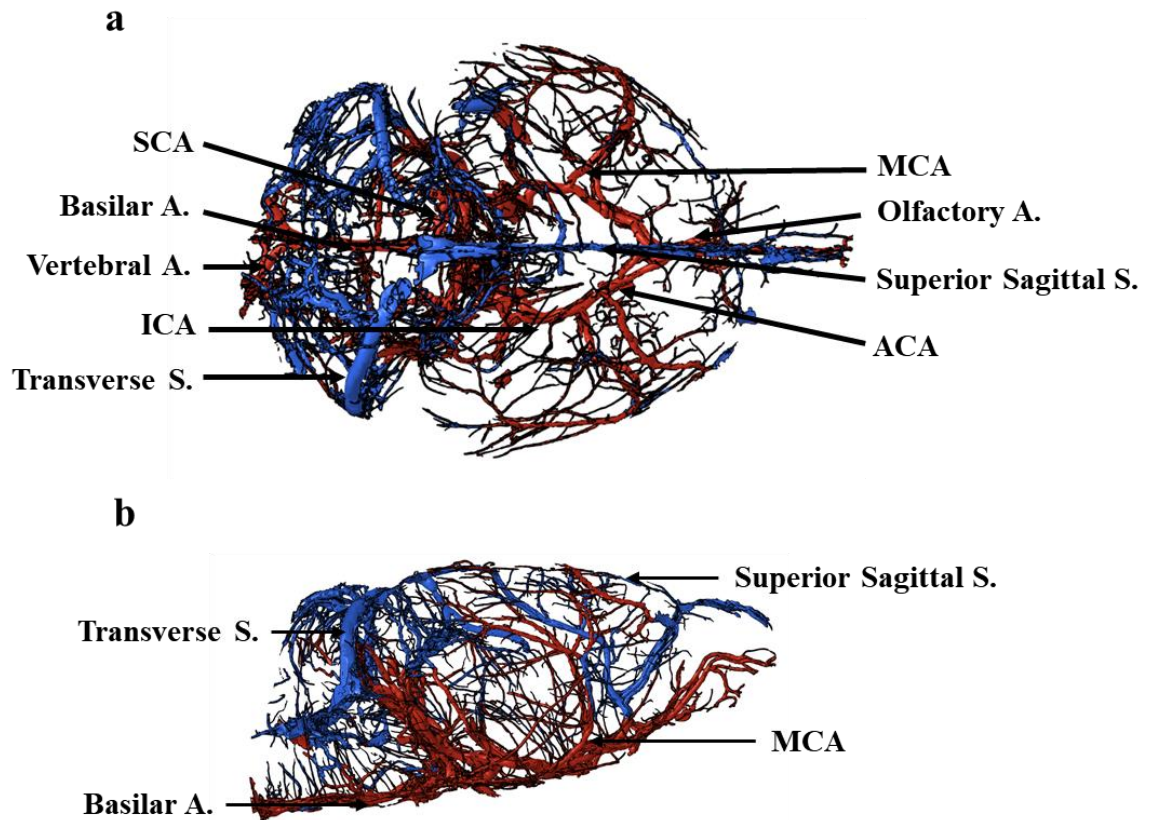


Figure 3.1 The top and side view of the geometry of the major arteries (dark red) and veins (blue).

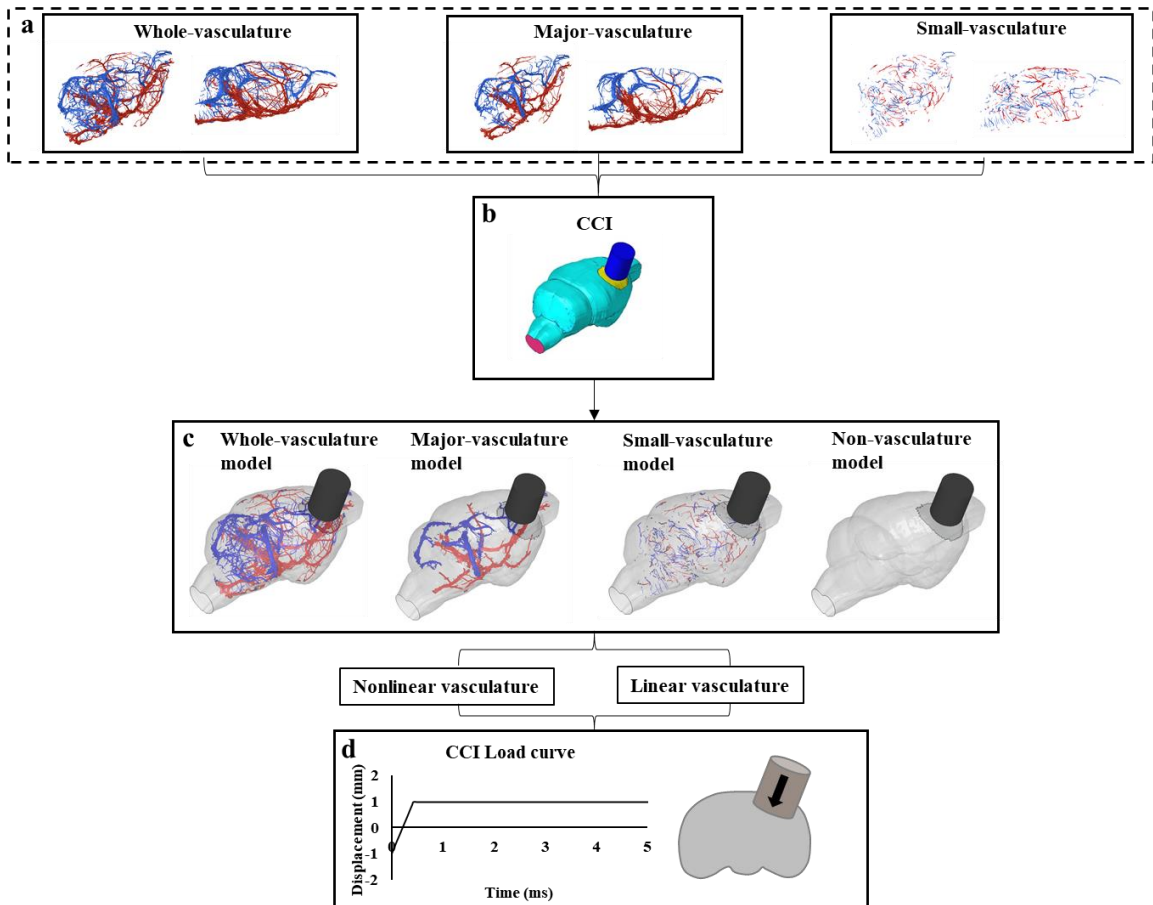


Figure 3.2 The process of developing 3D mouse brain models with different vasculature under CCI. CCI: controlled cortical impact.

Finite element (FE) brain models - The previously developed mouse brain FE model [55] contained most of the anatomically essential features, including the skull, dura matter, pia matter, hippocampus, corpus callosum, medulla oblongata, cerebral cortex, ventricle, internal capsule, cerebellum, spinal cord, optic tract, olfactory, pons, thalamus, and hypothalamus with a total of 258 thousand solid elements and a spatial resolution of 150 microns. The mouse brain model has been previously used to evaluate the effect of flat-shape and sphere-shape impactor tips during CCI [55] and a CCI with reduced impact rate [36] demonstrating correlations between brain strain predictions and histopathology observations (Figure 3.2b).

FE vasculature brain models – These vasculature models (Whole-vasculature, Major-vasculature, and Small-vasculature) were coupled into a 3D mouse model using

*CONSTRAINED_LAGRANGE_IN_SOLID available in LS-DYNA (Livermore Software Technology Corporation, Livermore, CA, USA) (Figure 3.2).

3.2.2 Material property

3.2.2.1 FE mouse brain material property

The linearly viscoelastic material law has been used in modeling the brain tissue simplifying the simulation. Eqn. 2 was used to calculate the shear modulus of a linearly viscoelastic material $G(t)$

$$G(t) = G_{\infty} + (G_0 - G_{\infty}) e^{-\beta t} \quad (2)$$

Where G_0 and G_{∞} are the short-term and long-term shear moduli, respectively. The decay constant and the duration is given by β and t , respectively. A previously developed FE mouse model was used. More detailed material properties can be referred to in previous publications [55, 56].

3.2.2.2 Vasculature material property

It is widely accepted that vasculature was nonlinear and almost incompressible with stress-strain property based on the assumption of cylindrical orthotropy [19, 20]. Quasi-static and dynamic tensile tests to collect experimental stress-strain curves were conducted [24]. The results demonstrated that longitudinally strain rate is quite important in the material model of the vasculature. A previous investigation by Monson et al. (2005) stated that the sources and sizes of the vessel affected vessel stiffness, which should be carefully referred in defining the material property of vasculature [96]. The stiffness of rat arteries was studied [101]. It demonstrated that the stiffness and peak stress of in vivo blood vessels were strain rate dependent from quasi-static levels while no rate dependency was found on the failure stretch of arteries. The stress-strain curves were obtained from the axial stretch test of rat arteries [101].

For nonlinear elastic vasculature, the Ogden constitutive model has been selected to represent the nonlinearity of the vasculature. Here representing the vasculature as an isotropic, incompressible material, the Ogden model was written with components λ ,

shear modulus μ , and constant α . The strain energy density function was written as Eqn. 3. Then we derived the engineering stress equations for compression/tension and shear modes and fit the stress-strain curves obtained from the axial stretch test of rat arteries to calculate the material parameters [101]. The shear modulus μ and constant α were 0.3515 MPa and 5.066, respectively.

$$W = \frac{2\mu}{\alpha^2} (\lambda_1^\alpha + \lambda_2^\alpha + \lambda_3^\alpha - 3) \quad (3)$$

For linear elastic vasculature, the material properties used for the vasculature were based on the stress-strain curve [101]. We assumed the average elastic modulus of the artery to be 3 MPa. Also, the elastic modulus of veins was assumed as 0.3 MPa, calculated based on the relationships of arteries and veins in the literature [18, 39]. The density of the vessel was 1.04E-06 kg/mm³ and the Poisson's ratio was 0.48 [18].

3.2.3 FE simulation of focal injury

The FE simulation of CCI was based on our established approach [102]. The CCI simulations were conducted in LS-DYNA (Livermore Software Technology Corporation, Livermore, CA USA). We simulated a 3 mm diameter flat tip impactor with 1 mm above the craniotomy. A 5 mm diameter craniotomy centered at 3.0 mm posterior to the bregma and 2.5 mm lateral to the midline was removed from the skull. The impact speed was 5 m/s. The impact depth was controlled at 1 mm (Figure 3.2).

Our trial simulations demonstrated that the highest MPS of the brain in CCI injury happened before 1.2 ms. Simulation results were plotted at every 0.1 ms. We investigated brain biomechanical responses for the seven vasculature models and quantified the effect of the detailed 3D cerebral vasculature during focal injuries at the tissue level.

3.3 Results

3.3.1 Brain strain contour

The strain contours were compared among the seven vasculature models and each model was simulated under CCI to reveal the effect of the vasculature on brain response for focal injury.

Figure 3.3 shows the MPS contours predicted by four models (NV, small-L, Major-L and Whole-L) and another four models (NV, small-NL, Major-NL and Whole-NL) at the time of maximum impact depth. Similar strain contours were observed in these models. The high MPS spread from the cortical layer into the deep brain in an ellipsoidal mode. Most of the high MPS regions were in the region directly under the impactor site. Some brain tissues were squeezed between the impactor and the edge of the craniotomy. These results show that including vasculature in the FE brain model has a minimal influence on the local brain tissue deformation in focal injury.

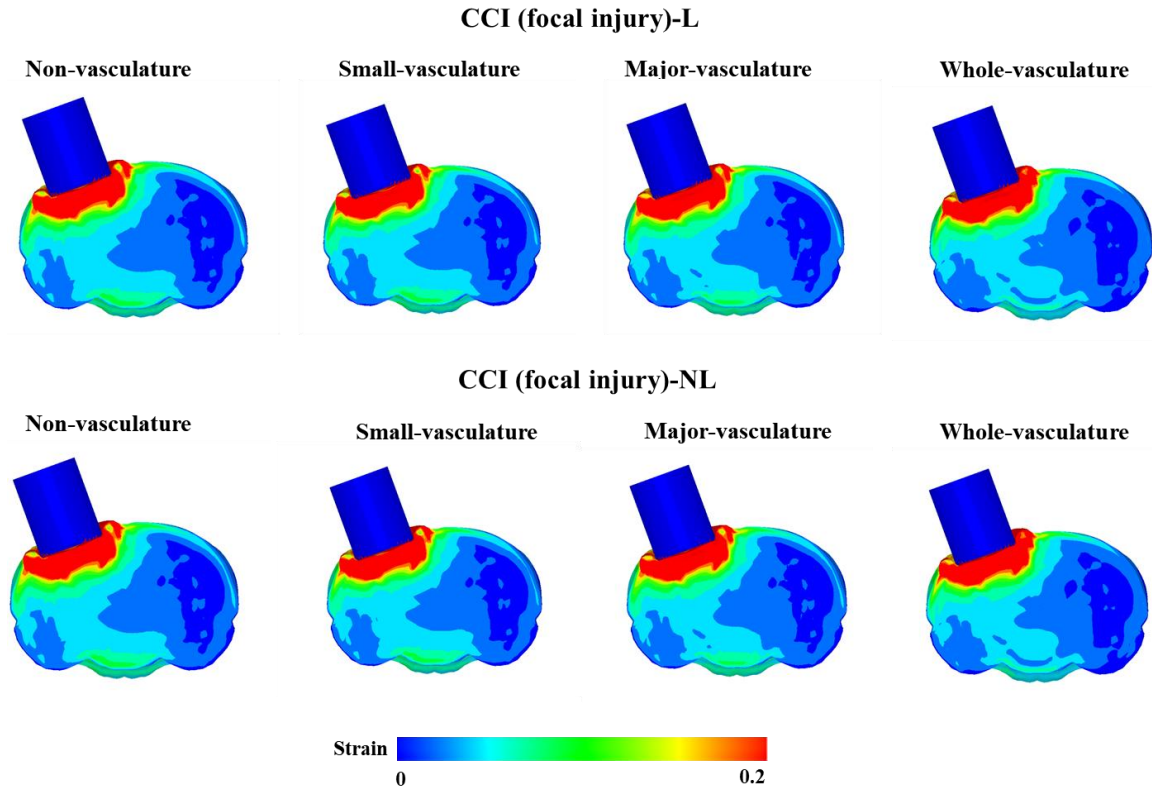


Figure 3.3 Comparison of the maximum principal strain contours of the brain for linear vasculature models in CCI. L: linear; NL: nonlinear. CCI: controlled cortical impact.

3.3.2 Cumulative strain damage measure (CSDM)

CSDM was used as the predictors to access brain responses induced by different impacts. CSDM values, for example, CSDM (0.10) means the percentage of the elements of which the strain exceeded 0.10, was used to describe the brain responses under focal injury.

Four brain locations, cerebral cortex, corpus callosum, hippocampus and thalamus, under the impactor were selected to how the vasculature affects the brain strain response for focal injury (Figure 3.4).

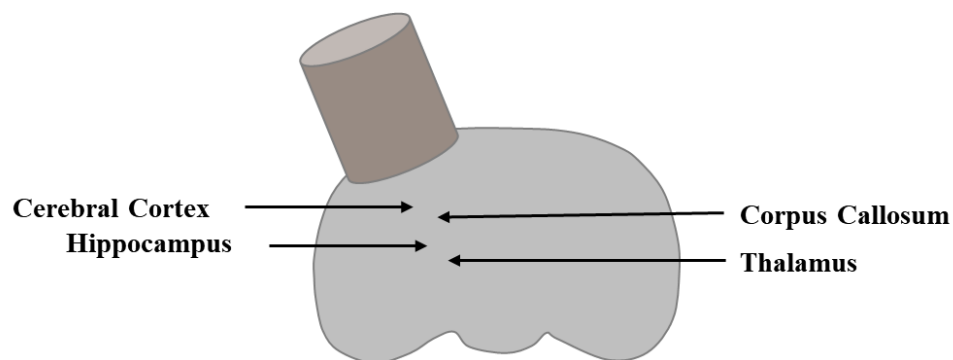


Figure 3.4 Four regions of brain selected for comparing strain of vasculature models in CCI. CCI: controlled cortical impact.

The CSDM results of all vasculature models in CCI were similar in these four regions for both linear and nonlinear vasculature (Figure 3.5). Less than 5% of CSDM reduction were found these four vasculature models in linear and nonlinear vasculature cases, except the whole nonlinear vasculature model which may experience over-brain-responses in some elements (9% of CSDM reduction). These results revealed that including linear and nonlinear vasculature in the brain had a minimum influence on brain strain prediction in CCI.

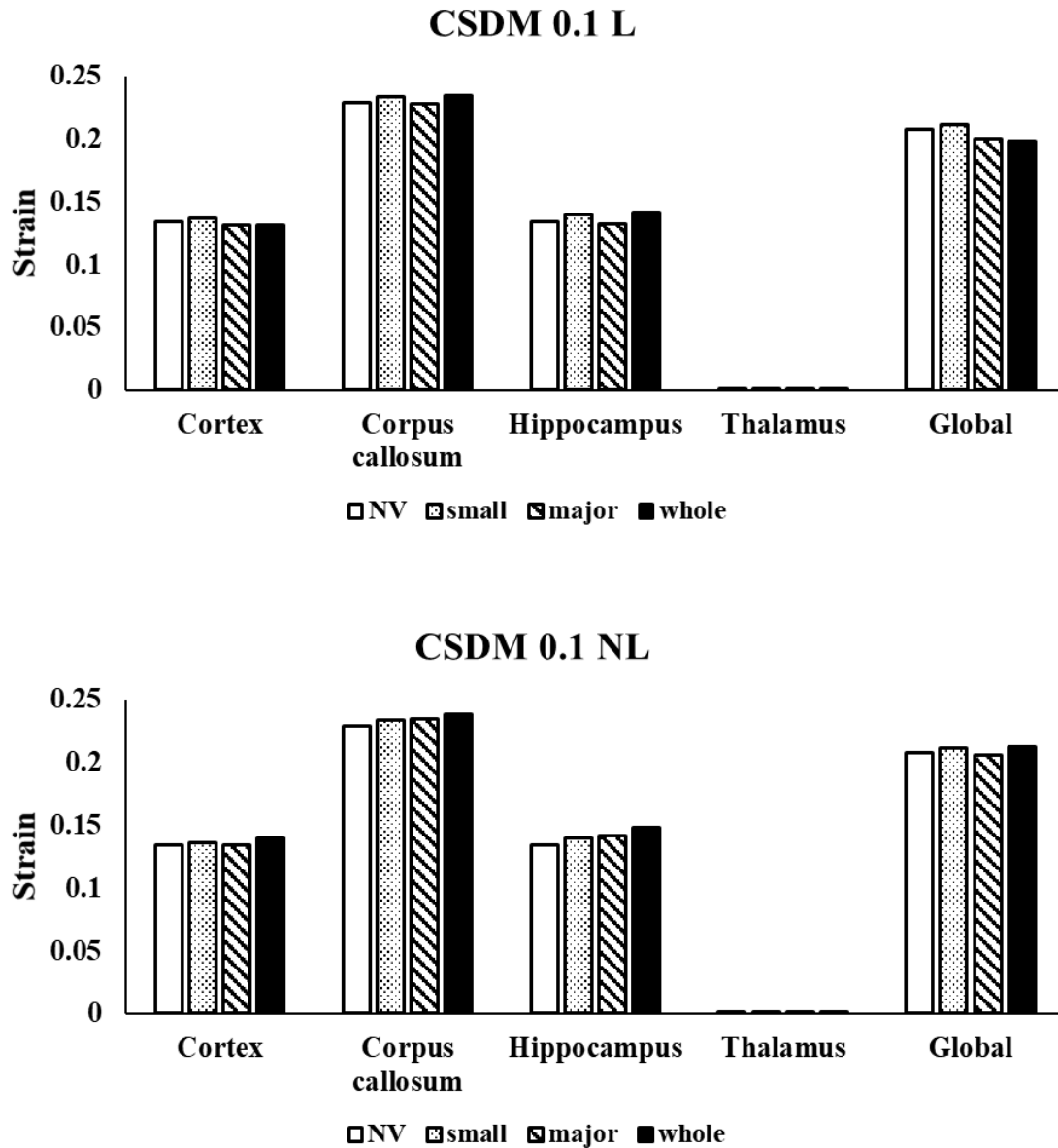


Figure 3.5 CSDM (0.1) of four selected brain regions in linear and nonlinear vasculature models in CCI. L: linear; NL: nonlinear. CCI: controlled cortical impact.

3.3.3 Maximum principal strain (MPS)

The peak MPS of the selected four regions including cortex, corpus callosum, hippocampus and thalamus were compared in Figure 3.6. The MPS of all vasculature models in CCI were similar in these four regions for both linear and nonlinear vasculature. Cortex had the highest MPS ranged from 0.36 to 0.40 among all these four

vasculature models for linear vasculature and ranged from 0.36 to 0.39 for nonlinear vasculature, followed by corpus callosum, hippocampus and thalamus. Less than 2% and 4% of strain reduction were found these four vasculature models in linear and nonlinear vasculature cases.

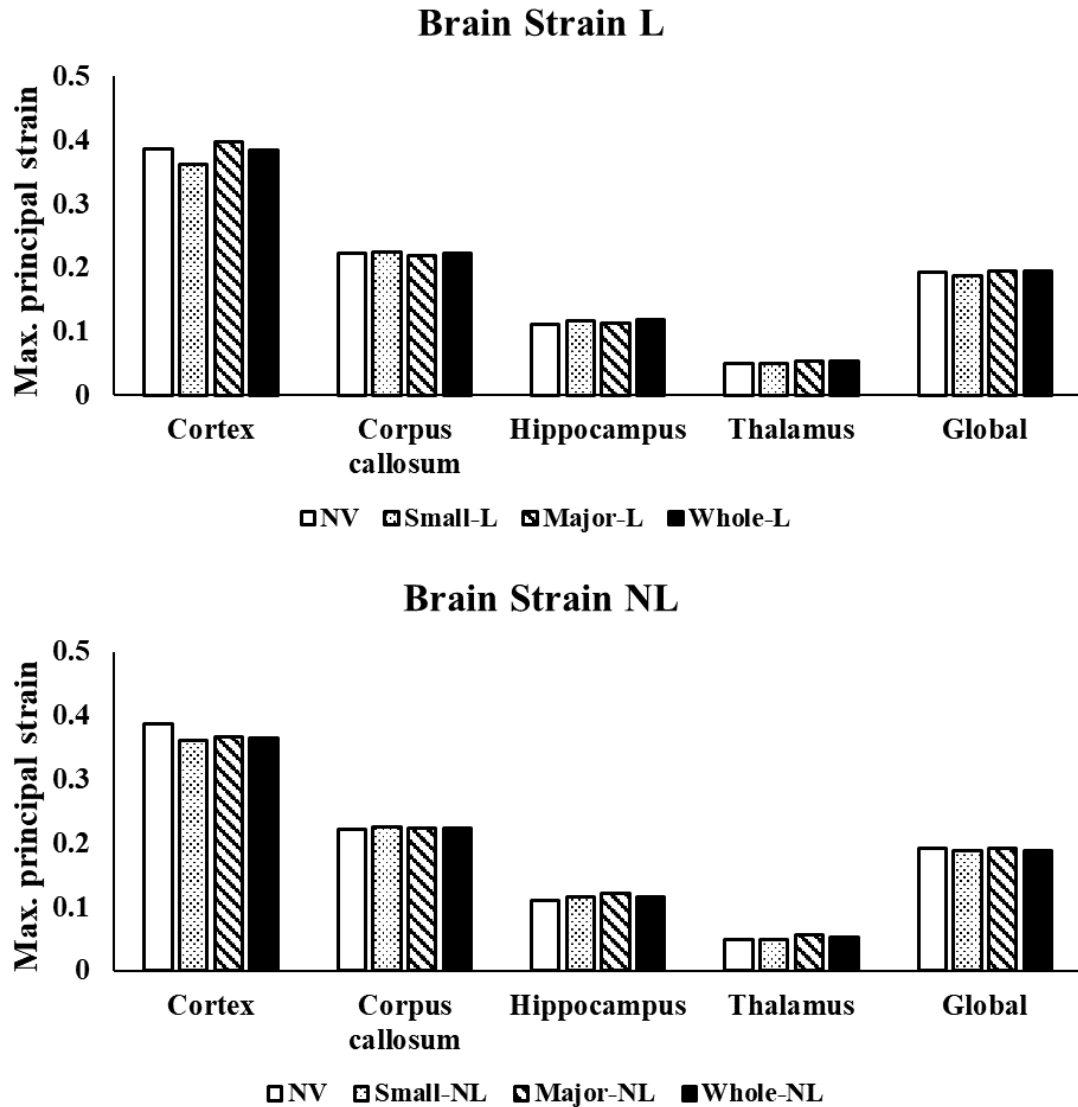


Figure 3.6 Comparison of predicted maximum principal strain in these four regions and the global brain in CCI for linear and nonlinear vasculature. L: linear; NL: nonlinear. CCI: controlled cortical impact.

3.4 Discussion

We developed seven vasculature models including a 3D, anatomically detailed vasculature model, major branches vasculature model, small branches of vasculature with nonlinear/linear vasculature and non-vasculature model to investigate the effect of the vasculature for focal injuries (CCI) on brain strain responses. The current study showed that vasculature had a small effect on focal injury. The contribution of the vasculature was limited, less than 5% for all the cases. It was concluded that vasculature has a small effect of brain response for focal CCI injury and the similar influences for the major and small branches of the vasculature.

The main significance of the current study was the developing of the FE mouse-brain-based model with the detailed 3D vasculature. Modeling detailed vasculature helps to improve the prediction accuracy of FE brain models. Some previously published brain models included a 2D vasculature model, a simple geometry model, or a 3D vasculature model with major branches, which were somewhat far from the actual brain with the vasculature. We realized that the vasculature details were different in these previous FE vasculature models, most of which had major branches of the vasculature and excluded the small vasculature. So, these results might be underpredicted or overpredicted the influence of the vasculature. That is because that the MPS results likely to rely on the locations of selected elements, and larger strain reductions in the elements closing to the major branches of the cerebral vasculature and somewhat smaller for the elements located at a distance. Ho et al. have reported that the reduction of MPS is less than 4% when including major branches in the with-vasculature model and excluding small vessels [25]. Therefore, how the detailed vasculature affect brain strain response should be investigated using an FE brain model with the detailed 3D vasculature. Although this study in 3D detailed vasculature brain model indicated that there is limited effect in focal CCI injury, this developed FE model will help to investigate the vasculature effect for diffuse injury in the future. Therefore, Incorporating the 3D detailed vasculature is still recommended to improve the prediction accuracy of FE brain models.

Modeling detailed vasculature also helps to study the vessel injury mechanisms in TBI. Generally, the cerebral vasculature is an essential and key cellular feature in the brain,

which is important to keep a healthy brain. Many researchers proved that almost all the moderate and severe TBI cases contain several degrees of damage to the cerebral vasculature, which has not been extensively studied [77-79]. The blood vessel injury can result in secondary injury in the form of hemorrhage, edema, change blood flow, and blood-brain barrier disruption [103]. Hence, the inclusion of the 3D vasculature could be helpful to explore brain vessel injury mechanisms in the future.

Modeling detailed vasculature also helps to study the vasculature responses, such as vasculature strain (shown in Figure 3.7), which could predict brain strain to a certain degree, to diagnose brain injury and develop treatments to improve the functional outcome after TBI. Compared with observing brain deformation, clinical data of vessel deformation is relatively easy to obtain because biomarkers in the cerebral vasculatures could be detected [104]. In this way, brain tissue injury could be predicted by the clinical tests of the cerebral vasculature, beneficial to diagnose brain injury. Also, the study of animal models has demonstrated that therapeutic intervention has successfully controlled the degree of injury after TBI because there are some nerves don't damage at the time of injury [105, 106]. The biomarker is critical to developing effective treatment, involving the molecular targets. Traumatic cerebral vascular injury (TCVI) usually happens after TBI, which may be the reason for functional deficits and TBI- related chronic diseases. TCVI could be a useful target for the therapeutic intervention after TBI because many developed pharmacological and non- drug therapies could improve vessel injury, which is beneficial for the TBI treatment [107, 108]. Therefore, modeling detailed vasculature could provide the basis for studying vasculature response, diagnosing TBI and exploring TBI treatment through brain vasculature.

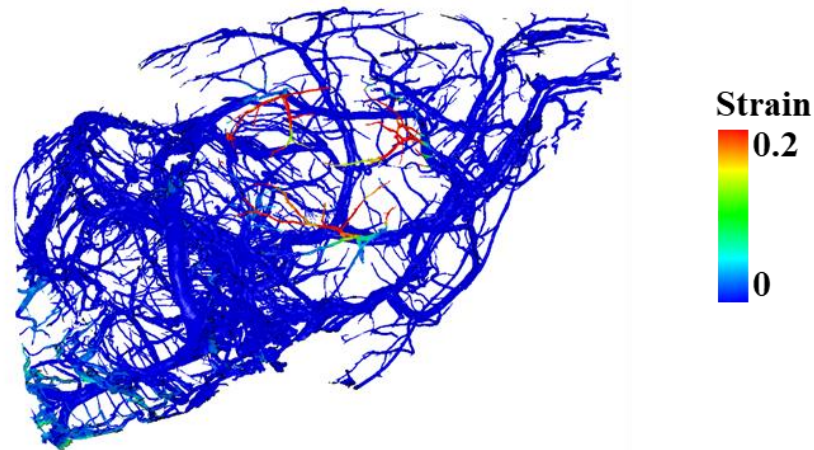


Figure 3.7 Vasculature strain in CCI. CCI: controlled cortical impact.

3.5 Conclusion

We conclude that during focal CCI injury, the contribution of the vasculature was limited, less than 5% for all the cases. This is because during CCI, the impactor tip was driven by either a pneumatic or electromagnetic device to reach a predefined impact distance, usually 1-3 mm. Hence, the added stiffness of the FE model with vasculature almost had no effect on the kinematics of the impactor tip, which determines how much brain surface would have been compressed. Though, incorporating the 3D detailed vasculature is still recommended to improve the prediction accuracy of FE brain models, especially for future diffuse-type brain injuries in which brain deformation will be affected by the brain's response to rotational forces.

Chapter 4

4 Investigating the mechanisms and thresholds of brain microvascular damage combining finite element modeling and experiments of CCI

The correlation between the vessel density map and the model predicted maximum principal strain (MPS) was evaluated. The brain microvascular damage mechanism and the associated threshold were investigated by comparing the histological data with finite element (FE) model predictions.

4.1 Introduction

3D cerebral blood vessels play an important role in brain metabolic activity after traumatic brain injury (TBI). Vessels may experience subtle deformation which is not severe enough to cause bleeding but can damage the microstructure of brain vessels, and even change their structure and function [80]. Also, cerebral blood flow (CBF) is an important parameter to evaluate the control of the vasculature function. The increase of vessel density may not raise the same amount of the blood flow [109]. Thus, there is a strong need to understand how the vasculature structure related to the CBF in TBI with the vasculature damage and vessel loss. Some studies investigated the relationship between CBF changes and vessel density and diameter [110, 111]. Vascular density in the hippocampus correlated with CBF in the rat fluid percussion (FP) injury [112]. Furthermore, the regions of increased metabolic activity usually have high vessel density [113]. Vessel density had been proved to be reduced after TBI [114].

The study of the vascular density was limited by the lack of 3D imaging techniques. 3D Imaging methodologies and automated techniques, such as Arterial spin labeling (ASL) magnetic resonance imaging (MRI) and Serial Two-Photon Tomography (STPT), have been combined to measure changes in cerebrovascular function and to characterize the 3D vascular architecture in mice. ASL MRI was used to quantify cerebral perfusion and 3D brain vasculature image was obtained by STPT [114]. A typical image of the microvasculature acquired with STPT is shown in Figure 4.1. The approach of using ASL MRI as a basis for producing vessel density maps has several advantages: First, vessel

density in the bioRxiv pre-print is also based on the vessel density at each ASL voxel, so there will be consistency across studies. Second, the ASL data also contains information on blood flow at each voxel under hypercapnia, which provides an opportunity to investigate the correlation between blood flow and brain strain.

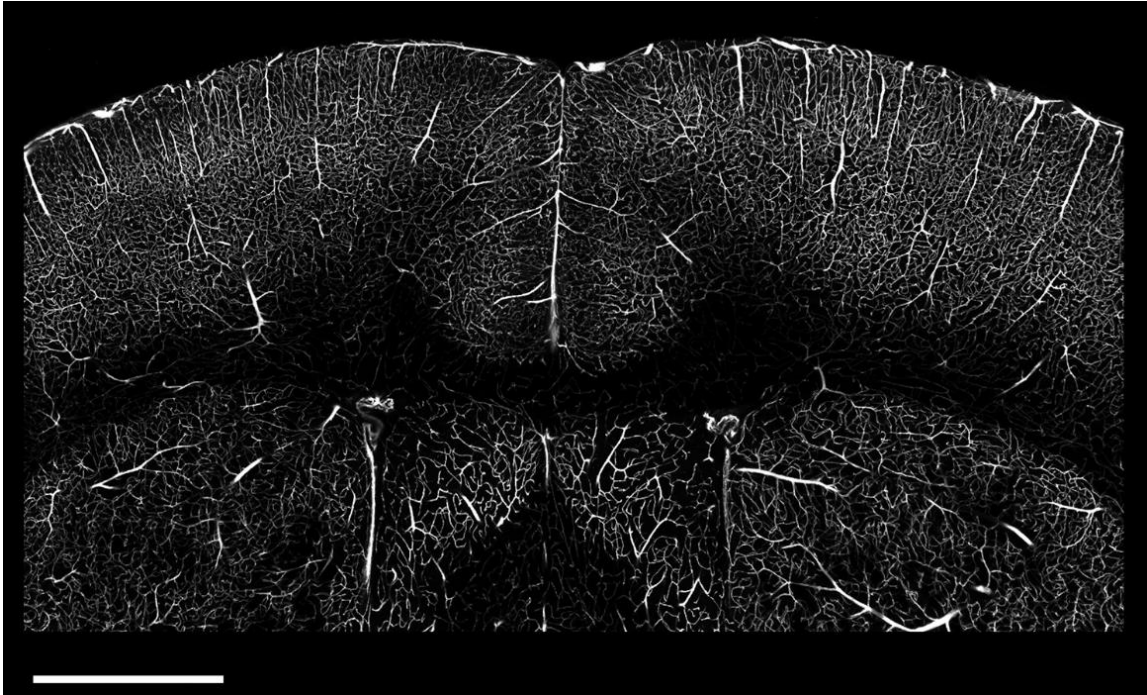


Figure 4.1 Microvasculature images with STPT from a healthy mouse. Maximum Intensity Projection (MIP) through 100 μm of tissue. Scale bar = 1mm. STPT: Serial Two-Photon Tomography [114].

Although high-resolution 3D imaging and automated techniques have been combined to measure changes in cerebrovascular function and to characterize the 3D vascular architecture in mice, little is known about the intracranial mechanical responses within cortical brain regions where the remarkable 3D cerebral microvascular length density changes during controlled cortical impact (CCI) [1]. Also, it remains unknown whether the stretches of brain tissues are related to microvascular damage and if so, how the extent of stretches determines microvascular damage. Therefore, the objective is to investigate mechanisms and thresholds of the brain microvascular damage combining FE modeling and experiments of CCI. We compared the vessel density map with model

predicted MPS and used logistic regression method to calculate the threshold for the brain microvascular damage.

4.2 Methods

4.2.1 CCI Experiments

Nine Cre x tdTomato mice were undergone CCI with 1 mm impact depth and 2 m/s impact velocity. A flat tip with a diameter of 1.5mm was used in CCI experiments. Each mouse was assigned its own ID. The impact center was targeted to bregma -2 mm and 1.7 mm lateral to the midline. For all mice except one, the injury center is located at about bregma -2 mm. However, for mouse 1049 the injury center is further moved back at about bregma -3 mm. The exact locations were further calculated from observed contusion cores.

4.2.2 Vessel density map and ASL MRI data

Microvascular damage was quantified using ASL MRI and the ex vivo STPT method. The vessel density map was calculated by registering the raw ASL data (voxel size 250 μm x 250 μm x 2 mm) in the same space as ex vivo MR (40 μm x 40 μm x 40 μm). Each ASL voxel had a corresponding vessel density calculated from the 2-photon images, and the signal in the attached vessel density map was the calculated density. Density units were the total length of all vessels within an ASL voxel divided by the ASL voxel volume (i.e. length/ mm^3). Since a single voxel in an ASL image contained many ex vivo MRI voxels, neighboring ex vivo MRI voxels were assigned the same density if they correspond to the same ASL voxel.

ImageJ (National institutes of Health and the Laboratory for Optical and Computational Instrumentation (LOCI, University of Wisconsin) Madison, WI, USA) was used to observe the ASL MRI of the mouse brain to obtain the vessel density map. The vessel density map of nine mice was shown in Figure 4.2. To label the injury center, only a single coronal slice was labeled, shown as a white dot in Figure 4.2. Mouse ID and related slice labeled with the injury center in TBI were listed in Table A.1. For comparison, the vessel density maps of seven sham mice were shown in Figure B.1. Also,

the mouse ID and related slice labeled with the injury center of seven sham mice were listed in Table A.2.

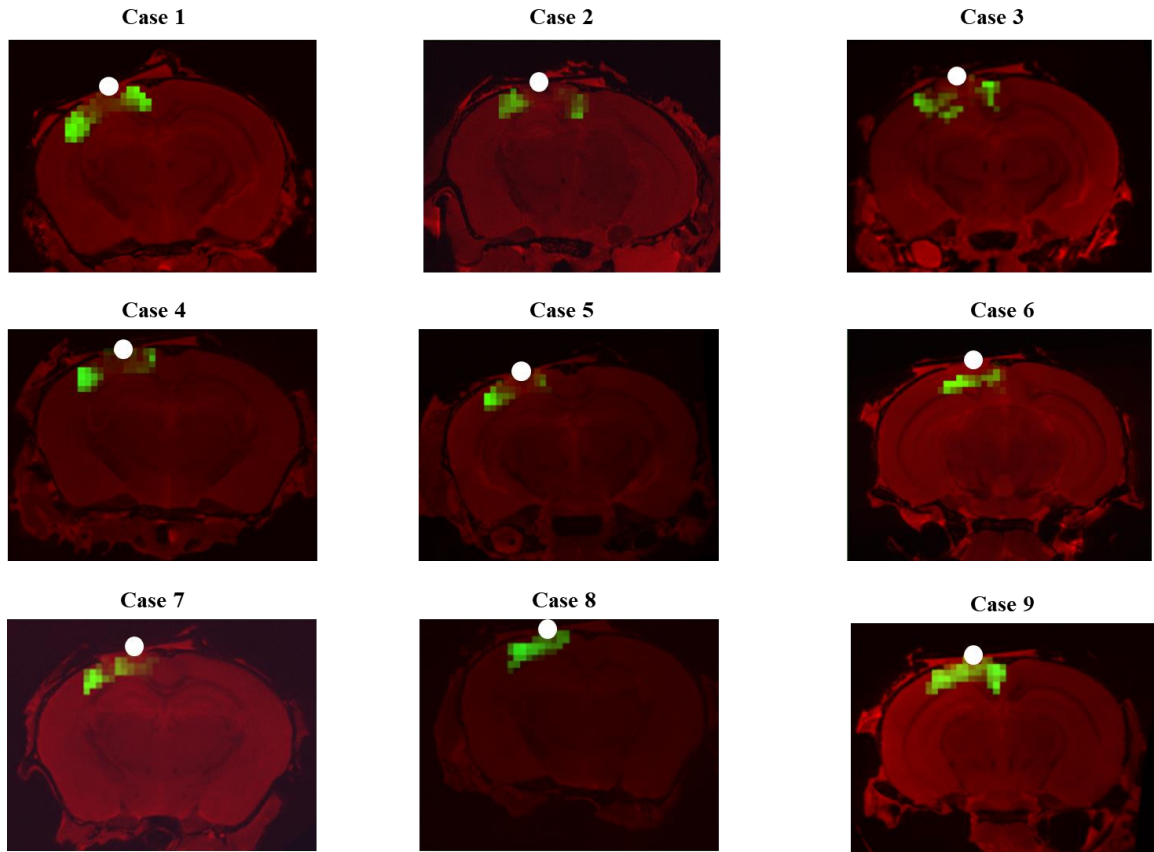


Figure 4.2 Vessel density map of all cases. The green ASL MRI boxes represents a different vessel length density. The white dot shows the impact center. ASL: Arterial spin Labeling, MRI: magnetic resonance imaging.

The different brightness of the green ASL MRI boxes represented a different vessel length density (Figure 4.2). The brighter ASL MRI box had a relative higher vessel length density, while the darker one had a lower vessel length density. The precise vessel density was given by the signal value of the voxel in the total length of vessels per mm^3 .

4.2.3 FE Simulation

The previously developed mouse brain FE model [55] contained most of the anatomically essential features, including the skull, dura matter, pia matter, hippocampus, corpus callosum, medulla oblongata, cerebral cortex, ventricle, internal capsule, cerebellum,

spinal cord, optic tract, olfactory, pons, thalamus, and hypothalamus with a total of 258 thousand solid elements and a spatial resolution of 150 microns. This FE mouse brain model with a detailed 3D vasculature, including 317,294 shell vasculature elements (Figure 4.3), was used to study intracranial responses in a series of CCI experiments. Each individual CCI impact was simulated according to the exact impact location. These FE model-predicted intracranial responses were further compared with the observed in vivo vessel length density map in the CCI experiment. We compared ASL boxes to finite element model and conducted injury-to-biomechanics comparison.

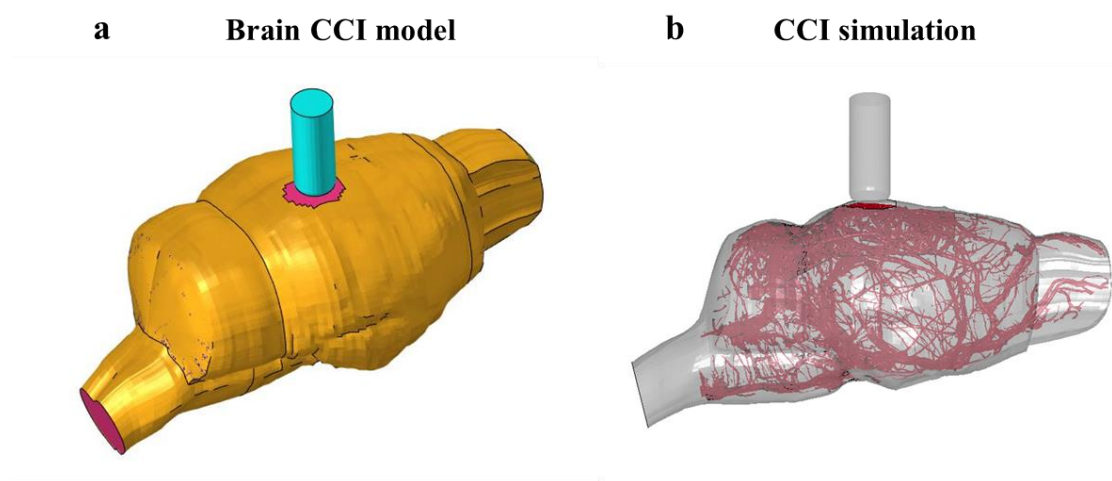


Figure 4.3 Mouse brain CCI model with vasculature **a. Brain CCI model** **b. CCI simulation with vasculature.** CCI: controlled cortical impact.

4.3 Results

4.3.1 Brain strain contour

The coronal view of the MPS contours at the time of maximum impact depth were illustrated in Figure 4.4. Similar strain contours were observed in nine cases. The high MPS spread from the cortical layer into the deep brain in an ellipsoidal mode. Most of the high MPS regions were in the region directly under the impactor site. High MPS was observed at the impact regions with a relatively low vessel length density (Figure 4.2 & Figure 4.4), indicating a higher brain microvascular damage. Overall, strain contours of nine cases were similar.

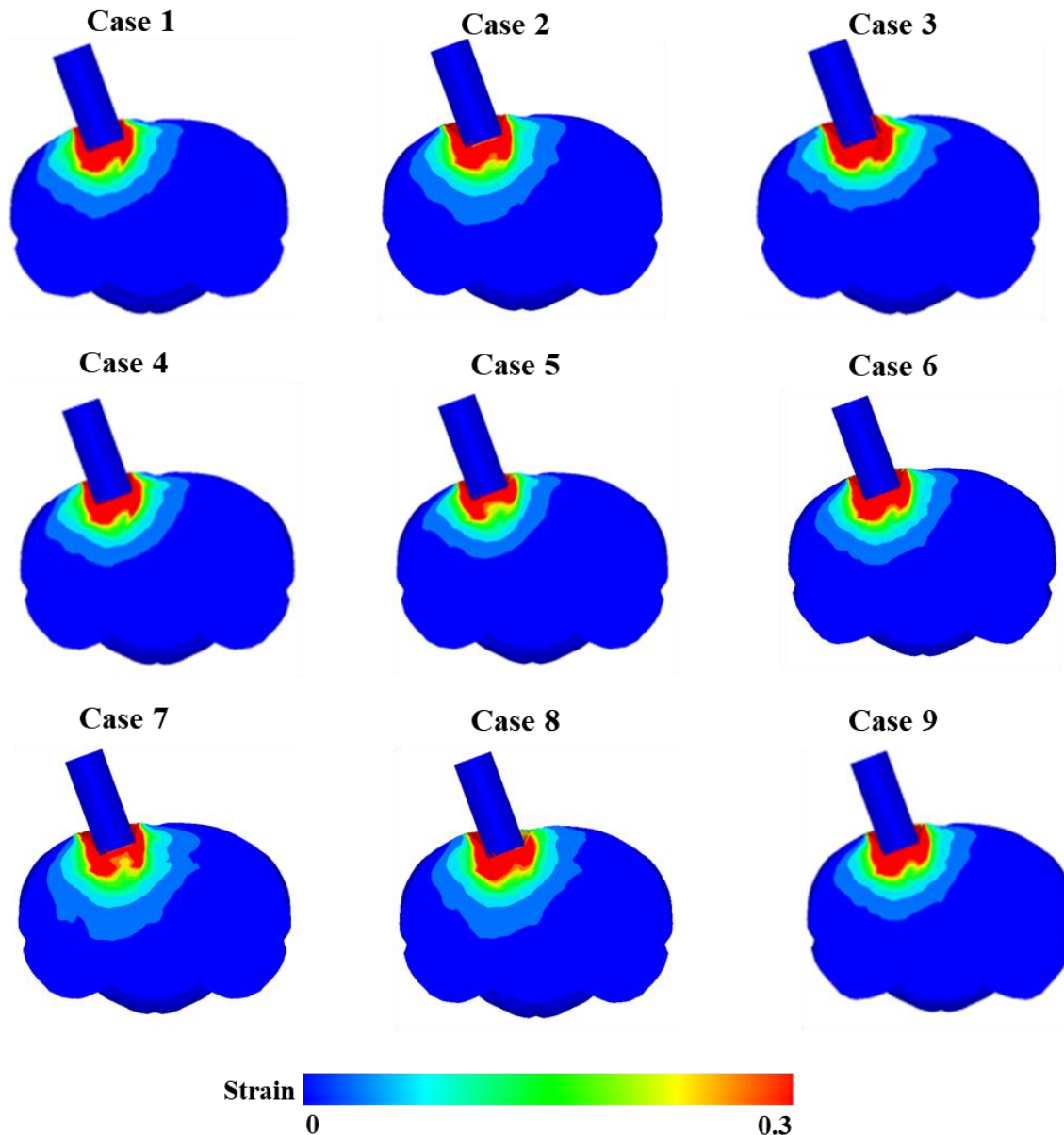


Figure 4.4 Maximum principal strain contours of the brain for all cases.

4.3.2 The correlation between the vessel length density and MPS

There was a clear correlation between the vessel length density and the predicted peak MPS during CCI for nine cases together when overlaying them at the same locations, shown in Figure 4.5. Also, the correlations for nine separated cases were shown in Figure 4.6. The R square of nine cases together was 0.3447. The R square for nine separated cases were 0.5387, 0.5434, 0.4293, 0.4481, 0.3801, 0.3515, 0.3432, 0.2792 and 0.3346,

respectively. When the strain was below 0.2, the vessel length density was relatively high, approximately 500 mm/mm³ or higher. However, nearly all the vessel length density of brain tissue under the impact site was below 500 mm/mm³ when the predicted brain strain was larger than 0.3. We found that larger strains induced more microvascular damage, while smaller strains close to 0.1 to 0.2 also induced some damage.

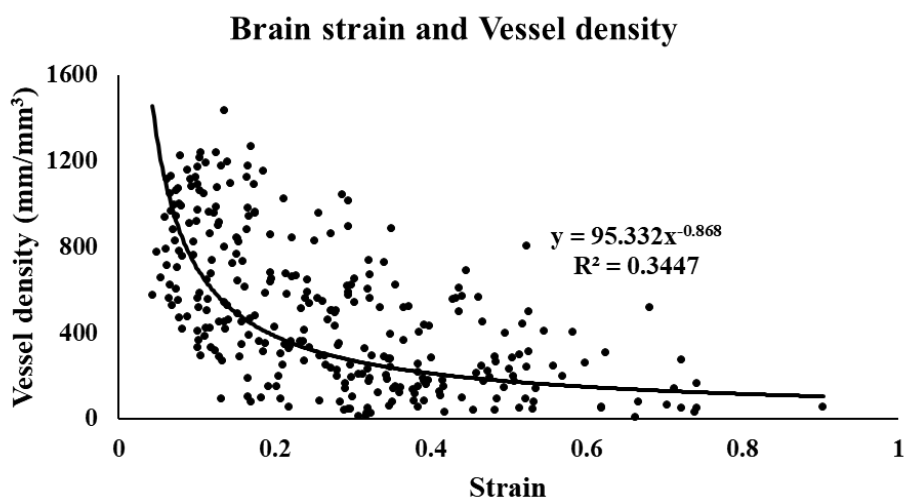


Figure 4.5 The correlation between vessel length density and maximum principal strain for nine cases together.

Brain strain and Vessel density

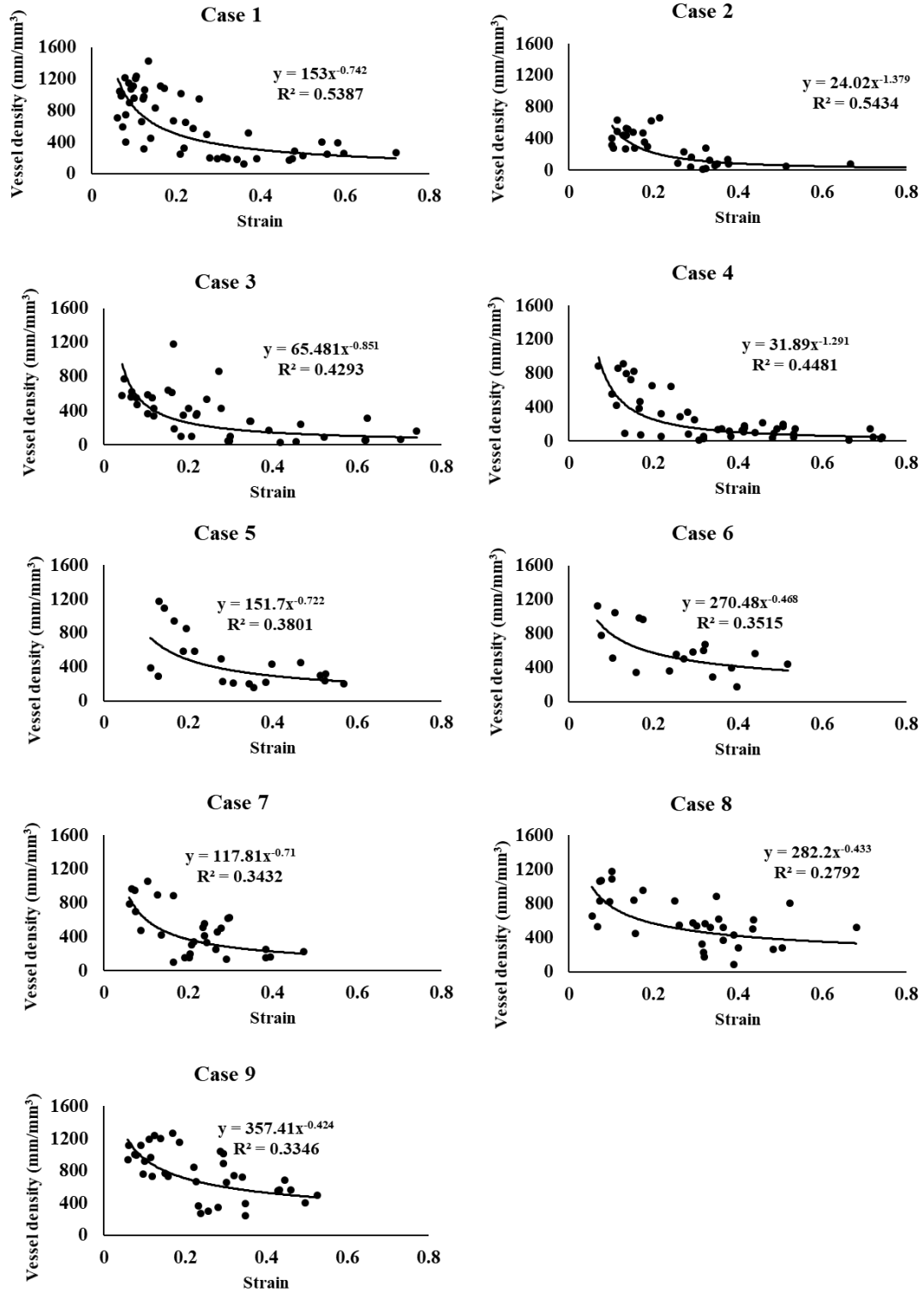


Figure 4.6 The correlation between vessel length density and maximum principal strain for nine separated cases.

4.3.3 Thresholds of the brain microvascular damage

The MPS corresponding to 50% risk of 800, 600, 400 and 200 mm/mm³ thresholds of brain microvascular damage for nine cases together were 0.08, 0.16, 0.27 and 0.43, respectively (Figure 4.7). Taking case 4 as an example, the MPS corresponding to 50% risk of 800, 600, 400 and 200 mm/mm³ thresholds of brain microvascular damage for case 4 were 0.11, 0.13, 0.19 and 0.27, respectively (Figure 4.8). The results of other cases were shown in Appendix C. As a reference, non-injured brain regions have a vessel density of 900 mm/mm³ roughly. For the MPSs corresponding to 50% risk of 800, 600, 400, 300 and 200 mm/mm³ thresholds were ranged from 0.09 to 0.18, 0.14 to 0.34, 0.18 to 0.49, 0.2 to 0.58 and 0.25 to 0.37, respectively.

The Logistic regression of nine cases

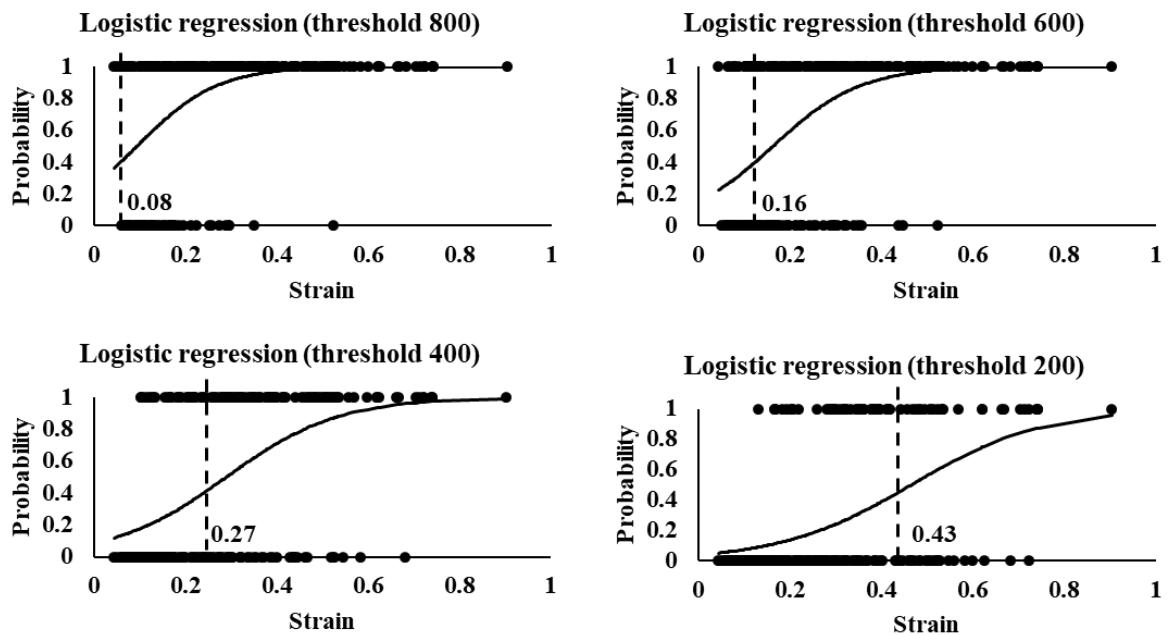


Figure 4.7 Logistic regression curves of nine cases together (800 mm/mm³ threshold, 600 mm/mm³ threshold, 400 mm/mm³ threshold, and 200 mm/mm³ threshold).

The Logistic regression of Case 4

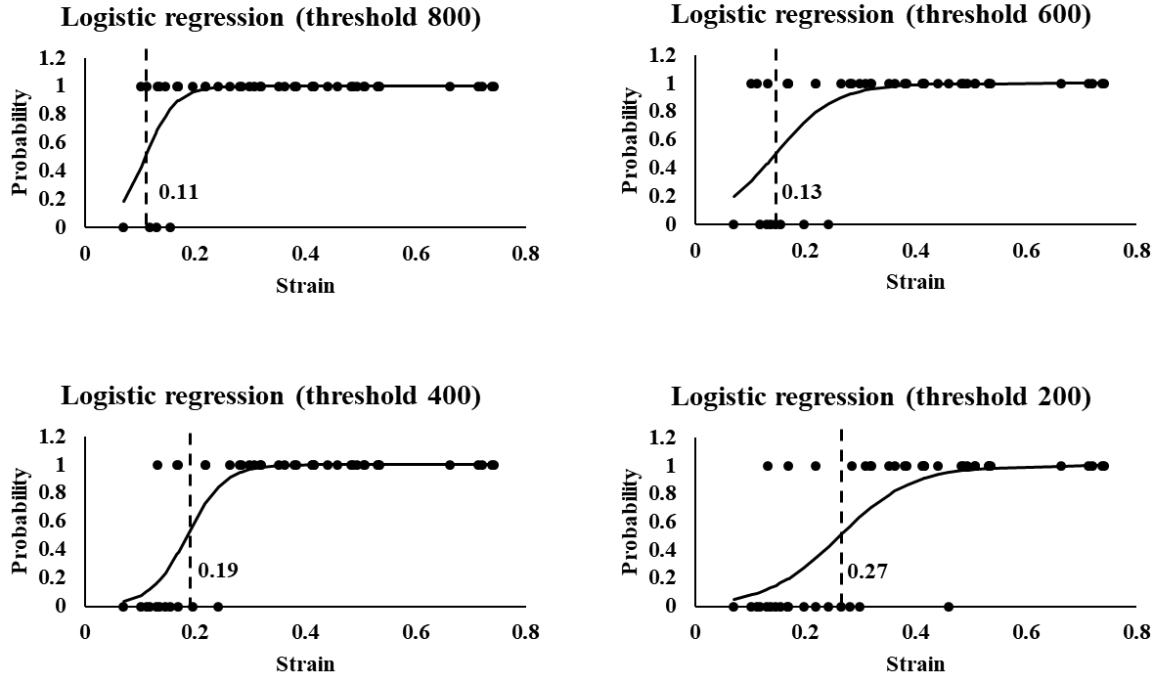


Figure 4.8 Logistic regression curves of case 4 (800 mm/mm³ threshold, 600 mm/mm³ threshold, 400 mm/mm³ threshold, and 200 mm/mm³ threshold).

4.4 Discussion

We used a FE mouse brain model to investigate the intercranial mechanical strain response within cortical brain region where the remarkable 3D cerebral microvascular length density changes in CCI. The clear correlation between the vessel length density and the predicted MPS of the microvascular in CCI. We found that larger strains induced more microvascular damage, while smaller strains close to 0.1 to 0.2 also induced some damage.

From ASL MRI images, we can only have a rough idea that there are lesions below the impact site (Figure 4.2). MRI just imaged the tissue at 40 μm resolution, but the STPT imaged the microvasculature at about 2 μm , which allowed observing the clear microvascular in the cortex region (Figure 4.1). However, because of the high-resolution and imaging scan time required for STPT, a whole-brain image was not acquired. Thus, high-resolution imaging was only done near the impact site.

Within the injury core where there were high strains, and there was a reduction in microvessel length density and blood flow. These parameters recovered within the cortex away from the injury core, like the strain map. Vessel damage was less for tissues outside the impact center. There was no obvious sign of vessel damage to the reconstruction data from the contralateral cortex. One study demonstrated that the contralateral cortical vasculature was affected in rat CCI 1-day post-injury [115]. However, the impact speed was 5 m/s, much faster than the 2 m/s velocity used in this study. Also, it was a different CCI because the rim of craniotomy should almost touch the midline (5 mm in diameter with the center being 3 mm to the midline) [115].

Microvessel damage is common across the spectrum of TBI-related injury. In the moderate to severe TBI, although big cerebral artery spasm could cause cerebral ischemia [116], the more common vessel damage happened in small vessels and microvessel [117]. In a study of the patients died in severe TBI, small arteries and microvessel damage were detected in the middle and deep layers of vascular areas in the cortex regions [118]. This study served first in its kind to correlate brain strains to microvessel damage.

The limitation of the FE mouse brain model used in the current study was that microvessel was not explicitly modeled. However, from the previous study (Chapter 3), it was found that the vasculature had a small effect on brain response during CCI, in which the skull was rigidly fixed while the exposed brain was deformed. Thus, it's postulated that the FE model without microvessel could still provide valid predictions of strain.

4.5 Conclusion

The brain microvascular damage mechanism and the associated threshold were investigated by comparing the histological data with FE model predictions. We observed that larger strains induced more microvascular damage, while smaller strains close to 0.1 to 0.2 also induced some damage. Considering the literature study reporting over 0.2 of brain strains for mild TBI/concussion cases, it is important to investigate microvascular damage in these mild TBI cases.

Chapter 5

5 Conclusion and future work

5.1 Conclusion

5.1.1 Using CCI while understanding its tip movement

CCI remains as one of the most used laboratory neurotrauma experimental methods and is expected to continue to be so as hundreds of, if not thousands of, labs have piled up brain injury data collected through CCI and will continue use similar settings for comparing with existing data. The CCI impact parameters such as impact depth and impact velocity were usually different across labs, which usually reported such depth and velocity for a cross-lab comparisons. However, the impact tip of electromagnetically and pneumatic driven CCI device both experienced repeated impacts and lateral movements, rather than a single axial impact. These tip movements were usually not observed or reported by labs. We found that the repeated impacts had minimal effect on peak brain strains. The lateral movements of tip greatly increased brain strains and affected large brain regions. Thus, we justify that CCI could be continuously considered as a single impact event and the repeated impacts could be characterized as part of this single event without affecting peak strains. However, our results show that lateral tip movements could play a major role in affecting brain injury such as increasing contusion volume. Hence, it is necessary to monitor and control lateral movement to ensure the accuracy and reproducibility of CCI, and for better across-lab comparisons.

5.1.2 Vasculature and microvasculature in CCI

The contribution of the vasculature on brain strains during the focal CCI was limited because the impactor tip was driven by either a pneumatic or electromagnetic device to

reach a predefined impact distance, usually 1-3 mm during CCI, with the animal skull being held still. Therefore, the added stiffness of the FE model with vasculature almost had no effect on the kinematics of the impactor tip, which determined how much brain surface would have been compressed.

The brain microvascular damage mechanism and the associated threshold were found by comparing the histological data with FE model predictions. We observed that larger strains induced more microvascular damage, while smaller strains close to 0.1 to 0.2 also induced some damage.

5.2 Contribution

CCI is a typical neurotrauma TBI model. During CCI, the brain is damaged by an impactor tip, which travels along its axial direction to a predefined depth at a preset speed. However, the high-speed image of an in-house pneumatically driven CCI device demonstrated CCI tip experienced lateral movement and second impact, which have long been ignored and not reported. The thesis was the first study using the finite element method to investigate how the lateral and repeat tip impact affect the brain strain responses -- which are the direct cause of neuronal damage and affect the accuracy of CCI. Our results proved that CCI could be continuously considered as a single impact event and the repeated impacts could be considered as part of this single event without affecting peak strains. However, lateral tip movement greatly affected brain responses and is suggested to be monitored. Meanwhile, caution should be practiced when comparing CCI results among different labs without knowing brain tissue responses.

Vasculature is an essential component in the brain and the roles of the vasculature in the dynamic response of the brain were studied by several teams. The previously published brain models included a two-dimensional (2D) vasculature model, a simple-geometry model, or a three-dimensional (3D) vasculature model with only major branches. There remains a controversial understanding of whether the vasculature greatly affects brain tissue deformation/strain. Therefore, the main contribution of the current study is to develop an FE mouse brain model with a new, detailed 3D vasculature model to further investigate the effect of the vessel on brain response. During focal CCI injury, the contribution of the vasculature was limited, less than 5% for all the cases. However, the vasculature is expected to have a large effect for diffuse-type brain injuries in which brain deformation will be affected by the brain's stiffness under rotational forces.

This study served as the first one to use the finite element method to study the brain microvascular damage mechanism and the associated injury threshold. The correlation between the vessel length density and the predicted MPS of the microvessel in CCI was reported. The finding that 0.1-0.2 strain-induced microvessel damage suggests that observing microvessel damage in mild TBI cases was needed, as similar strains were reported in concussion-level head impacts.

5.3 Limitations

The material property of the vasculature is known to be nonlinear, viscoelastic rather than elastic. Because of the limited time and computation power, and the lack of material testing, justification was made between the representation of physics and improvement of efficiency/stability. In the current study, nonlinear vasculature model was coupled into the FE mouse brain model.

There lacked a direct validation test for the developed FE mouse brain model with a 3D, anatomically detailed vasculature. However, as the basic model, the previously developed rat brain FE model was validated against the peak brain deformation data of CCI [56]. The mouse brain model was scaled based on the rat brain model. The correlations between experimentally observed injuries and input parameters, model responses and experimental injuries in CCI have been estimated [56]. Also, these FE models were well correlated through the linear relationship between the mechanical brain tissue strain and neural cell death [37]. Even though the simulations of repeated impacts lacked validation, the technique we used to simulate CCI on the mouse brain has been found to provide valid predictions when comparing brain strains to brain damage observed through histopathology.

5.4 Future study

The findings from the current study help to better develop a next-generation mouse brain model and investigate the influence of vasculature on brain strain response in the future.

5.4.1 Develop an FE brain model with detailed 3D nonlinear, visco-elastic and anisotropic vasculature

Though my MEng work, I learned how to determine material constants for non-linear vasculature and have gained a better understanding of how to work on complex FE models with half-million elements and many different types of elements. I also gained knowledge in constitutive equations, which will be further developed to model the vasculature as a nonlinear, visco-elastic and anisotropic material [119, 120]. I will develop an FE brain model with detailed 3D nonlinear, visco-elastic and anisotropic vasculature in the future. In this stage, I will determine the material constants for the non-

linear, visco-elastic vasculature and develop new constitutive equations to include the anisotropic behavior of vasculature. This can be achieved by combining nonlinear Ogden material with viscous terms.

5.4.2 Simulate the parcellated fiber axon clusters and blood flow

One of the unsolved challenges in developing high-quality brain models is to simulate the parcellated fiber axon clusters because the geometrical characteristics of the fiber orientation, fiber lengths, and fiber functionalities make the coupling engineering principles with medical imaging techniques and neuroscience difficult. So far, the FE brain model with the entire three-dimensional (3D) vasculature, parcellated fiber axon clusters, and blood flow has not been reported, which could be named as the next-generation mouse brain model. In this stage, I will incorporate parcellated fiber axon clusters into the model. I will use the high-quality mouse axon geometric dataset developed by Dr. Johnson's group at Duke University [121]. The methods I have learned during vessel meshes will be extended to develop axonal meshes. I expect to solve challenges such as incorporating extensive axon elements into solvable FE models.

5.4.3 Diffuse injury

Except for the focal brain injury, brain usually experiences diffuse brain injuries in which brain deformation will be affected by the brain's response to rotational forces, such as closed-head impact model of engineered rotational acceleration (CHIMERA). There remains a controversial understanding in literatures on whether the vasculature greatly affects brain tissue deformation/strain, or not for diffuse brain injury. Therefore, we will develop an FE mouse brain model with a new, detailed 3D nonlinear, visco-elastic and anisotropic vasculature model to further investigate the effect of the vasculature on brain

response under the diffuse injury in the future. An initial try was to use the linear elastic vasculature mouse brain model to study the effect of the vasculature under the diffuse injury, such as rotational acceleration. I found that the predicted peak maximum principal strains (MPS) ranged from 0.18 to 0.26 for the without-vasculature model (Figure 5.1a) and from 0.15 to 0.20 for the with-vasculature model (Figure 5.1b) for rotational acceleration.

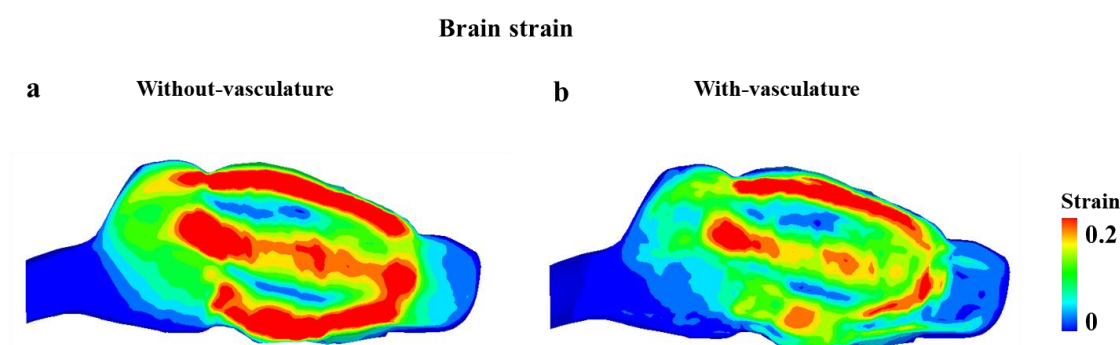


Figure 5.1 Brain strain and motion. Strain contours predicted by: (a) Without-vasculature model; (b) With-vasculature model.

5.4.4 Validation

Compared with the human FE brain model, animal FE brain model is relatively easy to be validated with animal experimental head model to mimic real-world head impact biomechanics. Therefore, the validation of the developed an FE brain model with detailed 3D nonlinear, visco-elastic and anisotropic vasculature, the parcellated fiber axon clusters and blood flow will be a challenging thing in the future, which may need the cooperation with other biological and biomechanical groups within and without the Western university.

5.5 Significance and novelty

The significance of the current study for a better understanding and use of CCI can be described as follows. First, caution should be practiced when comparing CCI results

among different labs without knowing brain tissue responses. A report of lateral movement is recommended besides reporting CCI parameters including impact depth, impact velocity, impactor tip shape and size, and craniotomy. Second, this study adopts an FE mouse model and helps to understand how the repeated impacts in milliseconds affect the tissue strain. Our data is unique in the literature, to the best of our knowledge. Third, the FE mouse brain model helps to explain the importance of monitoring lateral tip movements. Our studies proved that the lateral tip movement with contact was correlated well with the brain tissue strain (Table 2.2). Therefore, lateral tip movements should be monitored and those movements along with contact with the brain surface are expected to greatly affect brain responses. Fourth, the lateral tip movements in CCI devices are suggested to be added in the CCI FE modeling. In our previous work, CCI has been modeled as a single impact without considering the lateral tip movement. We could justify that previous CCI simulations might under-predict brain strain responses [37, 56]. To ensure the accurate prediction of brain response during CCI, lateral tip movements are suggested to be incorporated in simulations. Fifth, our study highlights that intracranial brain tissue responses are better predictors of TBI than external mechanical parameters because these tissue responses are directly related to injury rather than impact parameters such accelerations [74].

The main significance of developing of an FE mouse-brain-based model with the detailed 3D vasculature include: First, modeling detailed vasculature helps to improve the prediction accuracy of FE brain models. Some previously published brain models included a two-dimensional (2D) vasculature model, a simple geometry model, or a three-dimensional (3D) vasculature model with major branches, which were somewhat far from the actual brain with the vasculature. Second, modeling detailed vasculature also helps to study the vessel injury mechanisms in TBI. Many researchers proved that almost all the moderate and severe TBI cases contain several degrees of damage to the cerebral vasculature, which has not been extensively studied [77-79]. Third, modeling detailed vasculature also helps to study the vasculature responses, which could predict brain strain to a certain degree, to diagnose brain injury and develop treatments to improve the functional outcome after TBI.

The importance of the current study to investigate microvessel damage in the cortex region using the FE method is listed as follows: First, it is an innovation to use the FE method to investigate the microvessel damage. In the previous FE model studies, the research of the vasculature in FE model mainly focused on the big vasculature, such as arteries and veins. Little known was about the microvessel damage in FE model. Second, microvessel damage is common across the spectrum of TBI-related injury. In the medium to severe TBI, although big cerebral artery spasm could cause cerebral ischemia [116], the more common vessel damage in TBI happens in small vessels and microvessel [117]. In a study of the patients died in severe TBI, small arteries and microvessel damage were detected in the middle and deep layers of vascular areas in the cortex regions [118].

Bibliography

- [1] J. D. Corrigan, A. W. Selassie, and J. A. L. Orman, "The epidemiology of traumatic brain injury," *The Journal of head trauma rehabilitation*, vol. 25, no. 2, pp. 72-80, 2010.
- [2] H. Mao, "Modeling the head for impact scenarios," in *Basic Finite Element Method as Applied to Injury Biomechanics*: Elsevier, 2018, pp. 469-502.
- [3] G. Paxinos and C. Watson, *The rat in stereotaxic coordinates*. 1986.
- [4] M. D. Whiting, A. I. Baranova, and R. J. Hamm, "14 Cognitive Impairment following Traumatic Brain Injury," *Animal models of cognitive impairment*, p. 265, 2006.
- [5] N. C. Jones, L. Cardamone, J. P. Williams, M. R. Salzberg, D. Myers, and T. J. O'Brien, "Experimental traumatic brain injury induces a pervasive hyperanxious phenotype in rats," *Journal of neurotrauma*, vol. 25, no. 11, pp. 1367-1374, 2008.
- [6] J. Pierce, D. Smith, J. Trojanowski, and T. McIntosh, "Enduring cognitive, neurobehavioral and histopathological changes persist for up to one year following severe experimental brain injury in rats," *Neuroscience*, vol. 87, no. 2, pp. 359-369, 1998.
- [7] E. M. Umile, M. E. Sandel, A. Alavi, C. M. Terry, and R. C. Plotkin, "Dynamic imaging in mild traumatic brain injury: support for the theory of medial temporal vulnerability," *Archives of physical medicine and rehabilitation*, vol. 83, no. 11, pp. 1506-1513, 2002.
- [8] M. Dixon, A. Read, D. Donnai, A. Colley, J. Dixon, and R. Williamson, "The gene for Treacher Collins syndrome maps to the long arm of chromosome 5," *American journal of human genetics*, vol. 49, no. 1, p. 17, 1991.
- [9] R. L. West, "An application of prefrontal cortex function theory to cognitive aging," *Psychological bulletin*, vol. 120, no. 2, p. 272, 1996.
- [10] T. V. Bliss and G. L. Collingridge, "A synaptic model of memory: long-term potentiation in the hippocampus," *Nature*, vol. 361, no. 6407, p. 31, 1993.
- [11] S. M. Sherman and R. W. Guillery, *Exploring the thalamus and its role in cortical function*. MIT press, 2006.
- [12] H. M. Duvernoy, S. Delon, and J. Vannson, "Cortical blood vessels of the human brain," *Brain research bulletin*, vol. 7, no. 5, pp. 519-579, 1981.

- [13] H. Nonaka, M. Akima, T. Nagayama, T. Hatori, Z. Zhang, and F. Ihara, "Microvasculature of the human cerebral meninges," *Neuropathology*, vol. 23, no. 2, pp. 129-135, 2003.
- [14] S. Ghanavati, J. P. Lerch, and J. G. Sled, "Automatic anatomical labeling of the complete cerebral vasculature in mouse models," *Neuroimage*, vol. 95, pp. 117-128, 2014.
- [15] F. Reina-De La Torre, A. Rodriguez-Baeza, and J. Sahuquillo-Barris, "Morphological characteristics and distribution pattern of the arterial vessels in human cerebral cortex: a scanning electron microscope study," *The Anatomical Record: An Official Publication of the American Association of Anatomists*, vol. 251, no. 1, pp. 87-96, 1998.
- [16] H. Nonaka, M. Akima, T. Hatori, T. Nagayama, Z. Zhang, and F. Ihara, "Microvasculature of the human cerebral white matter: arteries of the deep white matter," *Neuropathology*, vol. 23, no. 2, pp. 111-118, 2003.
- [17] J. Meder, J. Chiras, J. Roland, P. Guinet, S. Bracard, and F. Bargy, "Venous territories of the brain," *Journal of neuroradiology. Journal de neuroradiologie*, vol. 21, no. 2, pp. 118-133, 1994.
- [18] L. Zhang *et al.*, "Computational study of the contribution of the vasculature on the dynamic response of the brain," in *SAE CONFERENCE PROCEEDINGS P*, 2002, pp. 145-164: SAE; 1999.
- [19] T. E. Carew, R. N. Vaishnav, and D. J. Patel, "Compressibility of the arterial wall," *Circulation research*, vol. 23, no. 1, pp. 61-68, 1968.
- [20] D. J. Patel, D. L. Fry, and J. S. Janicki, "The elastic symmetry of arterial segments in dogs," *Circulation research*, vol. 24, no. 1, pp. 1-8, 1969.
- [21] D. Mohan and J. W. Melvin, "Failure properties of passive human aortic tissue. I—uniaxial tension tests," *Journal of biomechanics*, vol. 15, no. 11, pp. 887-893, 1982.
- [22] D. C. Viano, "Biomechanics of nonpenetrating aortic trauma: a review," SAE Technical Paper0148-7191, 1983.
- [23] Y. Fung, "C. 1981 Biomechanics: Mechanical Properties of Living Tissues," ed: New York: Springer-Verlag.
- [24] K. L. Monson, "Mechanical and failure properties of human cerebral blood vessels," University of California, Berkeley, 2001.
- [25] J. Ho and S. Kleiven, "Dynamic response of the brain with vasculature: a three-dimensional computational study," *Journal of biomechanics*, vol. 40, no. 13, pp. 3006-3012, 2007.

- [26] J. D. Chalupnik, C. Daly, and H. C. Merchant, *Material properties of cerebral blood vessels*. Department of Mechanical Engineering, University of Washington, 1971.
- [27] H. J. Steiger, R. Aaslid, S. Keller, and H.-J. Reulen, "Strength, elasticity and viscoelastic properties of cerebral aneurysms," *Heart and vessels*, vol. 5, no. 1, pp. 41-46, 1989.
- [28] C. E. Dixon, J. W. Lighthall, and T. E. Anderson, "Physiologic, Histopathologic, and Cineradiographic Characterization of a New Fluid-Percussion Model of Experimental Brain Injury in the Rat," *Journal of neurotrauma*, vol. 5, no. 2, pp. 91-104, 1988.
- [29] D. H. Smith *et al.*, "A model of parasagittal controlled cortical impact in the mouse: cognitive and histopathologic effects," *Journal of neurotrauma*, vol. 12, no. 2, pp. 169-178, 1995.
- [30] Y. Kim, A. H. Fu, L. B. Tucker, J. Liu, and J. T. McCabe, "Characterization of controlled cortical impact devices by high-speed image analysis," *Journal of neuroscience research*, vol. 96, no. 4, pp. 501-511, 2018.
- [31] P. M. Kochanek *et al.*, "Severe controlled cortical impact in rats: assessment of cerebral edema, blood flow, and contusion volume," (in eng), *J Neurotrauma*, vol. 12, no. 6, pp. 1015-25, Dec 1995.
- [32] S. V. Kabadi, G. D. Hilton, B. A. Stoica, D. N. Zapple, and A. I. Faden, "Fluid-percussion-induced traumatic brain injury model in rats," *Nature protocols*, vol. 5, no. 9, p. 1552, 2010.
- [33] H. J. Thompson *et al.*, "Lateral fluid percussion brain injury: a 15-year review and evaluation," *Journal of neurotrauma*, vol. 22, no. 1, pp. 42-75, 2005.
- [34] Y. Xiong, A. Mahmood, and M. Chopp, "Animal models of traumatic brain injury," *Nature Reviews Neuroscience*, vol. 14, no. 2, p. 128, 2013.
- [35] S. R. Shultz *et al.*, "The potential for animal models to provide insight into mild traumatic brain injury: translational challenges and strategies," *Neuroscience & Biobehavioral Reviews*, vol. 76, pp. 396-414, 2017.
- [36] D. R. Namjoshi *et al.*, "Merging pathology with biomechanics using CHIMERA (Closed-Head Impact Model of Engineered Rotational Acceleration): a novel, surgery-free model of traumatic brain injury," *Molecular neurodegeneration*, vol. 9, no. 1, p. 55, 2014.
- [37] H. Mao *et al.*, "Finite element analysis of controlled cortical impact-induced cell loss," *Journal of neurotrauma*, vol. 27, no. 5, pp. 877-888, 2010.

- [38] L. Zhang *et al.*, "Recent advances in brain injury research: a new human head model development and validation," *Stapp Car Crash J*, vol. 45, no. 11, pp. 369-394, 2001.
- [39] K. Omori, L. Zhang, K. H. Yang, and A. I. King, "Effect of cerebral vasculatures on the mechanical response of brain tissue: a preliminary study," *ASME APPLIED MECHANICS DIVISION-PUBLICATIONS-AMD*, vol. 246, pp. 167-174, 2000.
- [40] Y. Hua, S. Lin, and L. Gu, "Relevance of blood vessel networks in blast-induced traumatic brain injury," *Computational and mathematical methods in medicine*, vol. 2015, 2015.
- [41] G. Unnikrishnan *et al.*, "A 3-D Rat Brain Model for Blast-Wave Exposure: Effects of Brain Vasculature and Material Properties," *Annals of Biomedical Engineering*, pp. 1-12, 2019.
- [42] D. M. Feeney, M. G. Boyeson, R. T. Linn, H. M. Murray, and W. G. Dail, "Responses to cortical injury: I. Methodology and local effects of contusions in the rat," *Brain research*, vol. 211, no. 1, pp. 67-77, 1981.
- [43] A. Marmarou, M. A. A.-E. Foda, W. v. d. Brink, J. Campbell, H. Kita, and K. Demetriadou, "A new model of diffuse brain injury in rats: Part I: Pathophysiology and biomechanics," *Journal of neurosurgery*, vol. 80, no. 2, pp. 291-300, 1994.
- [44] M. A. Flierl, P. F. Stahel, K. M. Beauchamp, S. J. Morgan, W. R. Smith, and E. Shohami, "Mouse closed head injury model induced by a weight-drop device," *Nature protocols*, vol. 4, no. 9, p. 1328, 2009.
- [45] C. R. Bass, M. B. Panzer, K. A. Rafaels, G. Wood, J. Shridharani, and B. Capehart, "Brain injuries from blast," *Annals of biomedical engineering*, vol. 40, no. 1, pp. 185-202, 2012.
- [46] R. R. Hicks, S. J. Fertig, R. E. Desrocher, W. J. Koroshetz, and J. J. Pancrazio, "Neurological effects of blast injury," *The Journal of trauma*, vol. 68, no. 5, p. 1257, 2010.
- [47] N. D. Osier, S. W. Carlson, A. DeSana, and C. E. Dixon, "Chronic histopathological and behavioral outcomes of experimental traumatic brain injury in adult male animals," *Journal of neurotrauma*, vol. 32, no. 23, pp. 1861-1882, 2015.
- [48] C. E. Dixon, G. L. Clifton, J. W. Lighthall, A. A. Yaghmai, and R. L. Hayes, "A controlled cortical impact model of traumatic brain injury in the rat," (in eng), *J Neurosci Methods*, vol. 39, no. 3, pp. 253-62, Oct 1991.

- [49] N. D. Osier and C. E. Dixon, "The Controlled Cortical Impact Model: Applications, Considerations for Researchers, and Future Directions," *Front Neurol*, vol. 7, p. 134, 2016.
- [50] D. L. Brody *et al.*, "Electromagnetic controlled cortical impact device for precise, graded experimental traumatic brain injury," *J Neurotrauma*, vol. 24, no. 4, pp. 657-73, Apr 2007.
- [51] D. Guo, L. Zeng, D. L. Brody, and M. Wong, "Rapamycin attenuates the development of posttraumatic epilepsy in a mouse model of traumatic brain injury," *PloS one*, vol. 8, no. 5, p. e64078, 2013.
- [52] S. Sangiorgi *et al.*, "Early-stage microvascular alterations of a new model of controlled cortical traumatic brain injury: 3D morphological analysis using scanning electron microscopy and corrosion casting," *Journal of neurosurgery*, vol. 118, no. 4, pp. 763-774, 2013.
- [53] M. C. LaPlaca, D. K. Cullen, J. J. McLoughlin, and R. S. Cargill, 2nd, "High rate shear strain of three-dimensional neural cell cultures: a new in vitro traumatic brain injury model," (in eng), *J Biomech*, vol. 38, no. 5, pp. 1093-105, May 2005.
- [54] B. Morrison, B. S. Elkin, J.-P. Dollé, and M. L. Yarmush, "In vitro models of traumatic brain injury," *Annual Review of Biomedical Engineering*, vol. 13, no. 1, pp. 91-126, 2011.
- [55] J. M. Pleasant, S. W. Carlson, H. Mao, S. W. Scheff, K. H. Yang, and K. E. Saatman, "Rate of neurodegeneration in the mouse controlled cortical impact model is influenced by impactor tip shape: implications for mechanistic and therapeutic studies," *Journal of neurotrauma*, vol. 28, no. 11, pp. 2245-2262, 2011.
- [56] H. Mao, L. Zhang, K. H. Yang, and A. I. King, "Application of a finite element model of the brain to study traumatic brain injury mechanisms in the rat," *Stapp car crash journal*, vol. 50, p. 583, 2006.
- [57] Y. Chen, H. Mao, K. H. Yang, T. Abel, and D. F. Meaney, "A modified controlled cortical impact technique to model mild traumatic brain injury mechanics in mice," *Frontiers in neurology*, vol. 5, 2014.
- [58] K. E. Saatman, K. J. Feeko, R. L. Pape, and R. Raghupathi, "Differential behavioral and histopathological responses to graded cortical impact injury in mice," *Journal of neurotrauma*, vol. 23, no. 8, pp. 1241-1253, 2006.
- [59] K. E. Schweteye, J. R. Cirrito, T. J. Esparza, C. L. Mac Donald, D. M. Holtzman, and D. L. Brody, "Traumatic brain injury reduces soluble extracellular amyloid- β in mice: a methodologically novel combined microdialysis-controlled cortical impact study," *Neurobiology of disease*, vol. 40, no. 3, pp. 555-564, 2010.

- [60] G. B. Fox, L. Fan, R. A. Levasseur, and A. I. Faden, "Sustained sensory/motor and cognitive deficits with neuronal apoptosis following controlled cortical impact brain injury in the mouse," *Journal of neurotrauma*, vol. 15, no. 8, pp. 599-614, 1998.
- [61] G. Onyszchuk, B. Al-Hafez, Y.-Y. He, M. Bilgen, N. E. Berman, and W. M. Brooks, "A mouse model of sensorimotor controlled cortical impact: characterization using longitudinal magnetic resonance imaging, behavioral assessments and histology," *Journal of neuroscience methods*, vol. 160, no. 2, pp. 187-196, 2007.
- [62] K. M. Guskiewicz *et al.*, "Cumulative effects associated with recurrent concussion in collegiate football players: the NCAA Concussion Study," *Jama*, vol. 290, no. 19, pp. 2549-2555, 2003.
- [63] J. J. Crisco *et al.*, "Frequency and location of head impact exposures in individual collegiate football players," *Journal of athletic training*, vol. 45, no. 6, pp. 549-559, 2010.
- [64] K. M. Guskiewicz *et al.*, "National Athletic Trainers' Association position statement: management of sport-related concussion," *Journal of athletic training*, vol. 39, no. 3, p. 280, 2004.
- [65] N. Osier and C. E. Dixon, "Mini Review of Controlled Cortical Impact: A Well-Suited Device for Concussion Research," *Brain Sci*, vol. 7, no. 7, Jul 20 2017.
- [66] H. L. Laurer *et al.*, "Mild head injury increasing the brain's vulnerability to a second concussive impact," *Journal of neurosurgery*, vol. 95, no. 5, pp. 859-870, 2001.
- [67] S. M. DeFord *et al.*, "Repeated mild brain injuries result in cognitive impairment in B6C3F1 mice," *Journal of neurotrauma*, vol. 19, no. 4, pp. 427-438, 2002.
- [68] V. Donovan *et al.*, "Repeated Mild Traumatic Brain Injury Results in Long-Term White-Matter Disruption," *Journal of Cerebral Blood Flow & Metabolism*, vol. 34, no. 4, pp. 715-723, 2014.
- [69] A. L. Petraglia *et al.*, "The spectrum of neurobehavioral sequelae after repetitive mild traumatic brain injury: a novel mouse model of chronic traumatic encephalopathy," *Journal of neurotrauma*, vol. 31, no. 13, pp. 1211-1224, 2014.
- [70] S. H. Friess *et al.*, "Repeated traumatic brain injury affects composite cognitive function in piglets," *Journal of neurotrauma*, vol. 26, no. 7, pp. 1111-1121, 2009.
- [71] C. V. Haar, D. M. Friend, D. B. Mudd, and J. S. Smith, "Successive bilateral frontal controlled cortical impact injuries show behavioral savings," *Behavioural brain research*, vol. 240, pp. 153-159, 2013.

- [72] G. Allen, D. Gerami, and M. Esser, "Conditioning effects of repetitive mild neurotrauma on motor function in an animal model of focal brain injury," *Neuroscience*, vol. 99, no. 1, pp. 93-105, 2000.
- [73] Y. C. Chen, D. H. Smith, and D. F. Meaney, "In-vitro approaches for studying blast-induced traumatic brain injury," *Journal of neurotrauma*, vol. 26, no. 6, pp. 861-876, 2009.
- [74] A. I. King, K. H. Yang, L. Zhang, W. Hardy, and D. C. Viano, "Is head injury caused by linear or angular acceleration," in *IRCOBI conference*, 2003, pp. 1-12: Lisbon, Portugal.
- [75] H. Mao, K. H. Yang, A. I. King, and K. Yang, "Computational neurotrauma—design, simulation, and analysis of controlled cortical impact model," *Biomechanics and modeling in mechanobiology*, vol. 9, no. 6, pp. 763-772, 2010.
- [76] D. H. Smith *et al.*, "Pre-Clinical Traumatic Brain Injury Common Data Elements: Toward a Common Language Across Laboratories," *J Neurotrauma*, vol. 32, no. 22, pp. 1725-35, Nov 15 2015.
- [77] D. S. DeWitt and D. S. Prough, "Traumatic cerebral vascular injury: the effects of concussive brain injury on the cerebral vasculature," *Journal of neurotrauma*, vol. 20, no. 9, pp. 795-825, 2003.
- [78] A. Jullienne, A. Obenaus, A. Ichkova, C. Savona-Baron, W. J. Pearce, and J. Badaut, "Chronic cerebrovascular dysfunction after traumatic brain injury," *Journal of neuroscience research*, vol. 94, no. 7, pp. 609-622, 2016.
- [79] K. Kenney *et al.*, "Cerebral vascular injury in traumatic brain injury," *Experimental neurology*, vol. 275, pp. 353-366, 2016.
- [80] E. D. Bell, J. W. Sullivan, and K. L. Monson, "Subfailure overstretch induces persistent changes in the passive mechanical response of cerebral arteries," *Frontiers in bioengineering and biotechnology*, vol. 3, p. 2, 2015.
- [81] R. Daneman and A. Prat, "The blood-brain barrier," *Cold Spring Harb Perspect Biol*, vol. 7, no. 1, p. a020412, Jan 5 2015.
- [82] E. M. Golding, "Sequelae following traumatic brain injury: the cerebrovascular perspective," *Brain research reviews*, vol. 38, no. 3, pp. 377-388, 2002.
- [83] C. Werner and K. Engelhard, "Pathophysiology of traumatic brain injury," *British journal of anaesthesia*, vol. 99, no. 1, pp. 4-9, 2007.
- [84] A. Holbourn, "Mechanics of head injuries," *The Lancet*, vol. 242, no. 6267, pp. 438-441, 1943.

- [85] I. Altman, A. Vinsel, and B. B. Brown, "Dialectic conceptions in social psychology: An application to social penetration and privacy regulation," *Advances in experimental social psychology*, vol. 14, pp. 107-160, 1981.
- [86] S. S. Margulies, L. E. Thibault, and T. A. Gennarelli, "Physical model simulations of brain injury in the primate," *Journal of biomechanics*, vol. 23, no. 8, pp. 823-836, 1990.
- [87] A. Ivarsson *et al.*, "Epidemic of coeliac disease in Swedish children," *Acta paediatrica*, vol. 89, no. 2, pp. 165-171, 2000.
- [88] J. S. Ruan, T. B. Khalil, and A. I. King, "Finite element modeling of direct head impact," SAE Technical Paper0148-7191, 1993.
- [89] R. Willinger, H.-S. Kang, and B. Diaw, "Three-dimensional human head finite-element model validation against two experimental impacts," *Annals of biomedical engineering*, vol. 27, no. 3, pp. 403-410, 1999.
- [90] T. Horgan and M. D. Gilchrist, "The creation of three-dimensional finite element models for simulating head impact biomechanics," *International Journal of Crashworthiness*, vol. 8, no. 4, pp. 353-366, 2003.
- [91] S. Kleiven, "Finite element modeling of the human head," KTH, 2002.
- [92] H. Mao *et al.*, "Development of a finite element human head model partially validated with thirty five experimental cases," *Journal of biomechanical engineering*, vol. 135, no. 11, p. 111002, 2013.
- [93] S. Ji *et al.*, "Parametric comparisons of intracranial mechanical responses from three validated finite element models of the human head," *Annals of biomedical engineering*, vol. 42, no. 1, pp. 11-24, 2014.
- [94] E. G. Takhounts *et al.*, "Investigation of traumatic brain injuries using the next generation of simulated injury monitor (SIMon) finite element head model," *Stapp car crash journal*, vol. 52, p. 1, 2008.
- [95] K. L. Monson, W. Goldsmith, N. M. Barbaro, and G. T. Manley, "Axial mechanical properties of fresh human cerebral blood vessels," *Journal of biomechanical engineering*, vol. 125, no. 2, pp. 288-294, 2003.
- [96] K. L. Monson, W. Goldsmith, N. M. Barbaro, and G. T. Manley, "Significance of source and size in the mechanical response of human cerebral blood vessels," *Journal of biomechanics*, vol. 38, no. 4, pp. 737-744, 2005.
- [97] K. L. Monson, V. Mathur, and D. A. Powell, "Deformations and end effects in isolated blood vessel testing," *Journal of biomechanical engineering*, vol. 133, no. 1, p. 011005, 2011.

- [98] A. Dorr, J. Sled, and N. Kabani, "Three-dimensional cerebral vasculature of the CBA mouse brain: a magnetic resonance imaging and micro computed tomography study," *Neuroimage*, vol. 35, no. 4, pp. 1409-1423, 2007.
- [99] S. Ghanavati, J. P. Lerch, and J. G. Sled, "Automatic anatomical labeling of the complete cerebral vasculature in mouse models," *Neuroimage*, vol. 95, pp. 117-28, Jul 15 2014.
- [100] B. Xiong *et al.*, "Precise Cerebral Vascular Atlas in Stereotaxic Coordinates of Whole Mouse Brain," *Front Neuroanat*, vol. 11, p. 128, 2017.
- [101] E. D. Bell, M. Converse, H. Mao, G. Unnikrishnan, J. Reifman, and K. L. Monson, "Material Properties of Rat Middle Cerebral Arteries at High Strain Rates," *Journal of biomechanical engineering*, vol. 140, no. 7, p. 071004, 2018.
- [102] L. Lu and H. Mao, "Quantifying the Effect of Repeated Impacts and Lateral Tip Movements on Brain Responses during Controlled Cortical Impact," *Journal of neurotrauma*, 2019.
- [103] A. Salehi, J. H. Zhang, and A. Obenaus, "Response of the cerebral vasculature following traumatic brain injury," *Journal of Cerebral Blood Flow & Metabolism*, vol. 37, no. 7, pp. 2320-2339, 2017.
- [104] J. A. Detre, H. Rao, D. J. Wang, Y. F. Chen, and Z. Wang, "Applications of arterial spin labeled MRI in the brain," *Journal of Magnetic Resonance Imaging*, vol. 35, no. 5, pp. 1026-1037, 2012.
- [105] N. Marklund, A. Bakshi, D. J. Castellbuono, V. Conte, and T. K. McIntosh, "Evaluation of pharmacological treatment strategies in traumatic brain injury," *Current pharmaceutical design*, vol. 12, no. 13, pp. 1645-1680, 2006.
- [106] T. K. McINTOSH, M. Juhler, and T. Wieloch, "Novel pharmacologic strategies in the treatment of experimental traumatic brain injury: 1998," *Journal of neurotrauma*, vol. 15, no. 10, pp. 731-769, 1998.
- [107] N. Nicolakakis, T. Aboukassim, A. Aliaga, X.-K. Tong, P. Rosa-Neto, and E. Hamel, "Intact memory in TGF- β 1 transgenic mice featuring chronic cerebrovascular deficit: recovery with pioglitazone," *Journal of Cerebral Blood Flow & Metabolism*, vol. 31, no. 1, pp. 200-211, 2011.
- [108] J. Wang *et al.*, "Omega-3 polyunsaturated fatty acids enhance cerebral angiogenesis and provide long-term protection after stroke," *Neurobiology of disease*, vol. 68, pp. 91-103, 2014.
- [109] J. Vogel, M. Gehrig, W. Kuschinsky, and H. H. Marti, "Massive inborn angiogenesis in the brain scarcely raises cerebral blood flow," *Journal of Cerebral Blood Flow & Metabolism*, vol. 24, no. 8, pp. 849-859, 2004.

- [110] N. M. Hayward, R. Immonen, P. I. Tuunanen, X. E. Nnode-Ekane, O. Gröhn, and A. Pitkänen, "Association of chronic vascular changes with functional outcome after traumatic brain injury in rats," *Journal of neurotrauma*, vol. 27, no. 12, pp. 2203-2219, 2010.
- [111] U.-W. Thomale, S.-N. Kroppenstedt, T. F. Beyer, K.-D. Schaser, A. W. Unterberg, and J. F. Stover, "Temporal profile of cortical perfusion and microcirculation after controlled cortical impact injury in rats," *Journal of neurotrauma*, vol. 19, no. 4, pp. 403-413, 2002.
- [112] N. M. E. A. Hayward, P. I. Tuunanen, R. Immonen, X. E. Nnode-Ekane, A. Pitkänen, and O. Gröhn, "Magnetic resonance imaging of regional hemodynamic and cerebrovascular recovery after lateral fluid-percussion brain injury in rats," *Journal of cerebral blood flow & metabolism*, vol. 31, no. 1, pp. 166-177, 2011.
- [113] B. Weber, A. L. Keller, J. Reichold, and N. K. Logothetis, "The microvascular system of the striate and extrastriate visual cortex of the macaque," *Cerebral cortex*, vol. 18, no. 10, pp. 2318-2330, 2008.
- [114] J. Steinman, L. S. Cahill, M. M. Koletar, B. Stefanovic, and J. G. Sled, "Acute and chronic stage adaptations of vascular architecture and cerebral blood flow in a mouse model of TBI," *NeuroImage*, vol. 202, p. 116101, 2019.
- [115] A. Obenaus *et al.*, "Traumatic brain injury results in acute rarefaction of the vascular network," *Scientific reports*, vol. 7, no. 1, p. 239, 2017.
- [116] N. A. Martin, C. Doberstein, C. Zane, M. J. Caron, K. Thomas, and D. P. Becker, "Posttraumatic cerebral arterial spasm: transcranial Doppler ultrasound, cerebral blood flow, and angiographic findings," *Journal of neurosurgery*, vol. 77, no. 4, pp. 575-583, 1992.
- [117] G. J. Bouma and J. P. Muizelaar, "Cerebral blood flow, cerebral blood volume, and cerebrovascular reactivity after severe head injury," *J Neurotrauma*, vol. 9, no. Suppl 1, pp. S333-S348, 1992.
- [118] A. Rodríguez-Baeza, F. Reina-de la Torre, A. Poca, M. Martí, and A. Garnacho, "Morphological features in human cortical brain microvessels after head injury: a three-dimensional and immunocytochemical study," *The Anatomical Record Part A: Discoveries in Molecular, Cellular, and Evolutionary Biology: An Official Publication of the American Association of Anatomists*, vol. 273, no. 1, pp. 583-593, 2003.
- [119] J. Cheung and C. Hsiao, "Nonlinear anisotropic viscoelastic stresses in blood vessels," *Journal of biomechanics*, vol. 5, no. 6, pp. 607-619, 1972.
- [120] J. Misra and B. Sahu, "Flow through blood vessels under the action of a periodic acceleration field: A mathematical analysis," *Computers & Mathematics with Applications*, vol. 16, no. 12, pp. 993-1016, 1988.

- [121] E. Calabrese, A. Badea, G. Cofer, Y. Qi, and G. A. Johnson, "A diffusion MRI tractography connectome of the mouse brain and comparison with neuronal tracer data," *Cerebral cortex*, vol. 25, no. 11, pp. 4628-4637, 2015.

Appendices

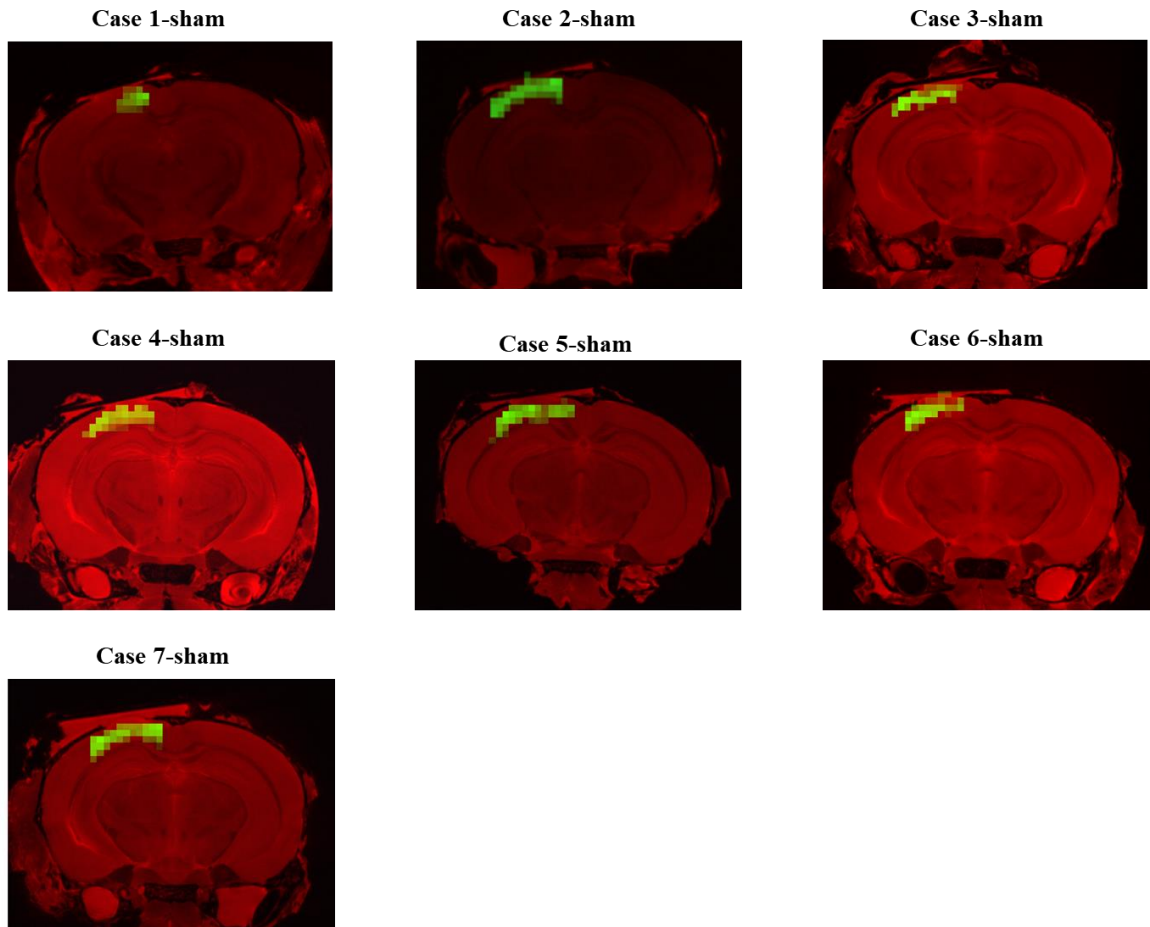
Appendix A Mouse ID and related slice labeled with the injury center

Table A.1 The mouse TD and related slice labeled with the injury center of nine cases in CCI.

Case No.	Mouse ID.	Slice labeled with the injury center
Case 1	1021	197
Case 2	1029	192
Case 3	1030	275
Case 4	1034	273
Case 5	1035	274
Case 6	1049	294
Case 7	1050	177
Case 8	1127	270
Case 9	1155	283

Table A.2 The mouse TD and related slice labeled with the injury center of seven sham cases.

Case No.	Mouse ID.	Slice labeled with the injury center
Case 1-sham	1156	281
Case 2-sham	1157	278
Case 3-sham	1193	281
Case 4-sham	1200	282
Case 5-sham	1204	281
Case 6-sham	1207	280
Case 7-sham	1208	277

Appendix B Vessel density maps of seven sham mice**Figure B.1 Vessel density map of seven sham mice.**

Appendix C **Logistic regression curves of nine separated cases (800 mm/mm^3 threshold, 600 mm/mm^3 threshold, 400 mm/mm^3 threshold, 300 mm/mm^3 and 200 mm/mm^3)**

The Logistic regression of Case 1

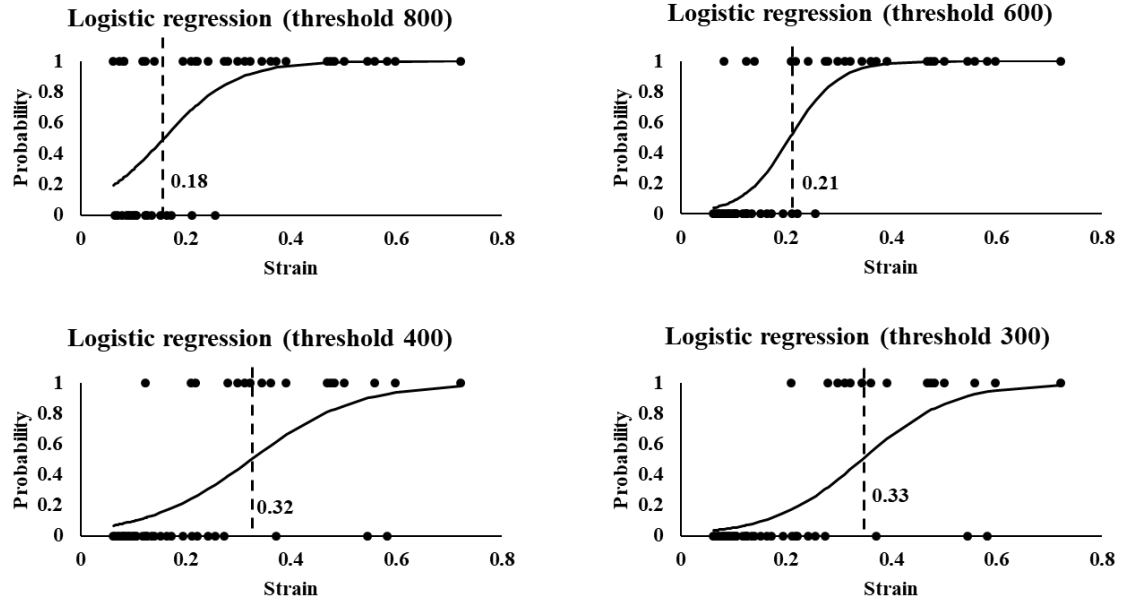


Figure C.1 Logistic regression curves of case 1 (800 mm/mm^3 threshold, 600 mm/mm^3 threshold, 400 mm/mm^3 threshold and 300 mm/mm^3 threshold).

The Logistic regression of Case 2

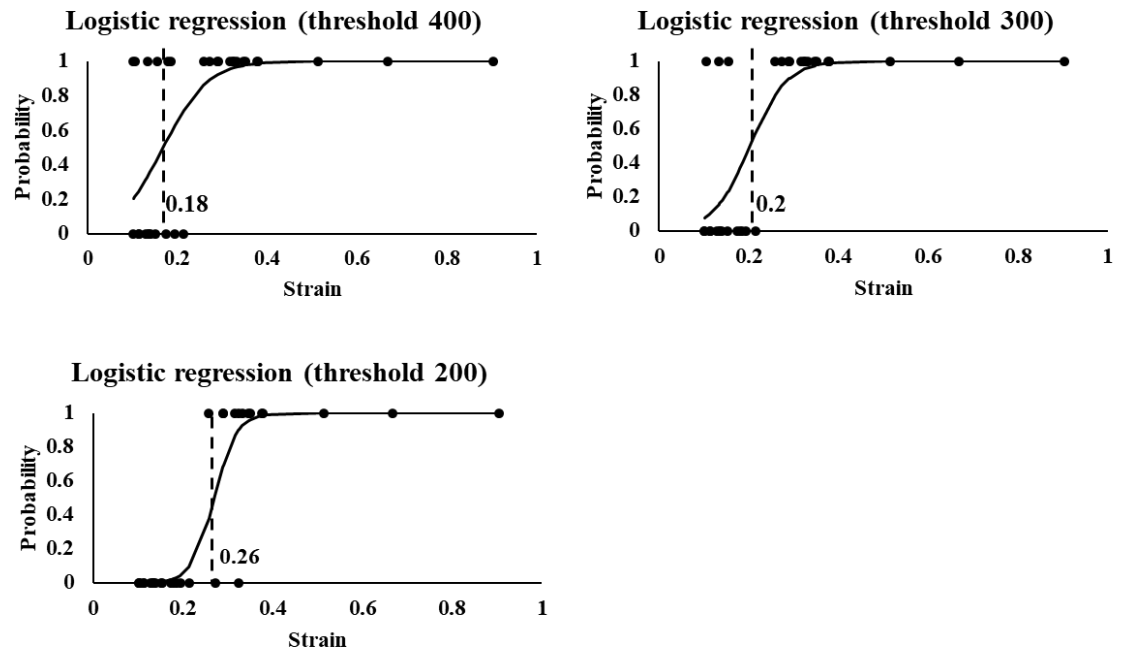


Figure C.2 Logistic regression curves of case 2 (400 mm/mm³ threshold, 300 mm/mm³ threshold and 200 mm/mm³ threshold).

The Logistic regression of Case 3

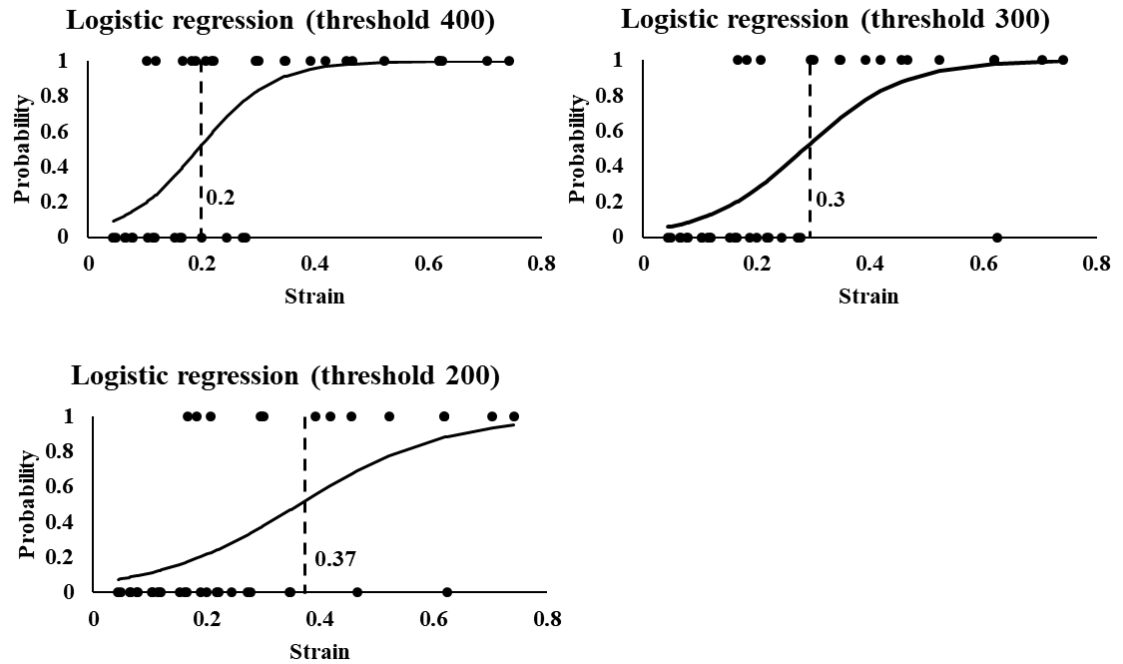


Figure C.3 Logistic regression curves of case 3 (400 mm/mm³ threshold, 300 mm/mm³ threshold and 200 mm/mm³ threshold).

The Logistic regression of Case 4

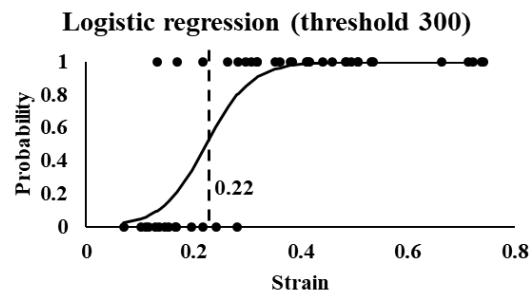


Figure C.4 The Logistic regression curve of case 4 (300 mm/mm³ threshold).

The Logistic regression of Case 5

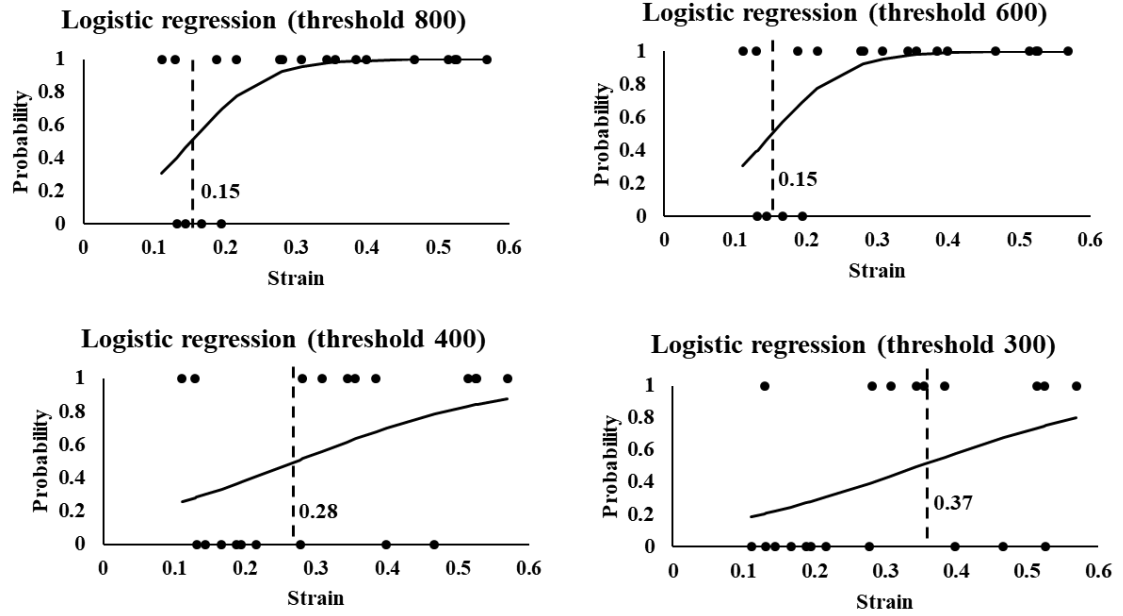


Figure C.5 Logistic regression curves of case 5 (800 mm/mm³ threshold, 600 mm/mm³ threshold, 400 mm/mm³ threshold and 300 mm/mm³ threshold).

The Logistic regression of Case 6

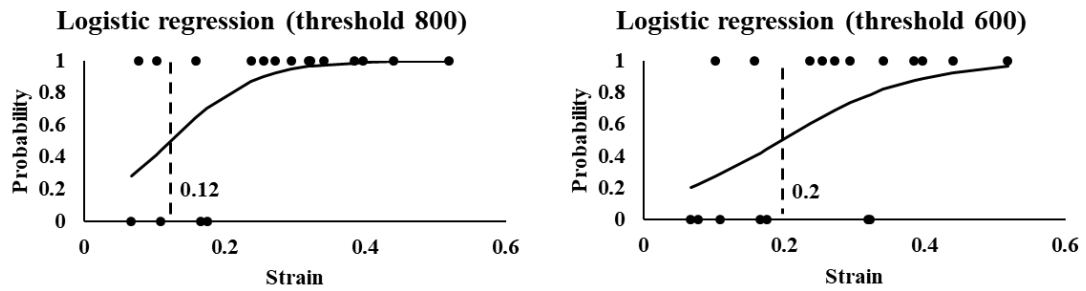


Figure C.6 Logistic regression curves of case 6 (800 mm/mm³ threshold and 600 mm/mm³ threshold).

The Logistic regression of Case 7

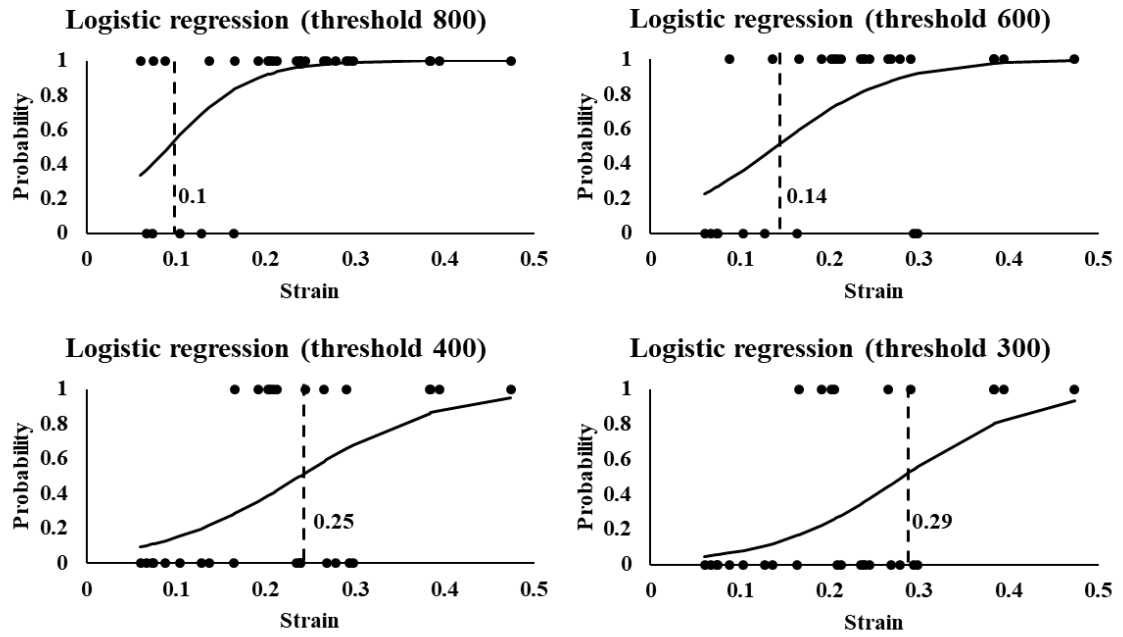


Figure C.7 Logistic regression curves of case 7 (800 mm/mm³ threshold, 600 mm/mm³ threshold, 400 mm/mm³ threshold and 300 mm/mm³ threshold).

The Logistic regression of Case 8

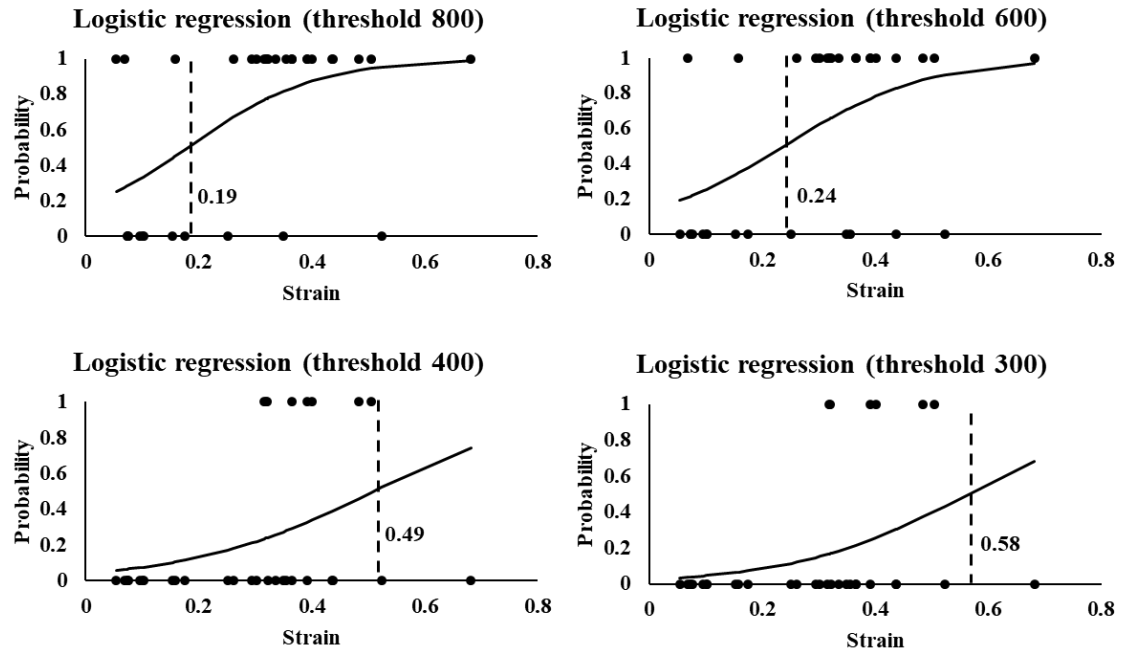


Figure C.8 Logistic regression curves of case 8 (800 mm/mm³ threshold, 600 mm/mm³ threshold, 400 mm/mm³ threshold and 300 mm/mm³ threshold).

The Logistic regression of Case 9

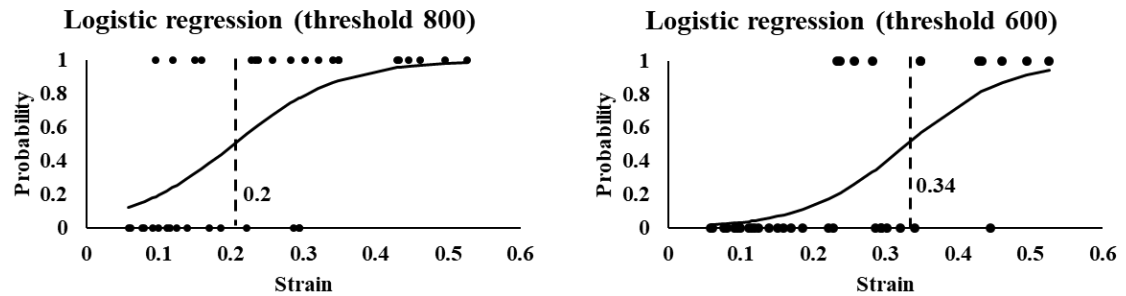


Figure C.9 Logistic regression curves of case 9 (800 mm/mm³ threshold and 600 mm/mm³ threshold).

Curriculum Vitae

Name: Lihong Lu

Post-secondary Education and Degrees: Xi'an University of architecture and technology
Xi'an, Shaanxi, China
2002-2006 B.Eng.

Western University
London, Ontario, Canada
2016-2017 M.Eng.

Western University
London, Ontario, Canada
2018-2019 M.ESc

Honors and Awards: Alexander Graham Bell-Canada Graduate Scholarship-Master's
2019 (CGSM)

Related Work Experience

Teaching Assistant
Western University
2018-2019

Postgraduate appointment
Western University
2017-2017

Publications:

Lu L, Mao H. Quantifying the Effect of Repeated Impacts and Lateral Tip Movements on Brain Responses during Controlled Cortical Impact[J]. *Journal of neurotrauma*, 2019, 36(11): 1828-1835.

Mao H, Lu L, Bian K, et al. Biomechanical analysis of fluid percussion model of brain injury[J]. *Journal of biomechanics*, 2018, 77: 228-232.

Lu L, Steinman J, Sled J, and Mao H. (2019) Investigating Mechanisms and Thresholds of Brain Microvascular Damage using a Controlled Cortical Impact Model. BMES 2019 Annual Meeting. Philadelphia (International Conference, Poster, M.E.Sc work)

Lu L, Bian K, and Mao H. (2019) A new way to link animal head kinematics to human head motion. CSME-CFDSC Congress 2019. London, Canada (International Conference, Oral presentation, M.E.Sc work)

Lu L, Bian K, and Mao H. (2019) A novel approach determining the scaling relationship between human and mouse brains in TBI. Ontario Biomechanics Conference. Alliston, Canada (Provincial Conference, Poster, M.E.Sc work)

Lu L, Bian K, and Mao H. A new scaling relationship between human and mouse brain to study concussion. ASME IMECE 2018, November 9-15, 2018, Pittsburgh PA. Selected as oral presentation.

Lu L, Sled J, and Mao H. Developing a novel mouse brain biomechanical model with 3-D vasculature. BMES 2018 Annual Meeting, October 17-20, 2018, Atlanta GA. Selected as oral presentation.

Lu L and Haojie Mao. Evaluating Electromagnetic Controlled Cortical Impact Device by Finite Element Analysis, BMES 2018 Annual Meeting, October 17-20, 2018, Atlanta GA.

Lu L and Haojie Mao. Should we engineer a better controlled cortical impact model with less lateral movement and minimized second impact of tip? Neurotrauma 2018, Toronto ON, August 11-16, 2018

Lu L, John G. Sled and Haojie Mao. Incorporating detailed three-dimensional brain vasculature into finite element modeling affects predictions of brain strains during impacts, Neurotrauma 2018, Toronto ON, August 11-16, 2018

Mao H and Lu L. Investigating pressures in the brain across multiple loading modalities. 8th World Congress on Biomechanics, Dublin Ireland 2018.